Characterization of B-Sands in Gambat Block using 3D Seismic Interpretation, Rock Physics Analysis, AVO Modelling & Post Stack Inversion Analysis

QUAID-I-AZAM UNIVERSITY

ISLAMABAD

Aqsa Afzal
M.Phil. Geophysics (2015-2017)
Department of Earth Sciences
Quaid-I-Azam University
Islamabad

IN THE NAME OF ALLAH,
THE MERCIFUL, THE COMPASSIONATE
And from Him do we seek help.
All praise be to ALLAH, the Sustainer of All the Worlds,
And blessings and peace be upon our master Muhammad (S.A.W.W),
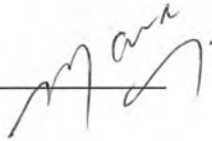*And on all his Family and Companions.*

CERTIFICATE

This dissertation submitted by **Aqsa Afzal** D/O **Muhammad Afzal** is accepted in its present form by the Department of Earth Sciences,

Quaid-I-Azam University Islamabad as satisfying the partial requirement for the award of M.Phil. Degree in Geophysics.

Dr. Muhammad Toqeer _____
(Supervisor)
Department of Earth Sciences

Dr. Mona Lisa _____
(Chairperson)
Department of Earth Sciences

ACKNOWLEDGEMENTS

ABSTRACT

Reservoir is characterized by integrating all available data to define physical properties by using different modelling techniques. The behavior of fluids is simulated in reservoir modelling which helps asset teams of E & P companies to develop optimal production techniques. In order to characterize the reservoir accurately, different geophysical techniques such as Petrophysical analysis, Rock Physics modelling, AVO modelling, Inversion, etc. are used and the results are correlated.

In the present study, B-Sands of Lower Goru Formation in Gambat Block, located in lower Indus Basin are characterized by applying all the above-mentioned techniques. Data set contains seismic data along with well data of four wells i.e. Tajjal_01, Tajjal_02, Tajjal_03 and Tajjal_04. Among these wells, Tajjal_01 and Tajjal_04 are gas producing wells while other two are abandoned ones.

In the zone of interest, saturation is changed from gas to 100% water in gas producing wells i.e. Tajjal_01 and Tajjal_04 using integrated modelling techniques and results are compared with in-situ water saturated wells i.e. Tajjal_02 and Tajjal_03.

Gassmann's Equation is applied to alter the saturation in the wells and VP is plotted against VS in all cases i.e. in-situ saturation conditions and modelled conditions. Results are compared and it is observed that VP is more effected by saturation as compared to VS.

Amplitude analysis of reflected data is carried out by using Aki-Richard's Equation on synthetic data and it is concluded class of reservoir sand is type IV.

Post stack seismic inversion is applied to extract porosity and pore pressure of the study area. Interval velocities are computed using model based seismic inversion which is a type of deterministic inversion. Porosity of reservoir ranges between 12-18% and results of pore pressure reveal that pore pressure remains almost same in adjacent sand-shale layers. However, slight increase in the pressure is observed in Ghazij shales which is bounded by limestone at its both ends.

Contents

List of Figures

1.　Introduction

Seismic interpretation conventionally implies picking and tracking horizontally reliable seismic to map geologic structures, reservoir character and stratigraphy. The ultimate goal is the detection of hydrocarbon accumulations, calculation of their lateral extent and volume. Seismic reflectors are mapped thoroughly in space and travel time, but amplitude variation is least considered. However, seismic interpreters are focusing on the quantitative techniques so that additional information regarding hydrocarbon anomalies can be validated to characterize reservoir in more accurate manner. These techniques include post-stack amplitude analysis, AVO analysis, elastic impedance inversion and forward seismic modeling. Seismic amplitudes can give information regarding porosity, lithology, saturation, as well as pore pressure (Coffeen, 1986).

1.1　Objective of the Study

Quantitative seismic interpretation helps to evaluate reservoir properties in more detail as compared to conventional interpretation. Practical implementation of the techniques mentioned above is helpful to observe behaviour of the reservoir by varying earth models and estimation of those reservoir properties which can't be estimated by conventional interpretation only. The objective of the study can be summarized as:

1. 3D Seismic Interpretation and Mapping of Subsurface Structure.
2. Generation of Synthetic Seismograms.
3. Rock Physics Modelling.
4. Seismic Attributes and AVO Modelling.
5. Post Stack Inversion

1.2　Study Area

The area of interest in this study is Gambat Block (2668-4) operated by the Österreichische Mineralölverwaltung (OMV), which lies on the eastern flank of the Khairpur high in the Lower Indus basin. Khairpur high area has a high geothermal gradient and it suffered through many stages of subsidence.

Gambat Block, a joint venture between OMV, PPL, ENI and GHPL. Gas discovery in the block was made in 2007 through exploratory well Tajjal-1 and the gas field is in Southern Pakistan's province of Sindh, it is situated almost 120 km south east of Sukkur. The proven gas reserves are

1

51 Bcf with daily average production of 3.24 MMscf. The geographical location of study area is shown as:
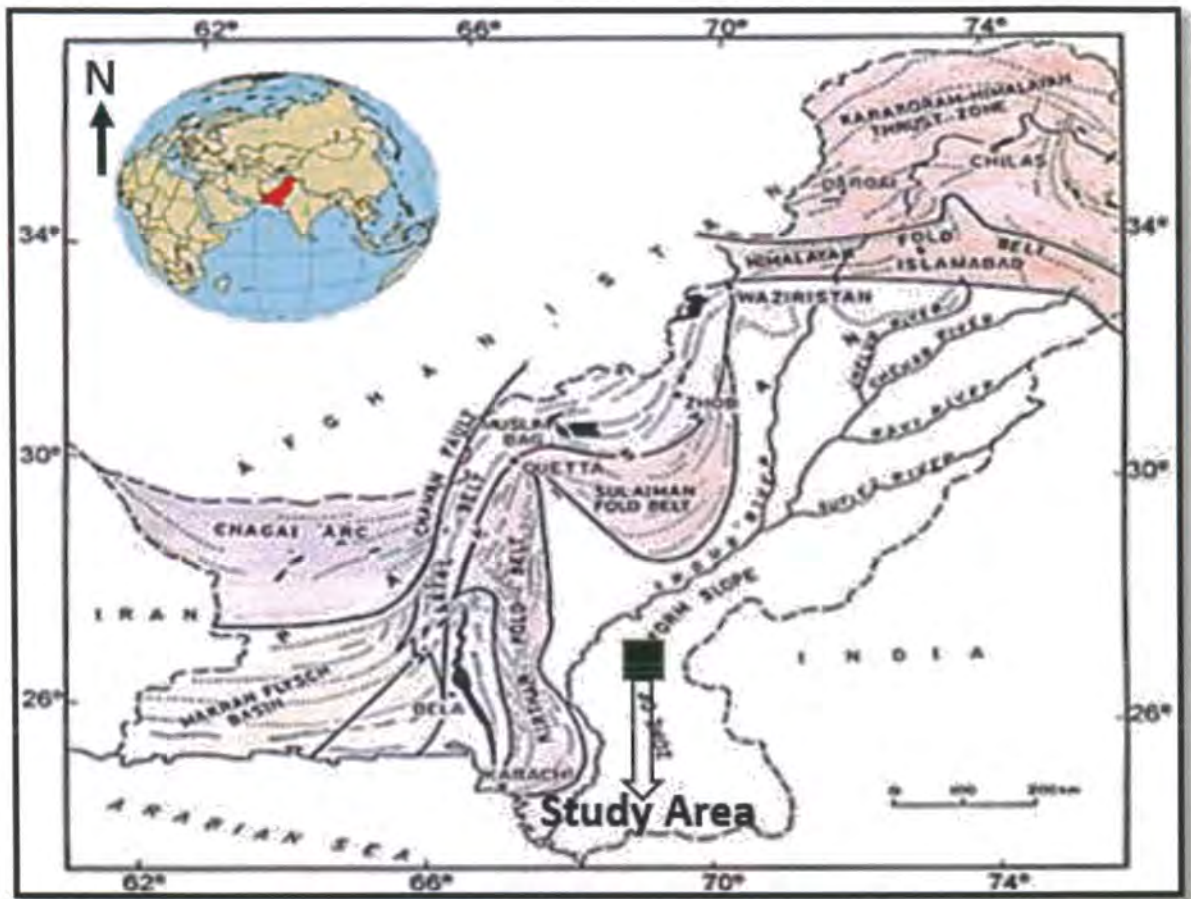
Figure 1.1: Location of study area (Younas et al., 2016)

1.3   Methodology

The methodology adopted to accomplish the above-mentioned objectives is generation of synthetic seismograms for all wells to confirm the horizons on seismic data. Petrophysical properties i.e. volume of shale and water saturation are calculated to identify hydrocarbon bearing zones. Fluid replacement modelling is carried out to build a relationship between P-wave and S-wave velocities using petrophysical properties as an input. These velocities are further used in AVO modelling to classify gas bearing sands based on AVO response. At the end, post stack inversion is applied on the data to extract reservoir properties i.e. porosity and pore pressures which can`t be extracted from seismic data only.

Seismic interpretation is done on Petrel while Rock Physics Modelling, AVO Modelling and Post Stack Inversion are carried out in Hampson and Russel (HRS).

1.4   Data Base

Seismic data is obtained by the formal permission from the Directorate General of Petroleum Concession (DGPC) through LMKR. Integrated geological and geophysical data used for the purpose is given as:

1. 3D Seismic Data
2. Wireline Log Data
    i.   Tajjal-01
    ii.   Tajjal-02
    iii.   Tajjal-03
    iv.   Tajjal-04
3. Well Tops
4. Shot Data Checking

The base map of the study area is given as:
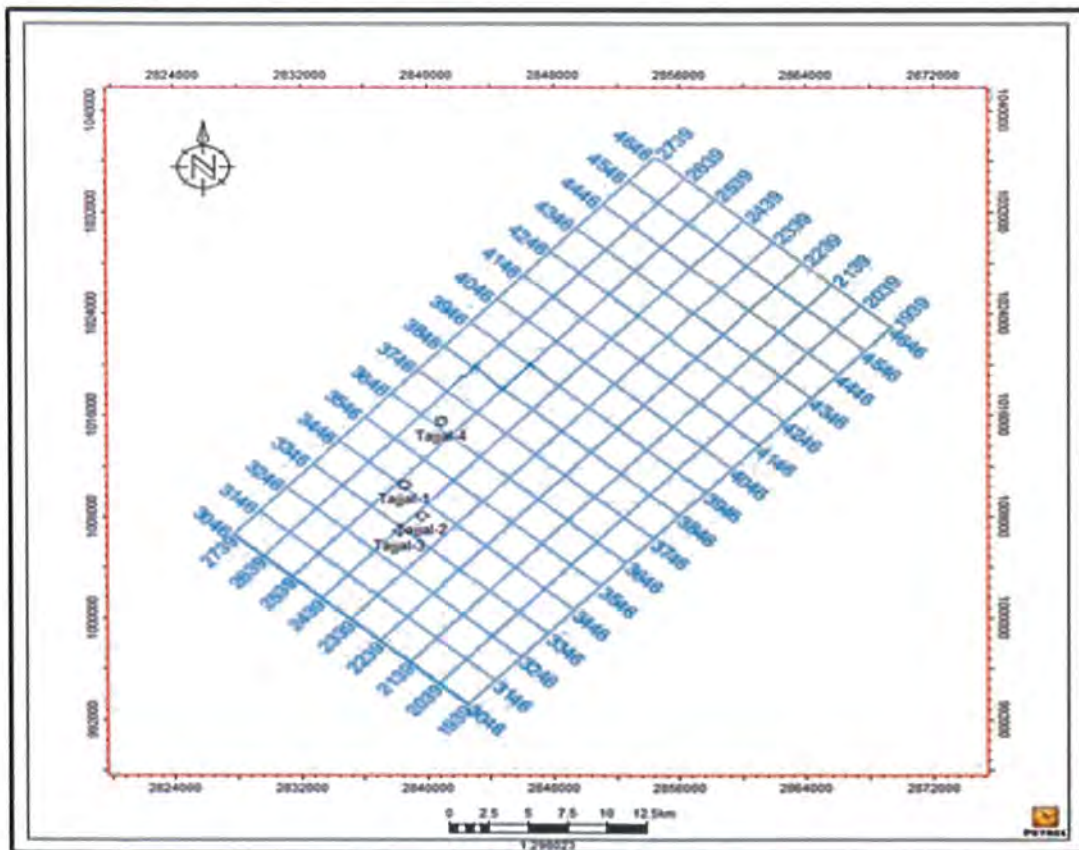
Figure 1.2: Base map of the study area

2. General Geology and Stratigraphy

The geography of Pakistan is a great combination of sceneries that includes forests, hills, plains, deserts and plateaus that extend from the coastal areas of the Arabian Sea in the south to the mountains of the Karakoram Range in the north (Kazmi and Jan, 1997).

2.1   Tectonic Zones of Pakistan

The Indian and the Eurasian tectonic plates geologically overlaps with Pakistan. On the north-western corner of the Indian plate the Sindh and Punjab provinces lie whereas within the Eurasian plate Baluchistan and most of the Khyber-Pakhtunkhwa lie which mainly consist of the Iranian plateau, some parts of the Middle East and Central Asia (Shah, 2009).

2.2   Geological Setting

Gambat Block lies in the southeastern part of prospective Kirthar Foredeep of Lower Indus Basin which is located on the continental shelf of the Indo-Pak plate (the northwest slope of the Indian Shield). Indus basin which covers 533,580 sq. km including continental shelf is divided into three parts based on structural features and positive highs. Those parts are Upper Indus Basin, Central Indus Basin and Lower Indus Basin (Kazmi and Jan, 1997).

Lower Indus Basin is principally a Cratonic Marginal Basin flanking northwestern side of Indian Shield having significant potential for testing of different exploration plays like structural, stratigraphic, combination, subtle, etc. It contains all essential ingredients for successful hydrocarbon exploration i.e. reservoir rocks, source rocks, structures, and seals which are all eventually filled by over 20,000 feet of Mesozoic sediment. Normal faults are generated because of entire southern basin displaying the extensional tectonics that describes the distinctive nature of the Horst and Graben structures. The main producing reservoirs are Cretaceous sandstones (Lower Goru Basal and Massive sands) which are un-conformably overlain by Deccan basaltic flows and thin Tertiary sediments. Rifting between the Madagascar Basin and Indian plate marked by the deposition of Lower Goru sands (Shah et al., 1977).

2.3   Tectonic Setting

Lower Indus Basin starts from the south of Sukkur Rift Zone which is a combined name of Jacobabad–Mari highs with an aerial extension between Indian Shield in the east and Baluchistan Basin in the west (Raza et al, 1989).

Kirthar Fold Belt is bounded by Main Frontal Thrust in the east along the western margin of the River Indus. West of Kirthar Fold Belt is an adjoining part of Chagi Arc System and Pishin Basin. The boundary is marked by the suture zones, developed along the different components of strike slip

4

movement of Chaman Fault & Ornach-Nal Fault. Ophiolites belt is present along this boundary in Bela and Muslim Bagh.

Kirthar Foredeep starts from the eastern edge of folded belt and extends eastward to Thar Platform. Thar Platform is a gentle sloping monocline with an extension towards Nagar Parker Uplift in the east; merges in to Karachi embayment and Kirthar trough in the SSW and bounded by Sulaiman Fold belt in NNW (Shah, 2009).

Rifting of Indian plate is followed by the Kimmeridgian-Oxfordian unconformity with a development of pelagic and bathyal shales on Jurassic limestone of the platform area with the onset of transgression resulted in Sembar Formation. This event was followed by changes in the sea level and tectonics at that time resulting into westerly prograding wedges of siliciclastic Sembar-Goru formations. After the deposition of Sembar sequences, relative sea level continued to change, causing overall retrogradation of the basin margin, which resulted into sand bearing facies of shore face, delta and Barrier Island in Lower Goru. This event was marked by constant change in sea level with different par sequence as upper sand, middle sand and basal sand of Lower Goru formation in Lower Indus basin. However, style of Lower Goru Sand changed from overall retrograding to prograding shale bearing sequence of Upper Goru in Early Cretaceous (Raza et al., 1989).

2.4   Stratigraphy

Gambat Block is entirely covered by alluvium of river Indus. Sedimentation intervals have been recorded throughout the geological time in the area; however, the important unconformities that are present in the stratigraphic succession drilled in the area are at the base of the Paleocene and Plio-Miocene. Chiltan limestone is the oldest formation penetrated in various wells drilled in and around the block.

Sedimentary succession younger than Eocene; comprising Nari (Oligocene) and Gaj formations (Miocene) is not encountered in most of the wells adjacent to the block. Oligocene and Miocene sequences are possibly either eroded due to Late Tertiary uplifting or never deposited in the surroundings of the block.

The stratigraphy of Lower Indus basin is given as:

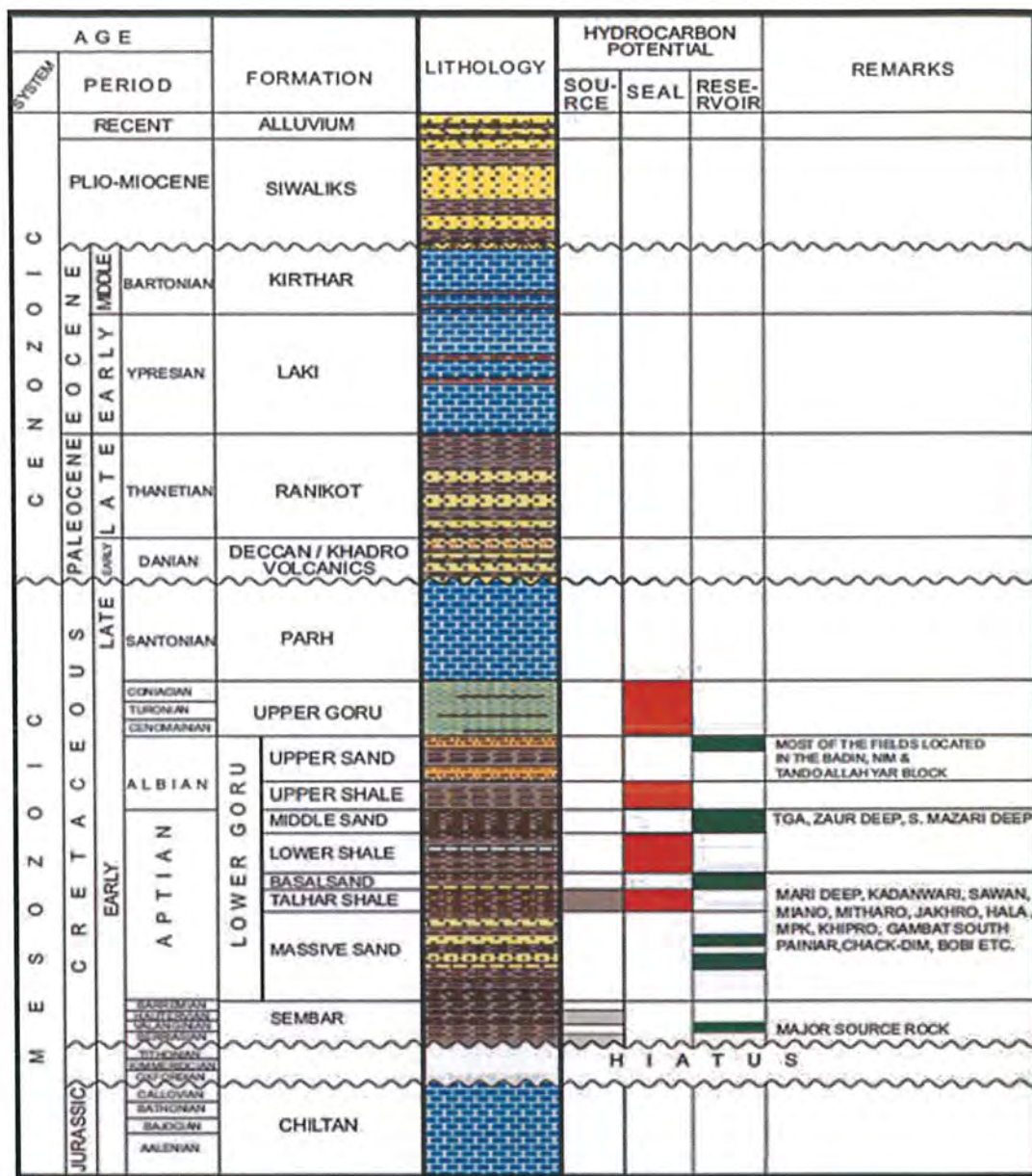| AGE				FORMATION	LITHOLOGY	HYDROCARBON POTENTIAL			REMARKS
SYSTEM	PERIOD					SOURCE	SEAL	RESERVOIR	
	RECENT			ALLUVIUM					
	PLIO-MIOCENE			SIWALIKS					
CENOZOIC	PALEOCENE — EOCENE	EOCENE	MIDDLE	BARTONIAN	KIRTHAR					
			EARLY	YPRESIAN	LAKI					
		PALEOCENE	LATE	THANETIAN	RANIKOT					
			EARLY	DANIAN	DECCAN / KHADRO VOLCANICS					
MESOZOIC	CRETACEOUS	LATE		SANTONIAN	PARH					
				CONIACIAN / TURONIAN / CENOMANIAN	UPPER GORU		■			
		EARLY	ALBIAN	LOWER GORU	UPPER SAND		■		■	MOST OF THE FIELDS LOCATED IN THE BADIN, NIM & TANDO ALLAH YAR BLOCK
					UPPER SHALE		■			
			APTIAN		MIDDLE SAND				■	TGA, ZAUR DEEP, S. MAZARI DEEP
					LOWER SHALE		■			
					BASAL SAND			■	■	MARI DEEP, KADANWARI, SAWAN, MIANO, MITHARO, JAKHRO, HALA, MPK, KHIPRO, GAMBAT SOUTH PAINIAR, CHACK-DIM, BOBI ETC.
					TALHAR SHALE			■		
					MASSIVE SAND				■	
			NEOCOMIAN etc.	SEMBAR		■		■	MAJOR SOURCE ROCK
	JURASSIC		TITHONIAN / KIMMERIDGIAN / OXFORDIAN / CALLOVIAN / BATHONIAN / BAJOCIAN / AALENIAN	CHILTAN		H I A T U S			

Figure 2.1: Stratigraphy of lower Indus Basin (Shah et al., 1977)

2.5   Petroleum System

In the Lower Indus Basin, the dominant petroleum system belongs to Cretaceous sequences. However, varieties of plays have been tested but most exploration success has come from sands of Lower Goru Formation, within "classic" up thrown traps.

6

The detachment of Indian Plate from the African Plate in the southern latitudes due to rifting initiated during Middle-Late Jurassic and continued till the close of the Cretaceous, resulting in the development of tilted fault blocks in the Lower Indus Basin. Tilted fault type traps (horsts and grabens) are productive within and immediately, S, E, NE, and SE of the block.

Hydrocarbon discoveries from several exploration wells within Lower Goru Formation inside Gambat South block and the discoveries in Hala, Khipro and Mirpurkhas blocks confirmed the viability of good reservoir quality in Lower Goru (Basal & Massive Sand units) of Lower Goru Formation (Raza et al., 1989).

2.5.1 Source Rock

Primary source rock in the area is Sembar Formation, a product of marine-deltaic deposition of late Jurassic / early Cretaceous age. It has been documented as a mature source rock in most of the areas in the Central and Southern Indus Basin. In the Late Cretaceous the hydrocarbons started generating and migrating and at some places it is still happening.

Presence of hydrocarbon gas/gas-condensate discoveries inside Gambat South block confirms the presence of active and mature hydrocarbon generating source rocks. Besides Sembar formation, Intra-formational shales of Lower Goru Formation especially Talhar Shale is also considered as effective potential source rock as proved from the geochemical analysis of well data of nearby wells located in adjacent blocks (Kazmi and Jan, 1977).

2.5.2 Reservoir Rock

The main reservoirs in the southern part of Lower Indus Basin are the stacked deltaic–marine shore face Lower Goru Sands of Early Cretaceous age. Basal Sand and Massive Sand of Lower Goru Formation separated by Talhar Shale & deeper Sembar Sands are the primary reservoir targets in the block. Goru Formation is a practical example of sand and shale layers with unique properties (Shah et al., 1977).

2.5.3 Seal Rock

The ultimate sealing rock is the Late Cretaceous shale/marl of Upper Goru Formation which is the regional top seal over the Lower Goru Sand reservoirs. The thickness of the Upper Goru Shales/marl varies from 350 to 1,200m based on the surrounded wells. The interbedded shales i.e. lower shale acts as a top seal for Basal sand and Talhar shale acts as top seal for Massive sand (Shah et al., 1977).

Shales of Sembar Formation and at lower section of Lower Goru Massive Sand are considered as top seal for deeper Sembar Sand

7

2.5.4 Trap

Oil and gas in Lower Goru sandstone trapped in tilted fault blocks resulted during Cretaceous rifting and sourced from Sembar and intra-formation shales of Goru Formation and sealed by shales of Upper Goru Formation. Horst and Graben structures are formed because of normal faulting where structural highs serve as repository for hydrocarbons and the associated faults may serve as migration conduits (Shah et al., 1977).

3. Seismic Interpretation and Petrophysical Analysis

The science of concluding the geology at some depth from the seismic record is seismic interpretation. While advance diverse channel data have increased the quality and quantity of interpretable data, the interpreters must have a geological understanding for a good interpretation so that they could pick the most probable interpretation from the various "logical" interpretations that the data allow (Robinson and Coruh, 1988).

There are two basic elements in the seismic record that are studied by the interpreter. The first is the time of the reflected or refracted ray coming back from a geological surface. The function of the thickness and velocity of layers of rocks is the accurate depth to that geological surface. The second is the shape of the reflection that shows the strength of the signal either its weak or strong, kind of frequencies it contains and their distribution over the entire pulse. This information can generally be used to assists conclusions about the fluid capacity of the seismic reflector being checked and the lithology (Telford et al., 1990).

The interpretation method can be partitioned into three comparable categories: lithologic, structural, and stratigraphic. Lithologic interpretation is intended at discovering changes in porosity, pore fluid, fracture intensity, lithology much more from seismic data. In the lithologic interpretation process employed elements are direct hydrocarbon indicators (DHI, HCIs, dim-outs or bright spots) (Robinson and Coruh, 1988).

Structural seismic interpretation is aimed toward the development of structural maps of the subsurface from the detected three-dimensional composition of arrival times. Stratigraphic interpretation describes the order of reflections watched to a model of periodic events of deposition. The main objective is to establish a chronostratigraphic frame of periodic, genetically related strata (Dobrin, 1988).

Seismic interpretation needs best possible seismic to well tie for effective results. Hence, synthetic seismograms must be accurate enough for a better comparison. It is highly based on the quality of data as well as generation or extraction of source wavelet from seismic data. In the present case, wavelets are not stable i.e. varying in amplitude and phase for each well location. Hence, an average wavelet is established to obtain best possible results.
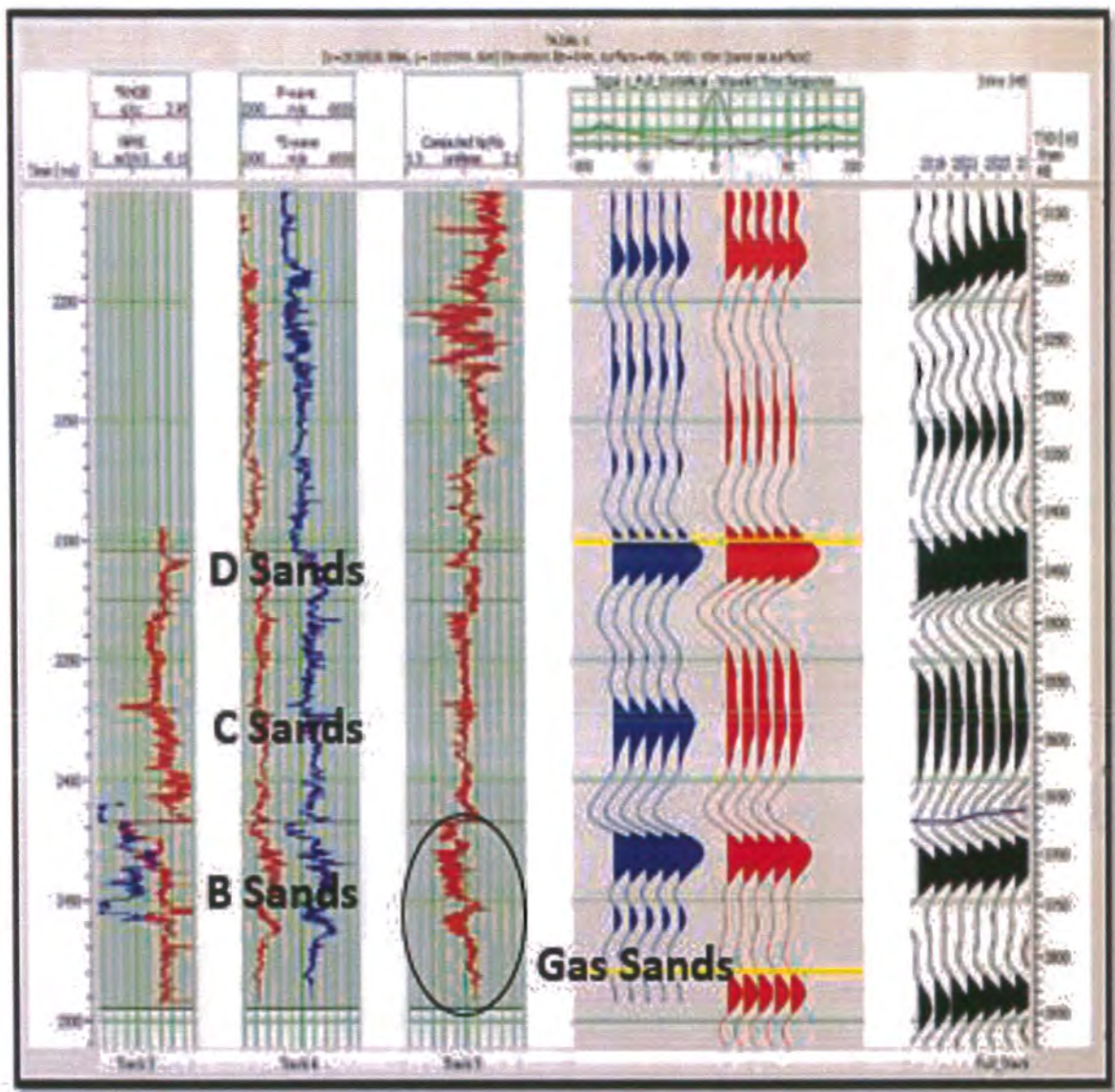
Synthetic seismogram of each well is shown as:

Figure 3.1: Synthetic seismogram of Tajjal_01 showing synthetic data calculated using V_P and V_S

Synthetic Seismogram shown above is generated by product of density log and sonic log. As well data contains both P-wave and S-wave velocity logs therefore two synthetics are shown. Blue one is generated using P-wave velocities while red one is generated using S-wave velocities. Black one is the original seismic data and it can be seen clearly that synthetic data is strongly correlating with original data. Extracted wavelet from seismic data is shown as well which is zero phased. In a similar way, synthetics are calculated for other wells.
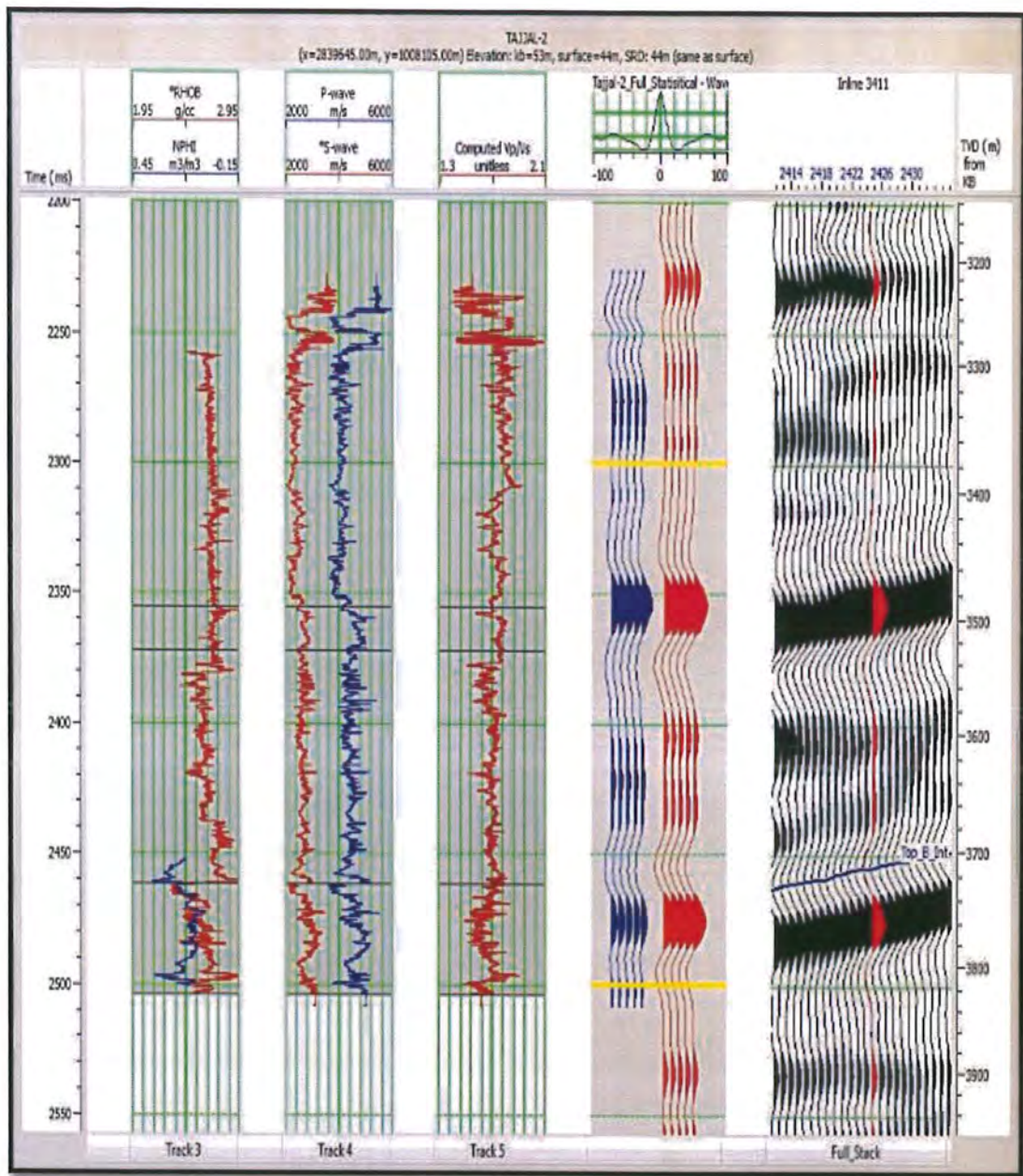
Figure 3.2: Synthetic seismogram of Tajjal_02 showing synthetic data calculated using V_P and V_S

In the above figure, synthetic seismogram is made on the same pattern for Tajjal_02 and synthetic data is correlating with seismic data. The marked zones shown are representing D-Sands, C-Sands and B-Sands. Top of B-Sands is shown on seismic data as well.
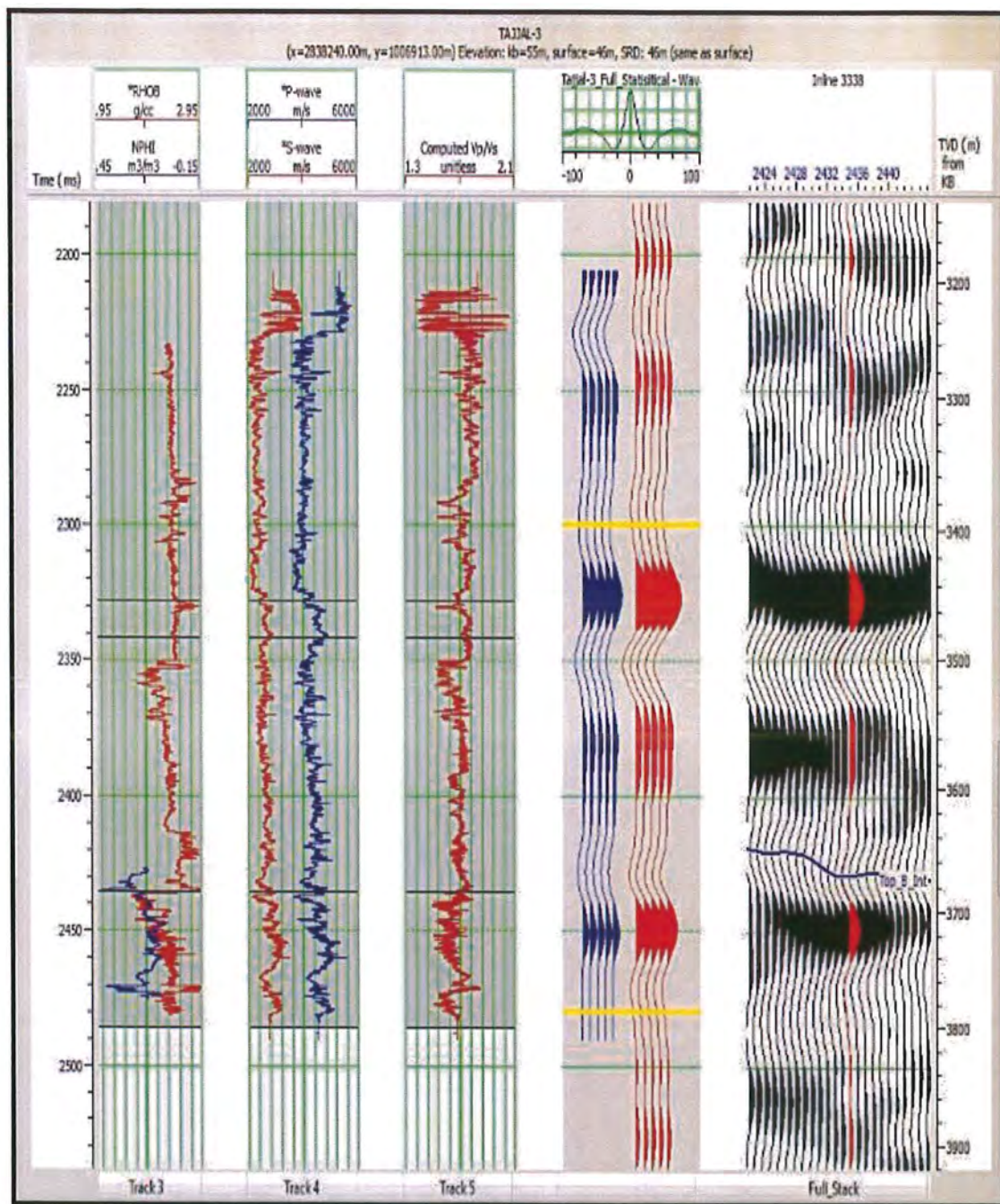
Figure 3.3: Synthetic seismogram of Tajjal_03 showing synthetic data calculated using V_P and V_S

In the above figure, synthetic seismogram is made on the same pattern for Tajjal_03. Top of B-Sands is same on synthetic as well as seismic data.
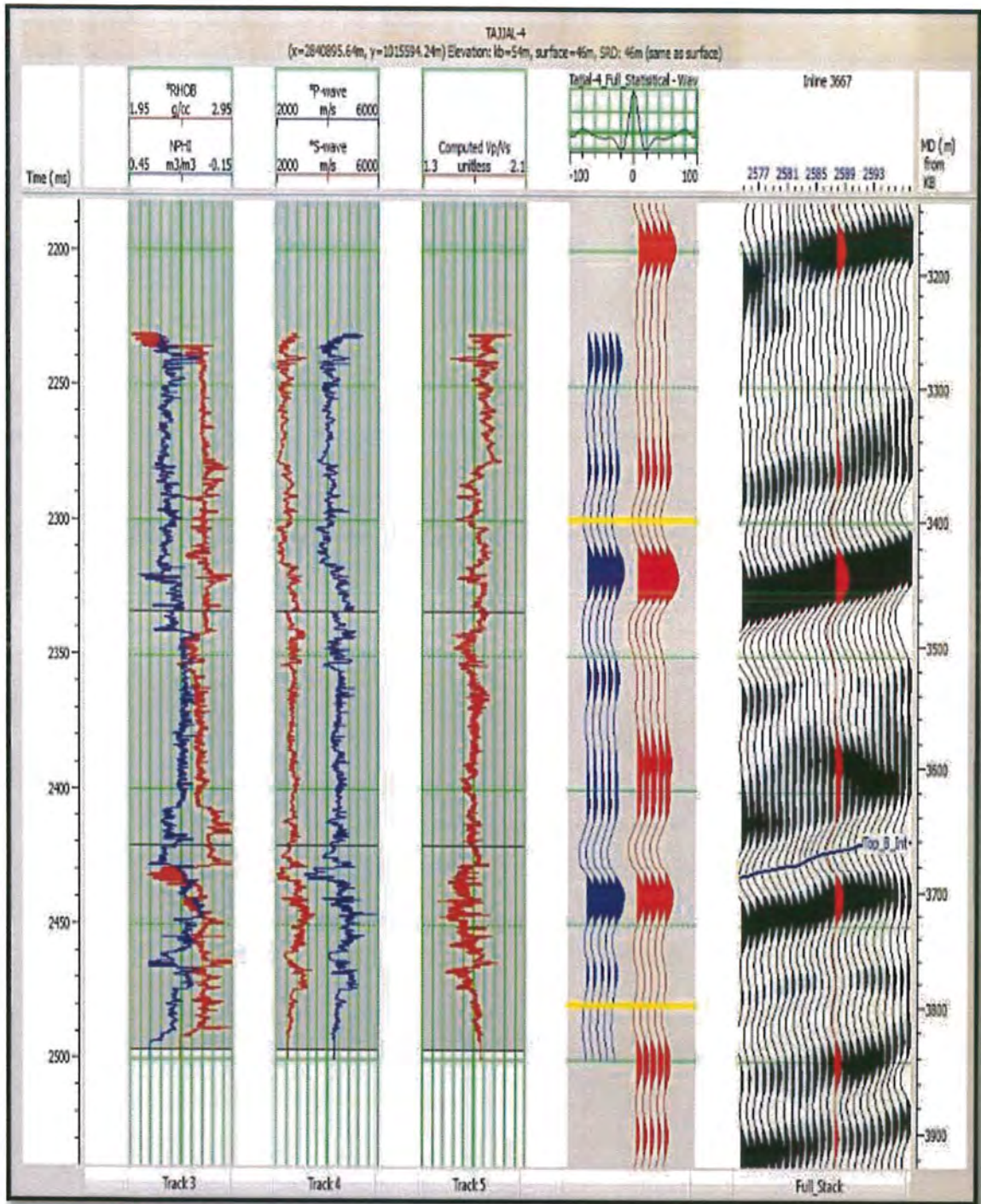
12

Figure 3.4: Synthetic seismogram of Tajjal_04 showing synthetic data calculated using V_P and V_S
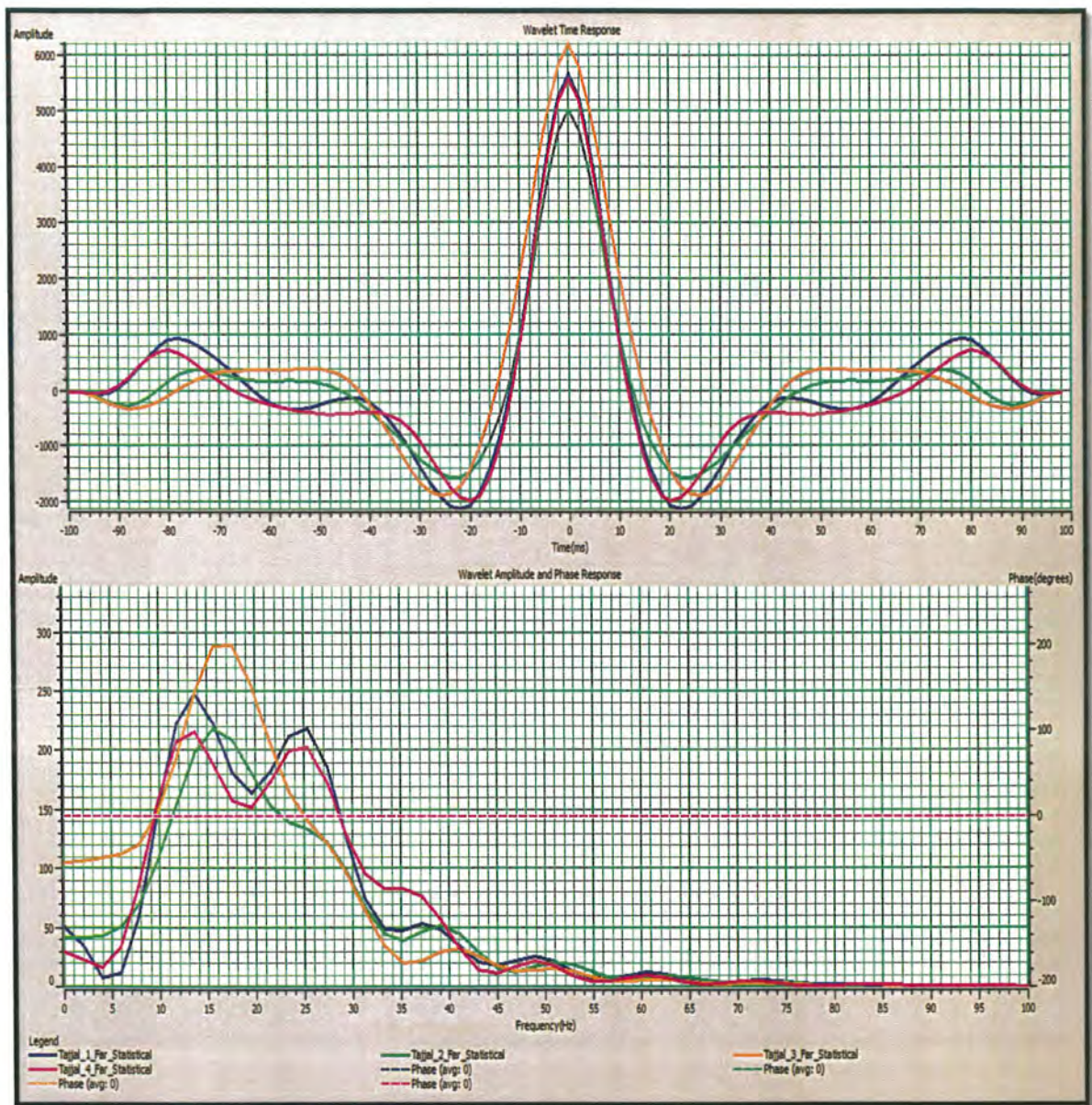
Fig 3.5: Time, amplitude and phase response of wavelets

The above figure shows time, amplitude and phase response of all extracted wavelets. Blue color is used for Tajjal_01, green for Tajjal_02, orange for Tajjal_03 and pink one for Tajjal_04. It can be seen that wavelets are zero phased, having maximum peaks between 5000-6000 amplitude units and frequency range is 0-50 Hz.
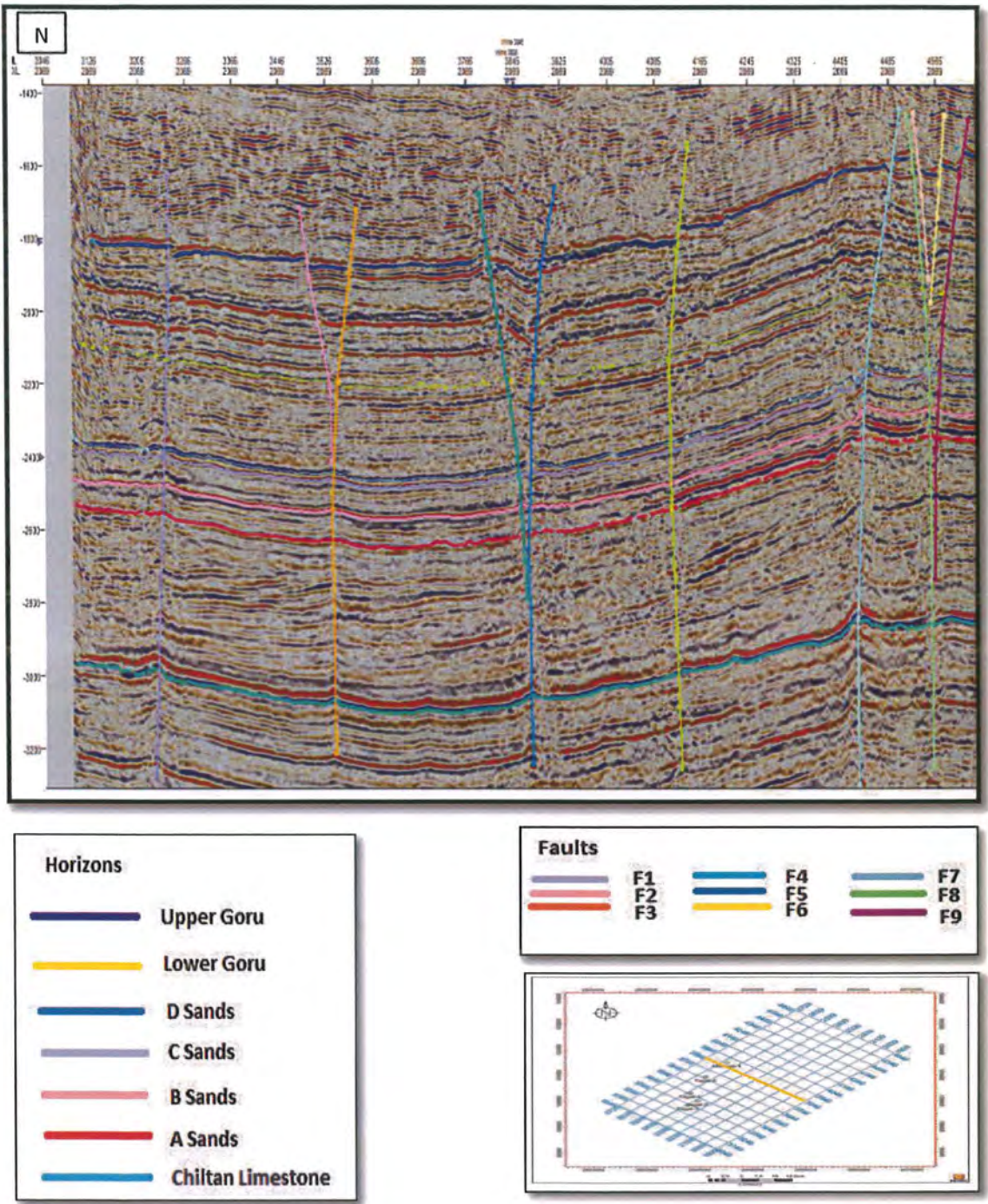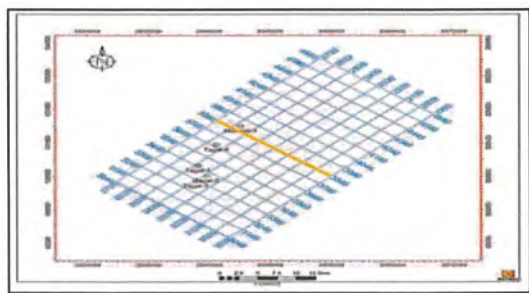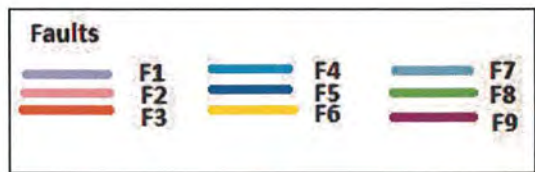
3.1   Seismic Interpretation

Figure 3.6: Seismic inline # 3846 (1)
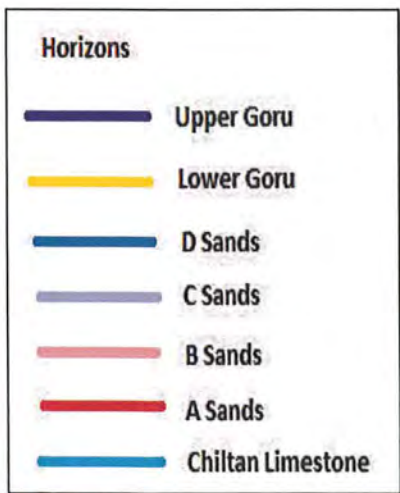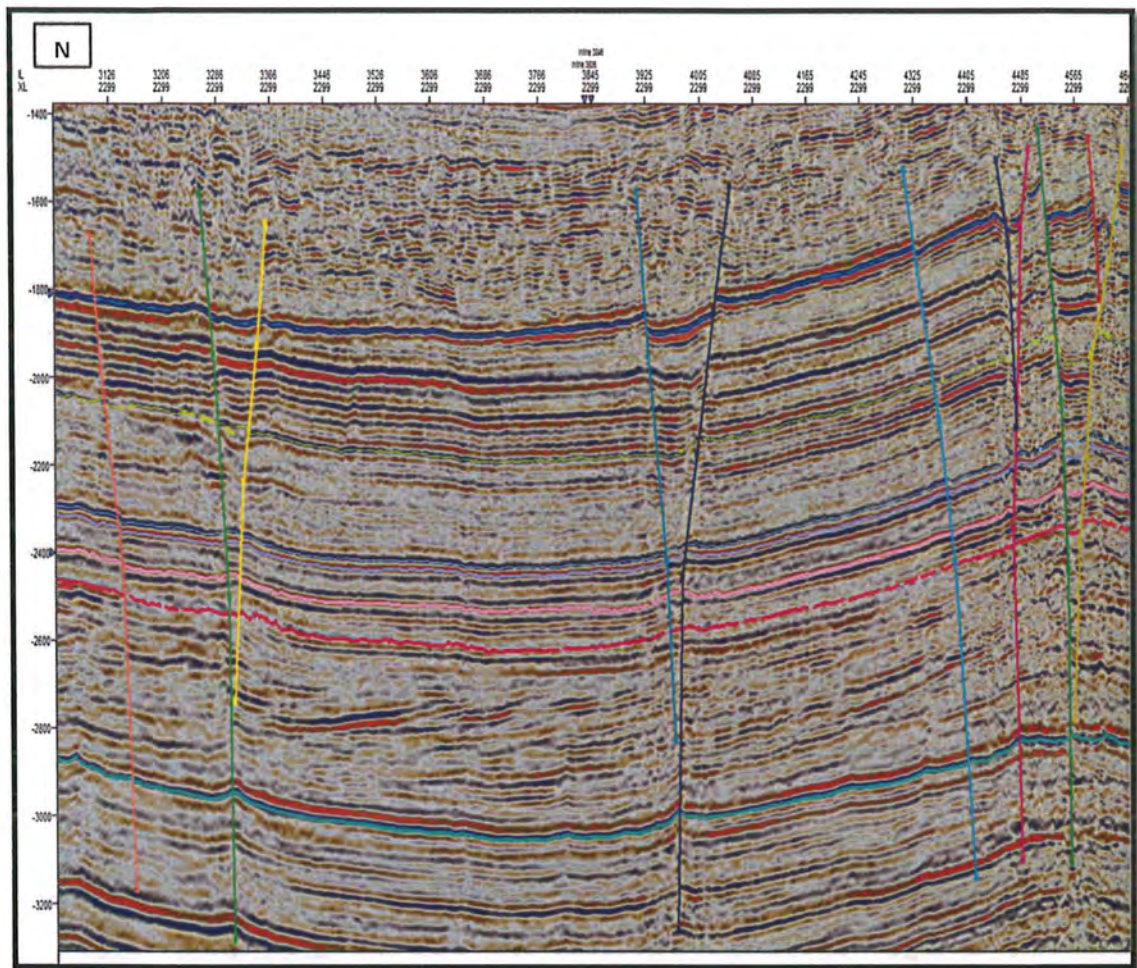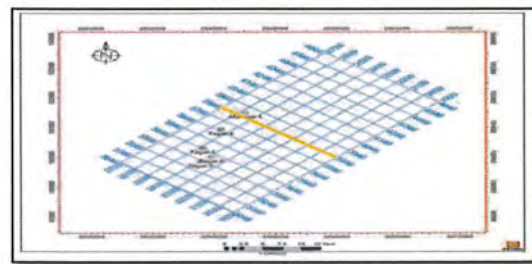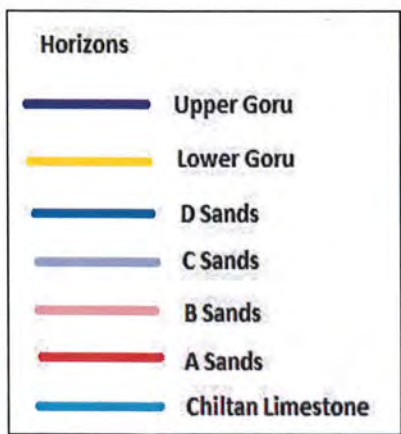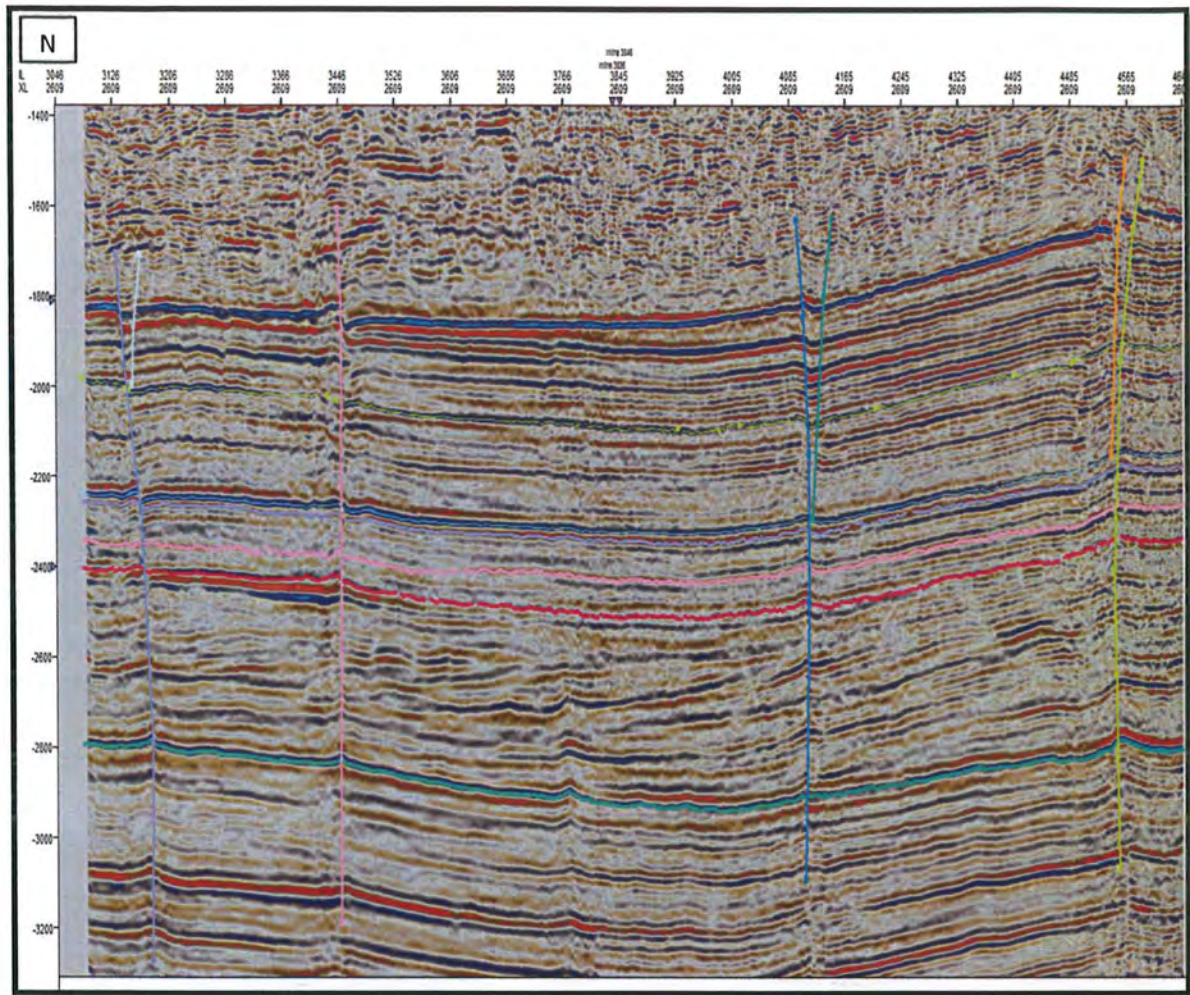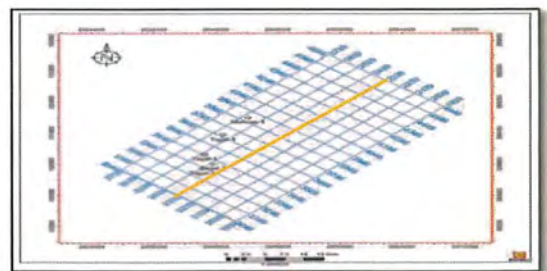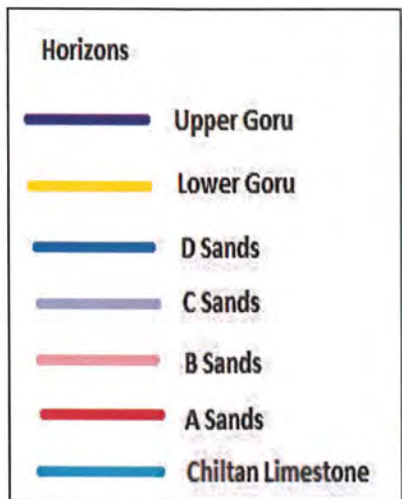
Figure 3.7: Seismic inline # 3846 (2)

Figure 3.8: Seismic inline # 3846 (3)
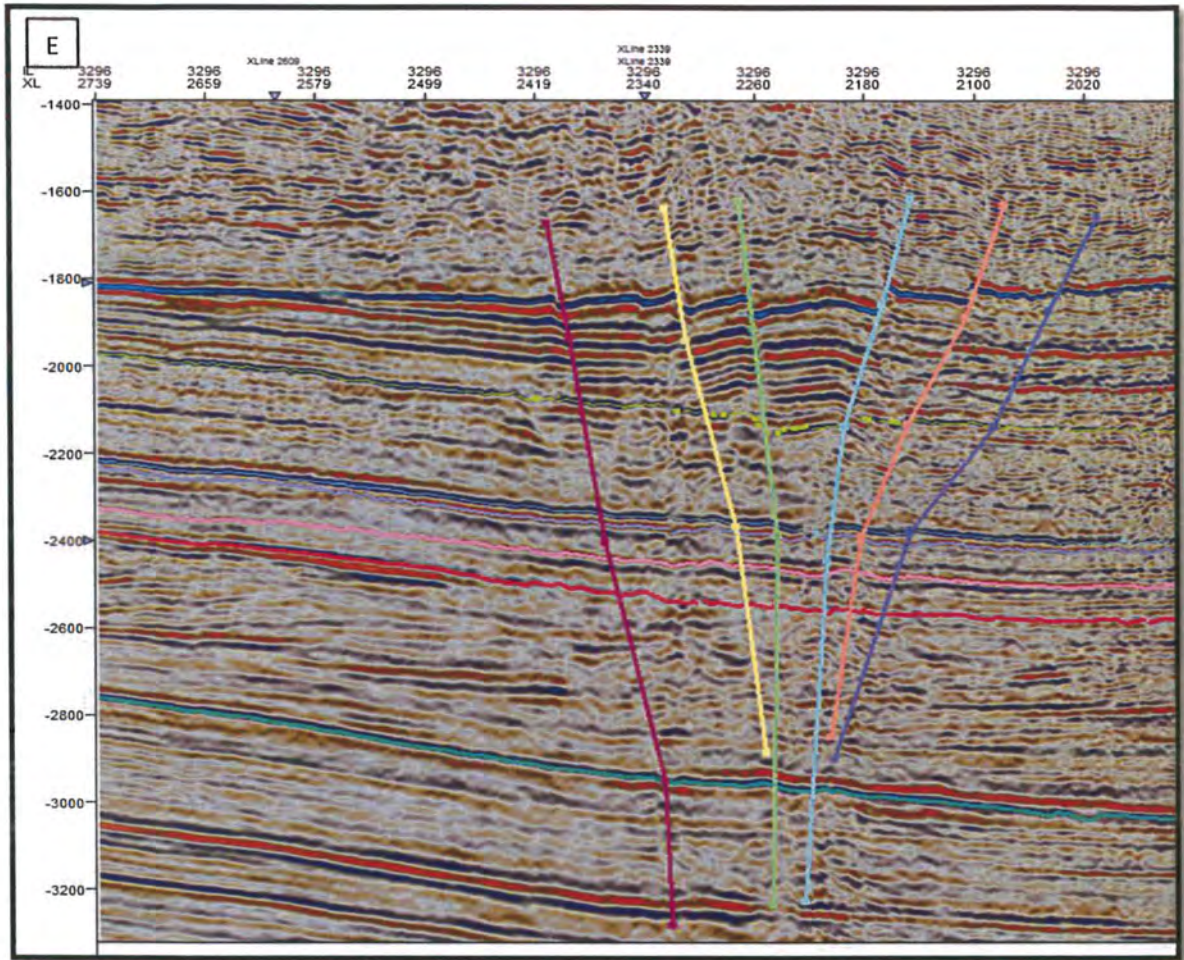
Figure 3.9: Seismic xline # 2339 (1)

Horizons

- Upper Goru
- Lower Goru
- D Sands
- C Sands
- B Sands
- A Sands
- Chiltan Limestone

Faults

F1	F4	F7
F2	F5	F8
F3	F6	F9
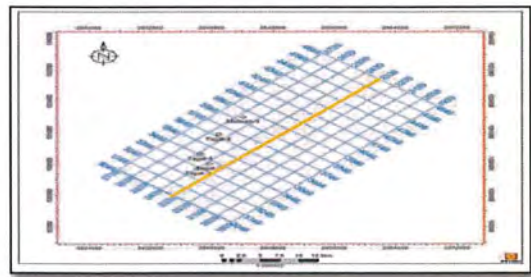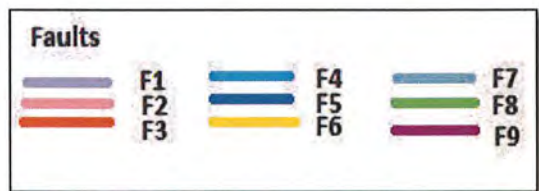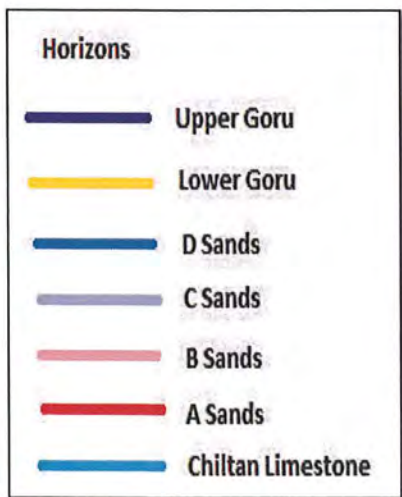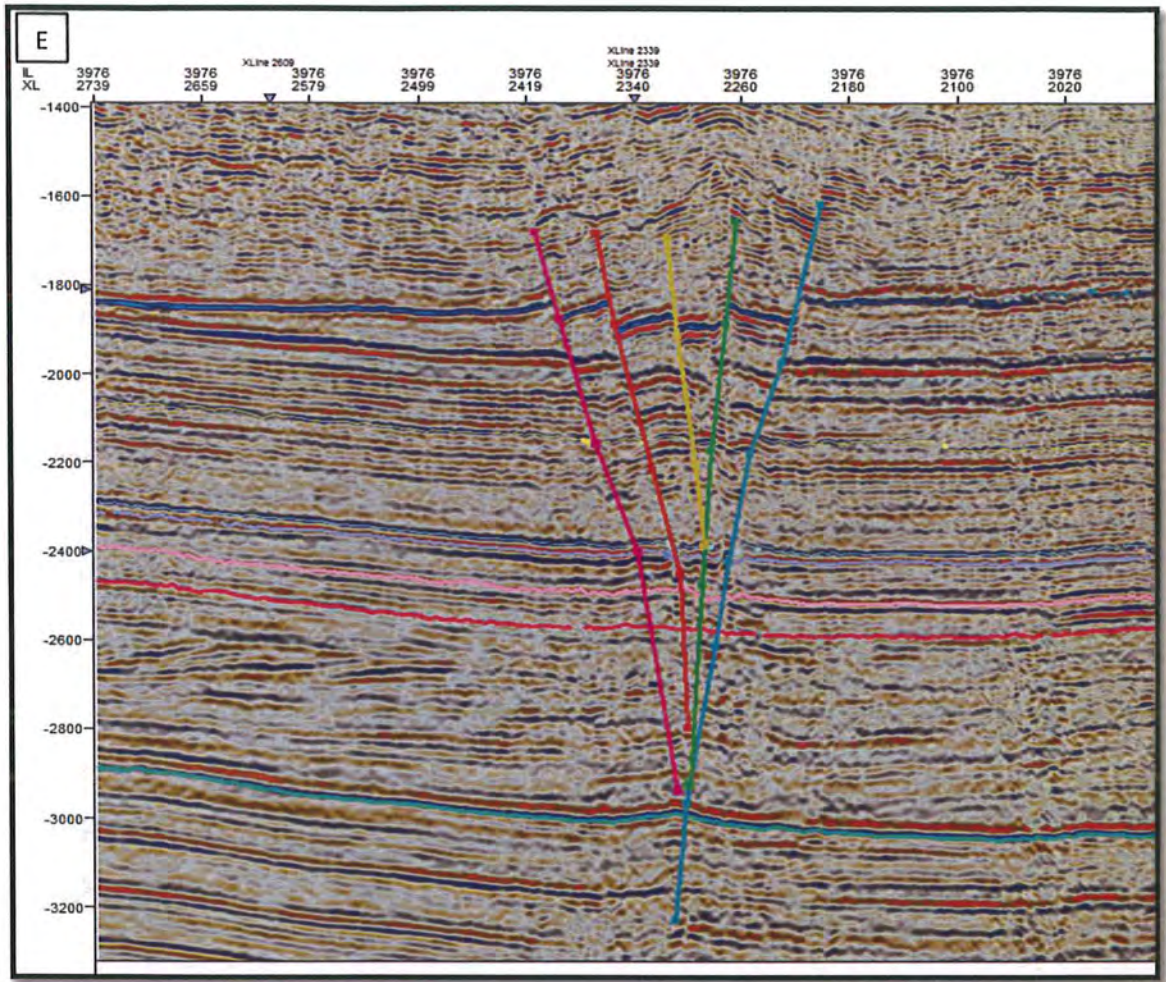
Figure 3.10: Seismic xline # 2339 (2)
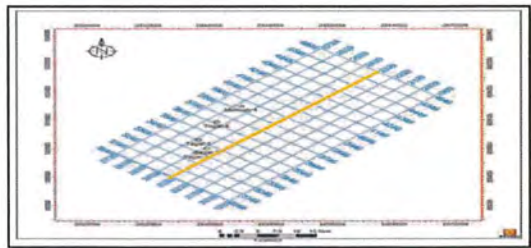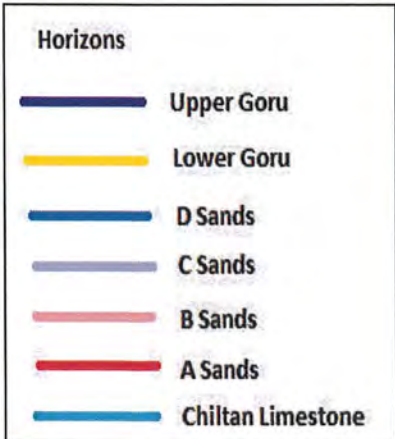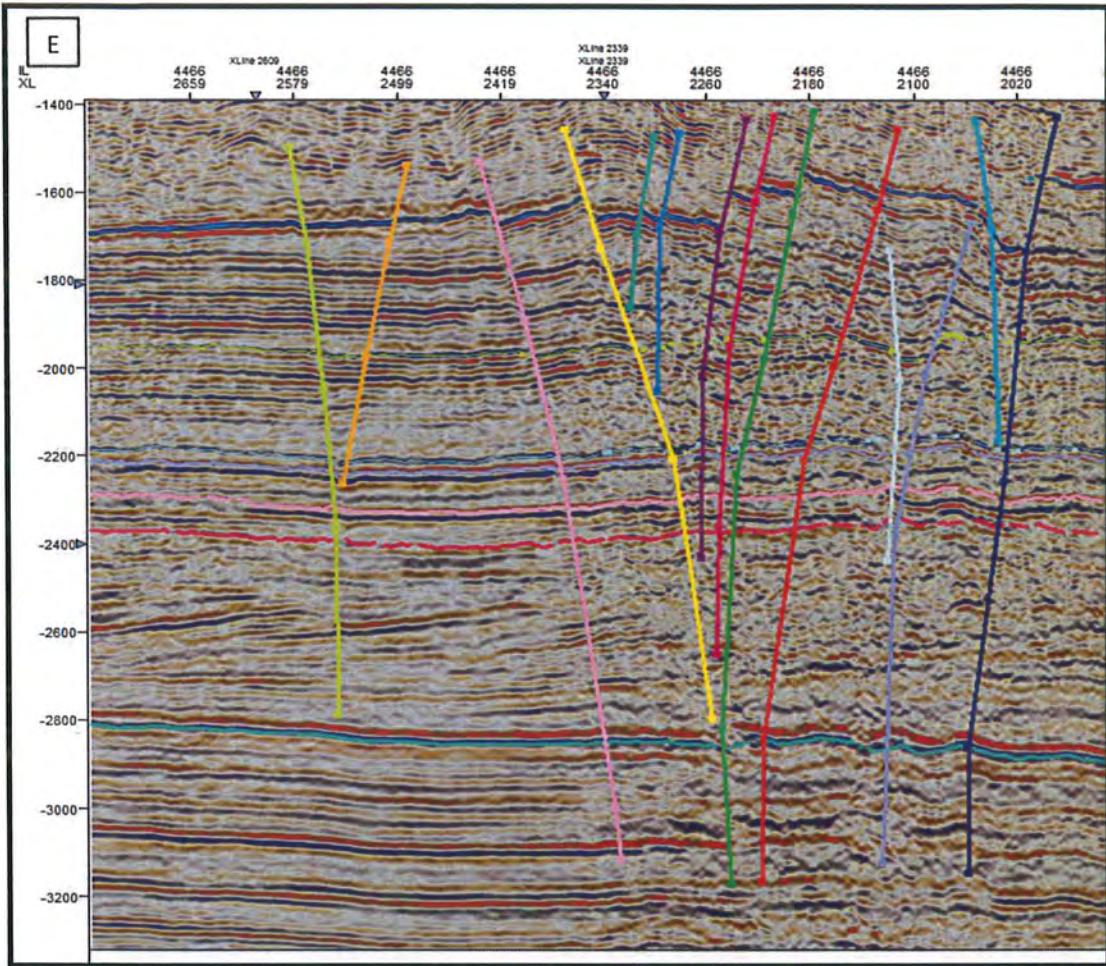
Figure 3.11: Seismic xline # 2339 (3)

Seismic interpretation shows that area is highly subjected to strike slip faulting having NW-SE trend and as a result, flower structures are formed. The faults are deep rooted i.e. extended up to Chiltan Limestone. The target horizon i.e. B-Sands is observed at 2300msec. Time contour map for top of B-Sands is shown as:
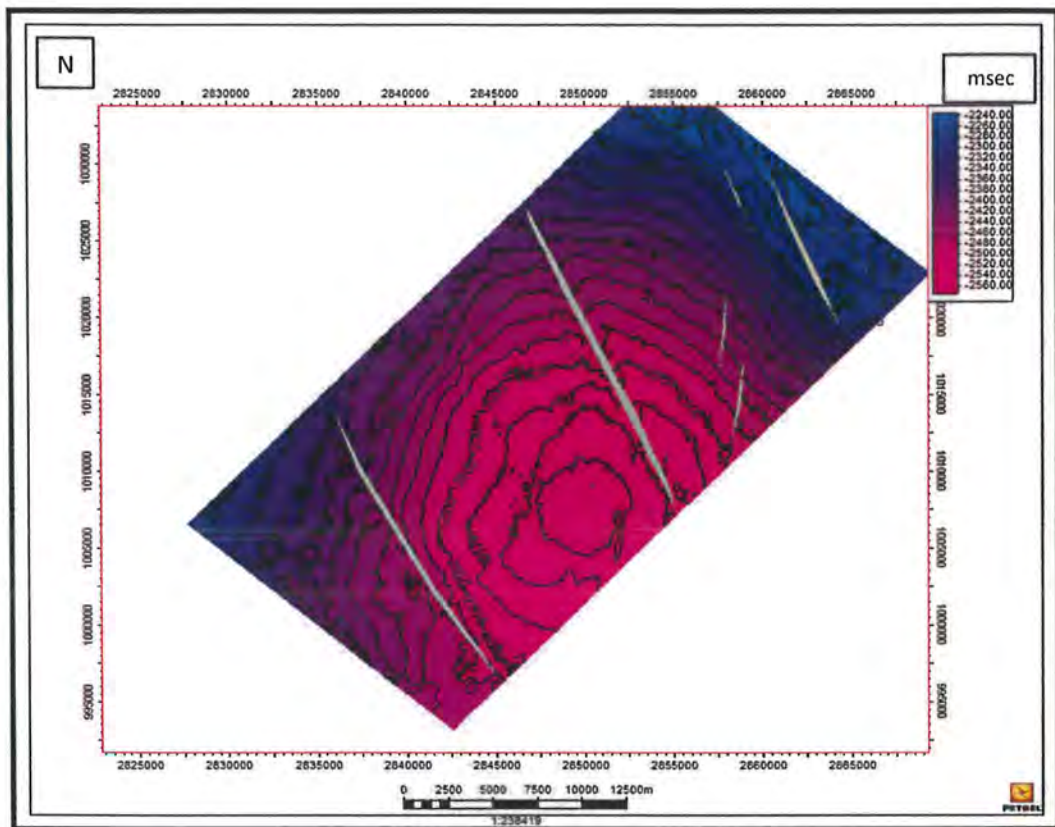
Figure 3.12: Time contour map of B-sands

Time contour map shows that arrival time varies between 2240-2560 msec. The extent of major faults is shown on entire data volume in NE-SW direction. This shows that area is subjected to extensive faulting making en-echelon pattern.

3.2   Petrophysics

The study of the properties of rocks and interaction of rocks with fluids at different conditions is Petrophysics. It also explains about the chemistry of pores of the subsurface and how they are linked and helps in predicting the migration and accumulation of hydrocarbons. While explaining the physical and chemical properties, Petrophysics also explains many other related terms such as lithology, water saturation, density, porosity and permeability (Johansen et al., 2013).

In petroleum survey, the geological model is established and then by drilling it is confirmed, disproved, or altered. The later promotion declarations are placed on the actuality of hydrocarbons within the pores of the reservoir rock under the condition of the downhole.

When a hydrocarbon-carrying formation is cored and the core is brought to surface the characteristics of the fluid in the pores changes. Most of the more effervescent items drip off at the time of surface handling and the decompression process (Johansen et al., 2013).

Hence wireline logging, was established. The science of petrophysics was developed to understand the geological significance of the output from these logs. The objective of petrophysics is to discover, calculation on rock samples, and from measurements in borehole with instruments, the hydraulic conductivity called permeability; the depository volume of the rock called porosity; the fragment of the pore space occupied by hydrocarbons called saturation; and the acoustic velocity (Johansen et al., 2013).

In the study area, well data contains following logs:

1. Gamma Ray Log
2. Resistivity Log (Shallow & Deep)
3. P-Wave Log
4. S-Wave Log
5. Density Log
6. Neutron Porosity Log

The zone of interest is B-Sands of Lower Goru and there is remarkable decrease in velocities at Top B-Sands. In this zone, resistivity values are low due to the presence of conductive minerals and water saturation is 20%. Fluid substitution modelling for gas producing wells i.e. Tajjal_01 and Tajjal_04 is performed at 100% water saturation and results are comparable with other in-situ water saturated wells. The results are shown as:
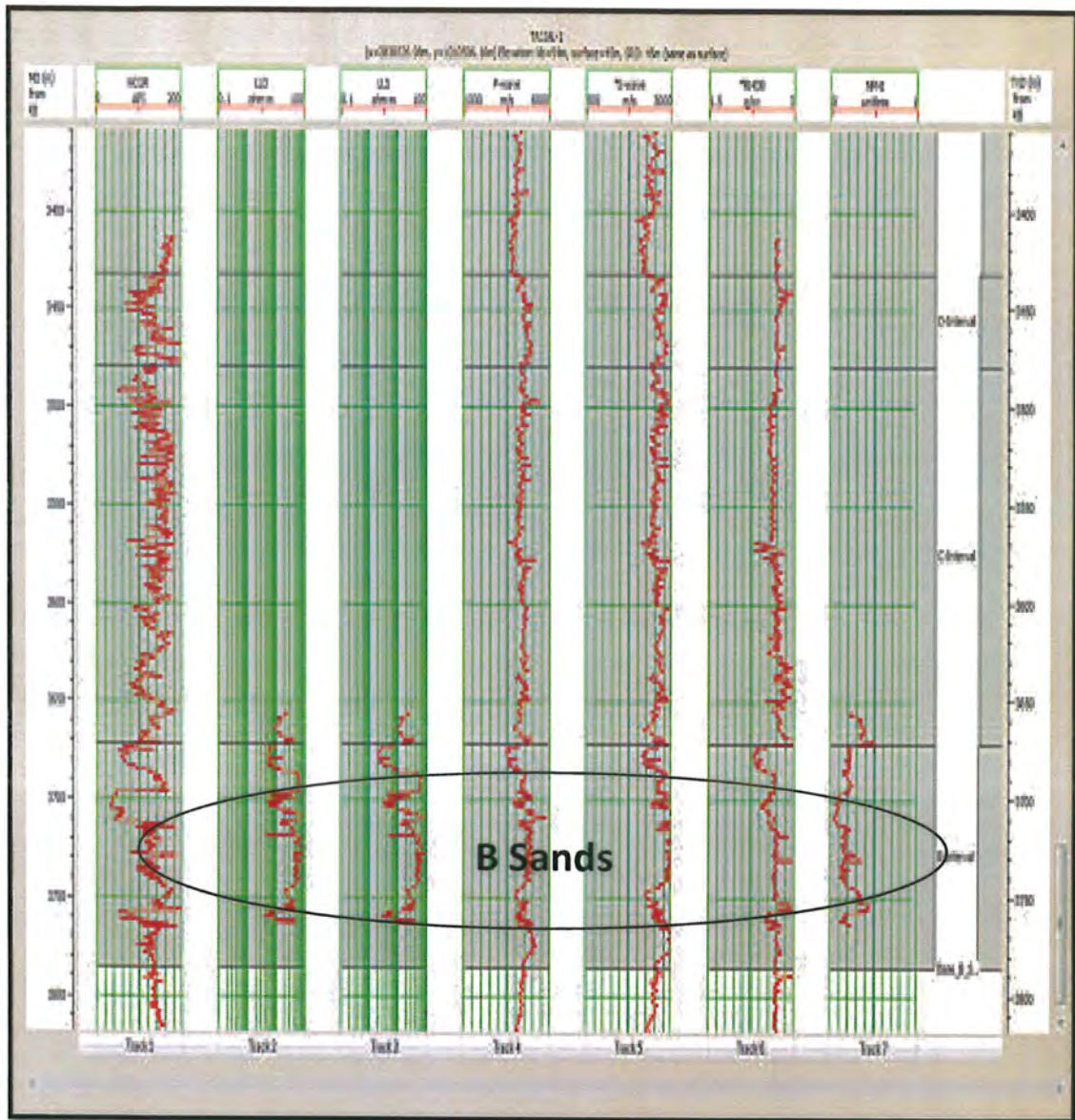
Figure 3.13: Well log data of Tajjal_01 (In-situ Gas)

In the above figure, GR log, resistivity logs, P-wave velocities log, S-wave velocities log, density log and neutron porosity log are shown in track 1, track 2, track 3, track 4, track 5, track 6 and track 7 respectively. There are three marked zones as shown above i.e. D-Sands, C-Sands and B-Sands respectively with measured depth on left scale and total depth on right scale. Among all these logs, resistivity logs and neutron porosity log are shown for B-Sands only.

23
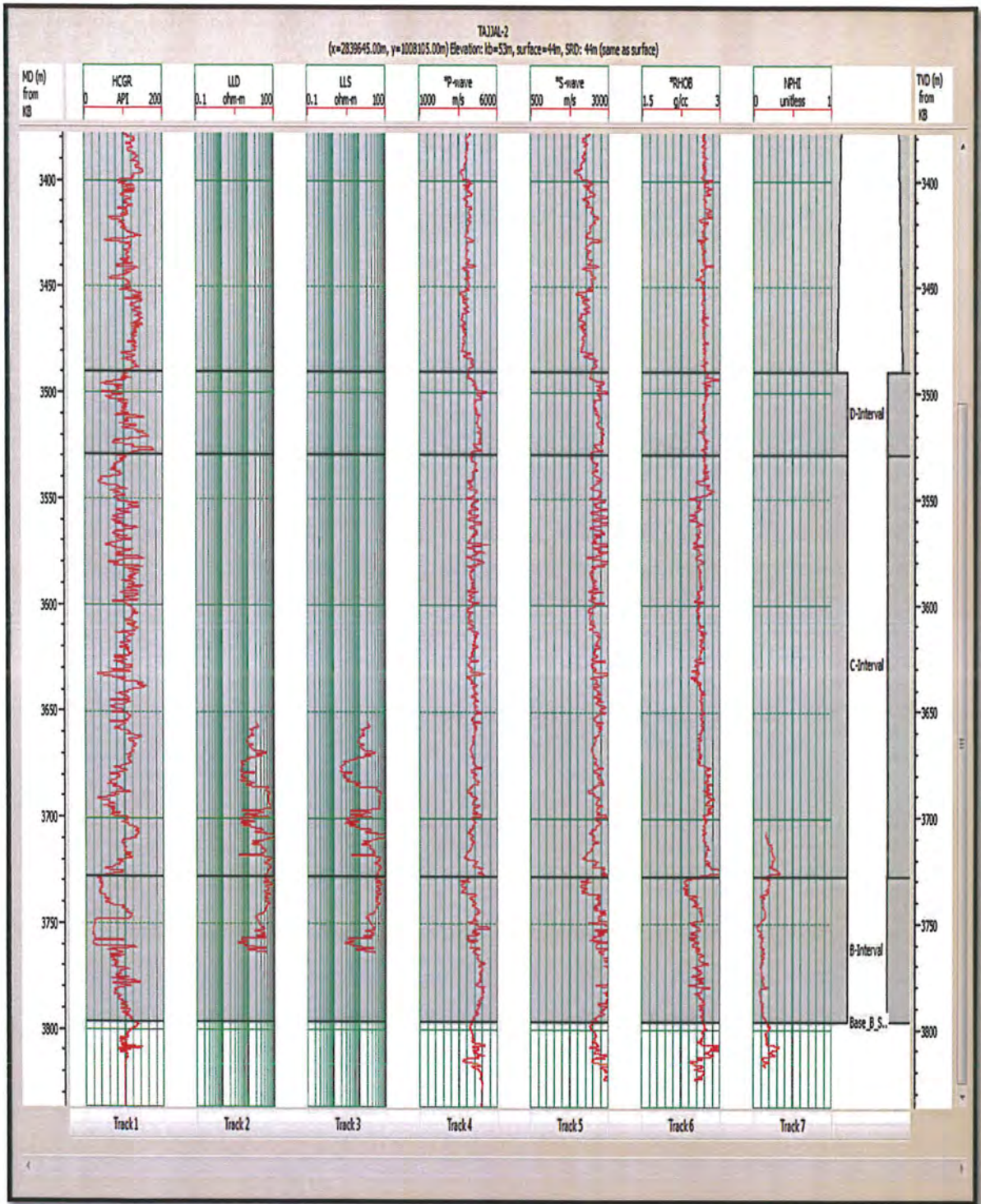
Figure 3.14: Well log data of Tajjal_02 (In-situ Water)
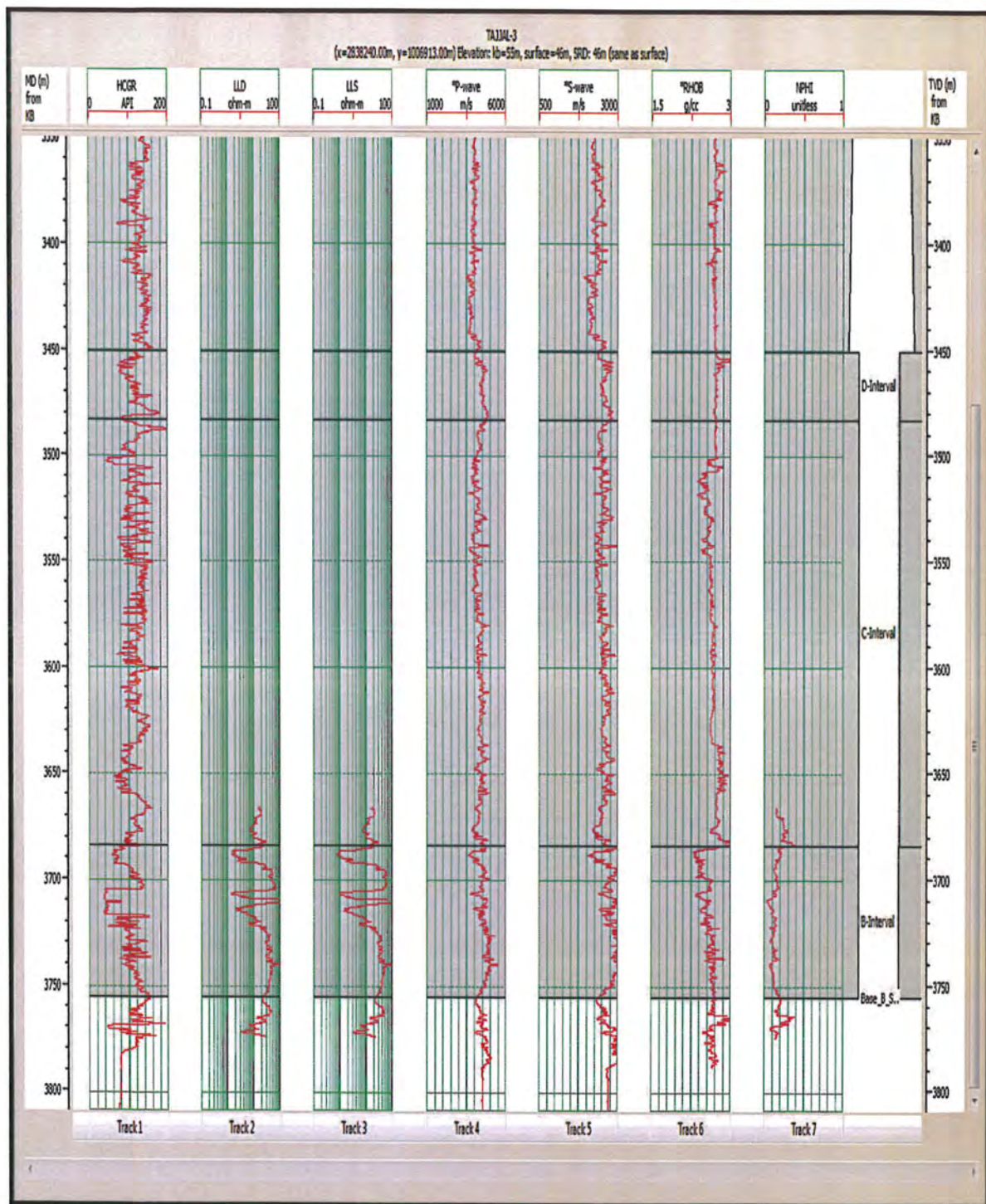
Figure 3.15: Well log data of Tajjal_03 (In-situ Water)
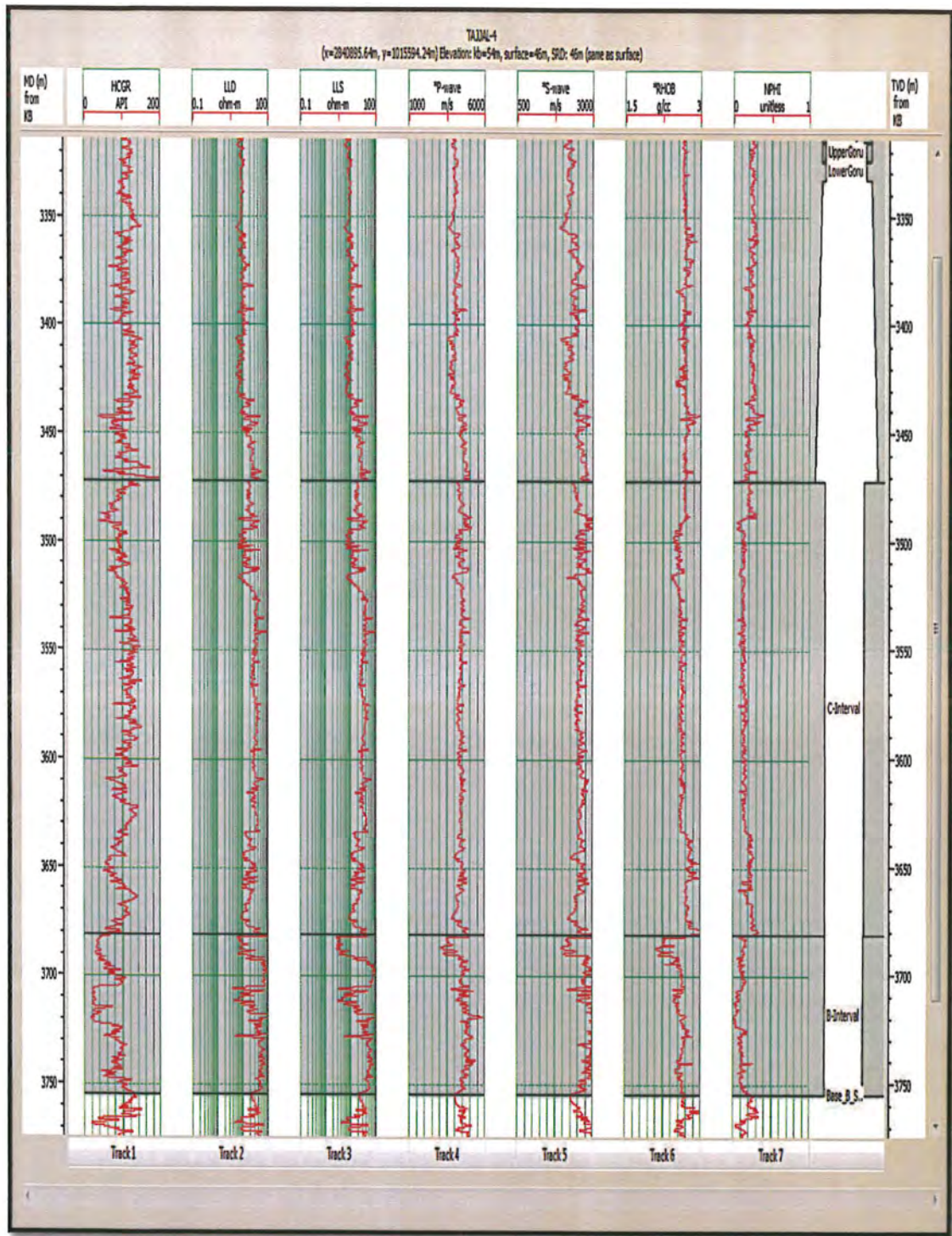
Figure 3.16: Well log data of Tajjal_04 (In-situ Gas)
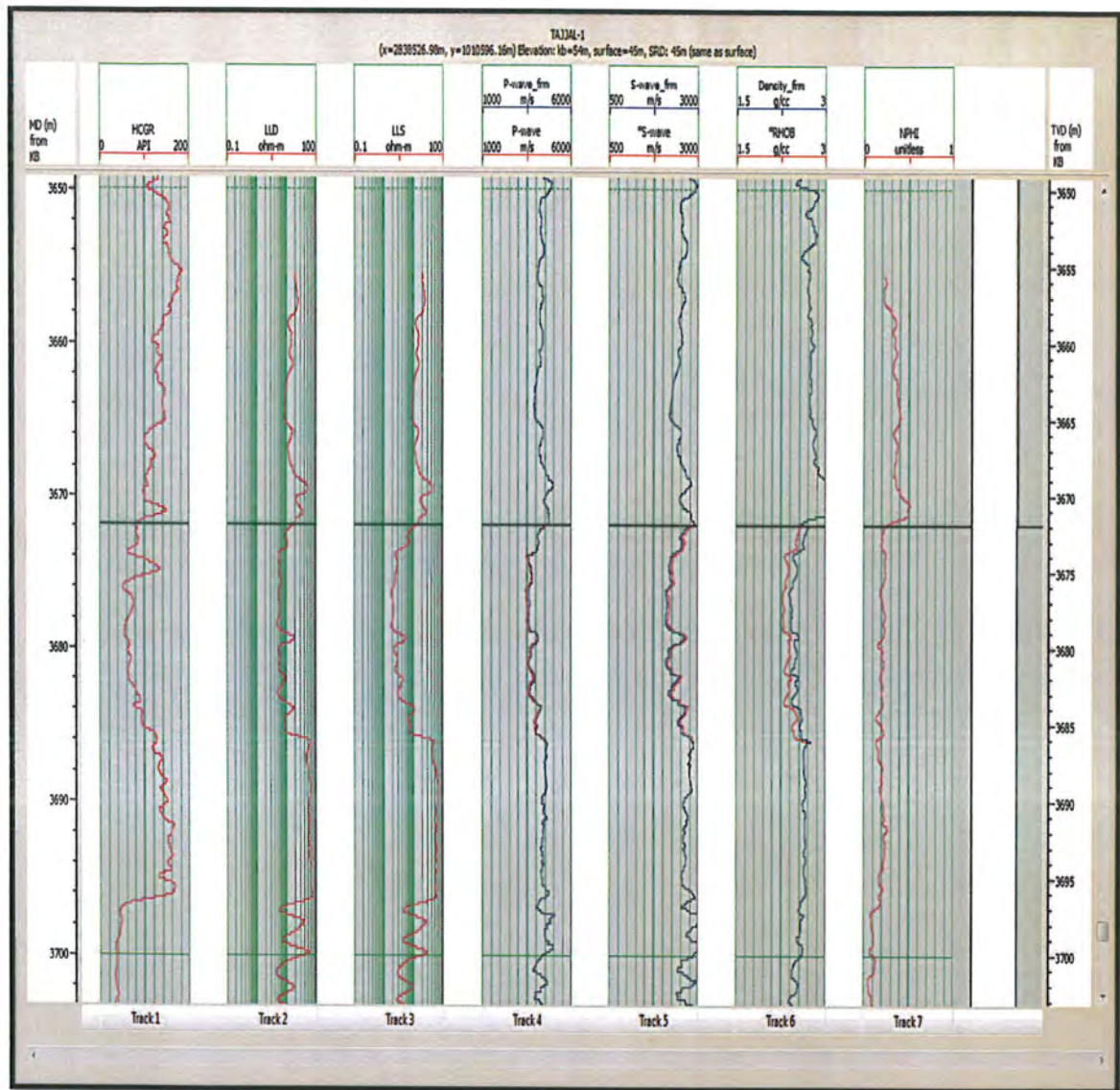
Figure 3.17: Well log analysis of Tajjal_01 (100% water saturation)

In the above figure, P-wave velocities log, S-wave velocities log and density log curves are generated after changing the fluid saturation in B-Sands i.e. water (originally, it is a gas saturated well). Log trend is comparative with Tajjal_02 and Tajjal_03 which are in-situ water saturated wells. It shows that fluid saturation highly effect the reservoir properties such as velocities and densities of the medium.

27
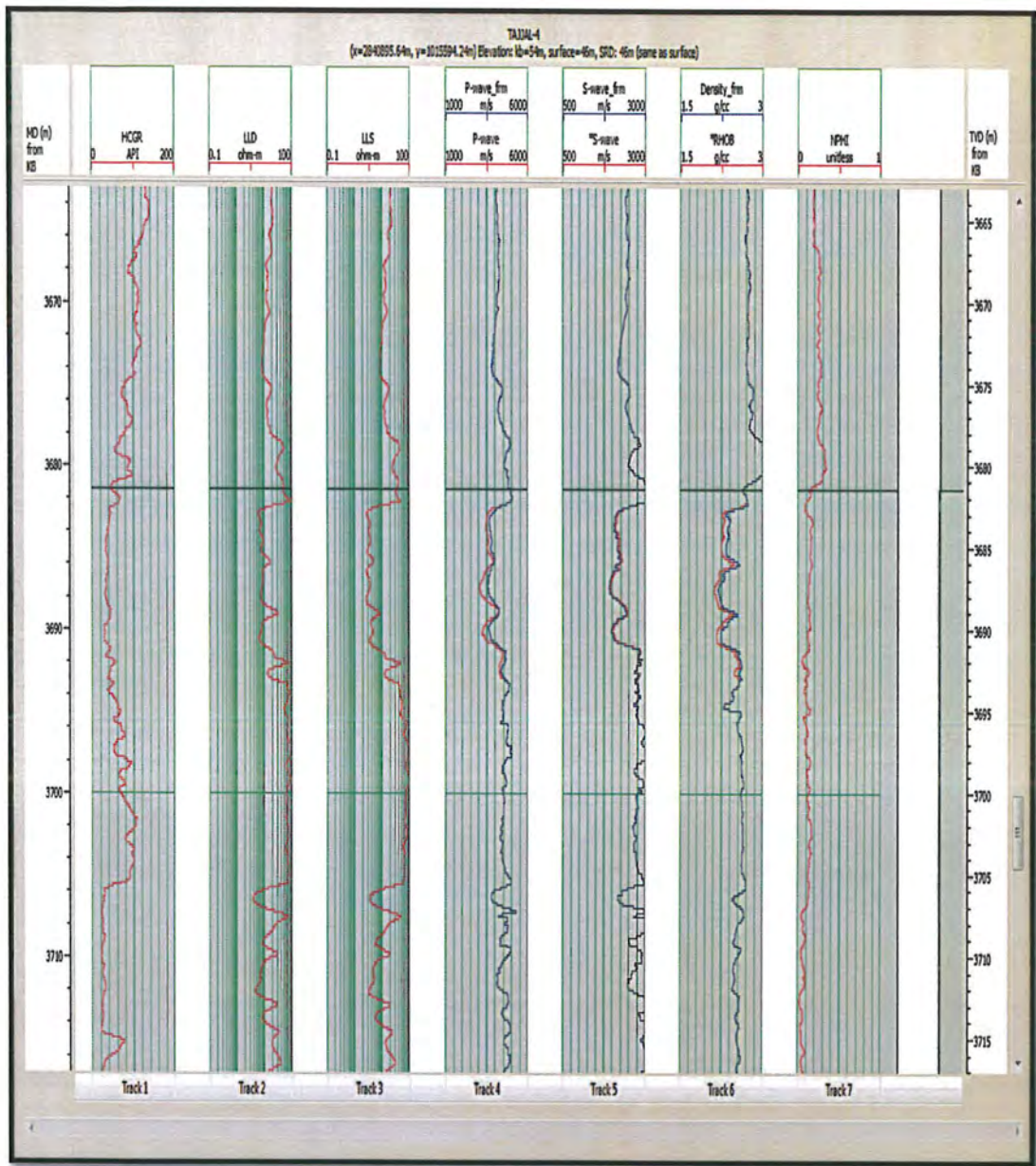
Figure 3.18: Well log analysis of Tajjal_04 (100% water saturation)

Tajjal_04 is also a gas producing well and similar curves are generated as for Tajjal_02 after changing the fluid saturation and similar results are obtained.

4. Rock Physics Analysis

4.1 Introduction

Rock physics modelling set up a relation among the qualitative characteristics of the reservoir (porosity, water saturation, fracture density, etc.) and the quantitative properties (P-Impedance, S-Impedance, etc.). Quantitative seismic interpretation and reservoir characterization are based on these model. Combination of rock physics models and mathematical tools can reduce uncertainty of the data because most of the geophysical measurements are uncertain. Elastic properties can be predicted applying probability theory approach using probability distributions rather than definite values. In such a way analytical solutions of rock physics models can be extracted in which the exact value of input random variable is unknown but its probability distribution is known. The uncertainty in rock physics model prediction can then be quantified by using probability derived approach (Grana, 2014). A great number of different rock physics models are developed to get the link between reservoir and seismic properties and this relevance is constrained by the type of lithology, textural complexity, porosity range, dynamics of the pore fluid and the saturation conditions. As the numbers of rock physics parameters are often higher than the seismic parameters, this is said to be an underdetermined problem with no unique solutions. To evaluate the validity of several models of rock physics for a given set of data modeling procedure can be used. It also provides the most robust data parameter combinations to use for either pore fluid prediction, or porosity, lithology, whenever a specific rock physics model has been selected for the cause (Grana, 2014).

4.2 Rock Physics Modelling

Gassmann's equation, a rock physics model is used to observe the effect of varying fluid saturation on seismic properties i.e. V_P and V_S. S-wave velocities can be predicted through P-waves by varying fluid saturation in the reservoir.

Gasman's (1951) equations are mostly used to determine changes in velocity coming from distinct fluid saturated pores. Nevertheless, the input parameters are frequently roughly predicted, and the resulting guess of fluid effects can be unreal. In rocks, features like density, porosity, and velocity are not liberated, and values should be conserved constrained and consistent. In the analysis of direct hydrocarbon indicators (DHI), such as amplitude bright spots time-lapse reservoir monitoring and amplitude variation with offset (AVO) these equations are noticeable (Grana, 2014).

29

Important feature of these equations is not being comprehensively checked despite the popularity of Gassmann's equations and their usage for seismic reservoir interpretation in most software packages. For common reservoir rocks and fluids most of the basic assumptions are invalid. In Gasman's equation, the full implications of parameter interactions are not well apprehending in the first place so, no compulsions are kept on input parameters and there is no cross check of the results. Problems arise in automated analysis in which results are commonly taken at nominal value exclusively.

4.3   Gassmann`s Equation

For determining the effect of fluid-saturation on bulk modulus a simple model is provided by the Gasman's equations. The equation used is given as;

$$K_s = K_d + \Delta\, K_d \qquad (4.1)$$

$$\Delta K_d = \frac{K_o\left(1 - {K_d}/{K_o}\right)^2}{1 - \emptyset - {K_d}/{K_o} + \emptyset * {K_o}/{K_f}} \qquad (4.2)$$

$$\mu_s = \mu_d \qquad (4.3)$$

In this set of equations, K_o is the bulk moduli of the mineral grain, K_f is for fluid, K_d for the dry rock and K_s is the bulk moduli for the saturated rock frame, φ is porosity and μ_s and μ_d are the shear moduli of saturated and dry-rock respectively. ΔK_d is an accession of bulk modulus because of dry rocks fluid saturation. These equations show that the pores containing fluid will affect bulk modulus but not shear modulus.

4.3.1   Assumptions
The equation is based on the following assumptions:

1. The material is elastic, isotropic, monomineralic and similar.
2. In pressure equilibrium, the pore spaces are connected.
3. There is no pore fluid movement across the boundaries, hence the medium is close spaced.
4. Shear Modulus remains constant.
5. Frequency Effects are negligible.

4.4   Effect of Fluid Saturation on Seismic Properties

The seismic reaction of geological events is straight guarded by shear (S-wave) and compression (P-wave) velocities Vs and V_P respectively together with densities. Dry and water-saturated S-wave and P-wave velocities of sandstone are a function of distinctive pressure. P-wave velocity boosts hardly with water saturation, whereas S-wave velocity on a small-scale decline. Because of the pairing between S- and P-waves by way of the bulk density and shear modulus, both P and S wave velocity is the excellent signal of any fluid saturation influence (Han and Batzle, 2004).

To water saturation Bulk modulus is more sensitive so, bulk-volume distortion is generated by a passing seismic wave causes a pressure increase in pore fluid (water) and results in a pore-volume change. Stiffens of the rock frame increases due to this pressure and creates a raise in bulk modulus. Shear distortion does not bring out a pore-volume change, and thus distinct fluids do not influence shear modulus. Thus, any effect on fluid-saturation must be correlated to a bulk modulus change. (Han and Batzle, 2004).

In the study area, gas producing wells are Tajjal-1 and Tajjal-4 while Tajjal-2 and Tajjal-3 are abandoned wells. Gassmann's Equation is applied to compare the effect of gas saturated and water saturated wells.

The results are compared by cross plotting V_P against Vs under different conditions. The results are shown as;

31
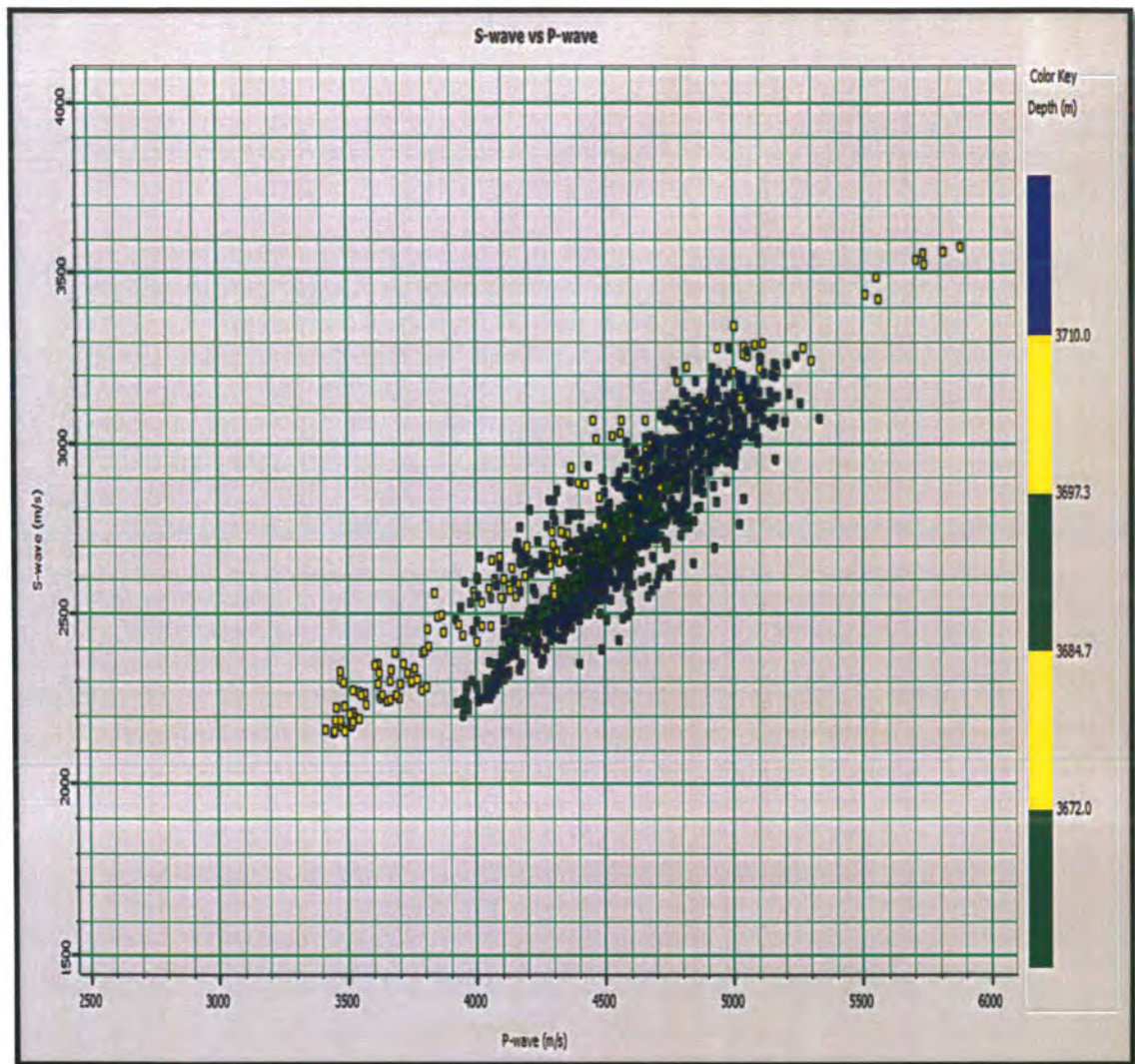
Figure 4.1: V_P/V_S cross plot of Tajjal-01 (In-situ Gas)

In the above figure, P-wave velocities are plotted against the S-wave velocities at a specific depth interval i.e. 3600 to 3750 meters. Well data is used for this purpose and data trend is observed for different zones. Generally, there is a strong positive relation between two parameters. Rock physics modelling is applied at short interval of almost 12 meters i.e. 3672 to 3684 meters. In the present case, data values are comparatively scattered away from general trend as shown with yellow points. The zone is gas saturated and hence, velocity values are highly effected.
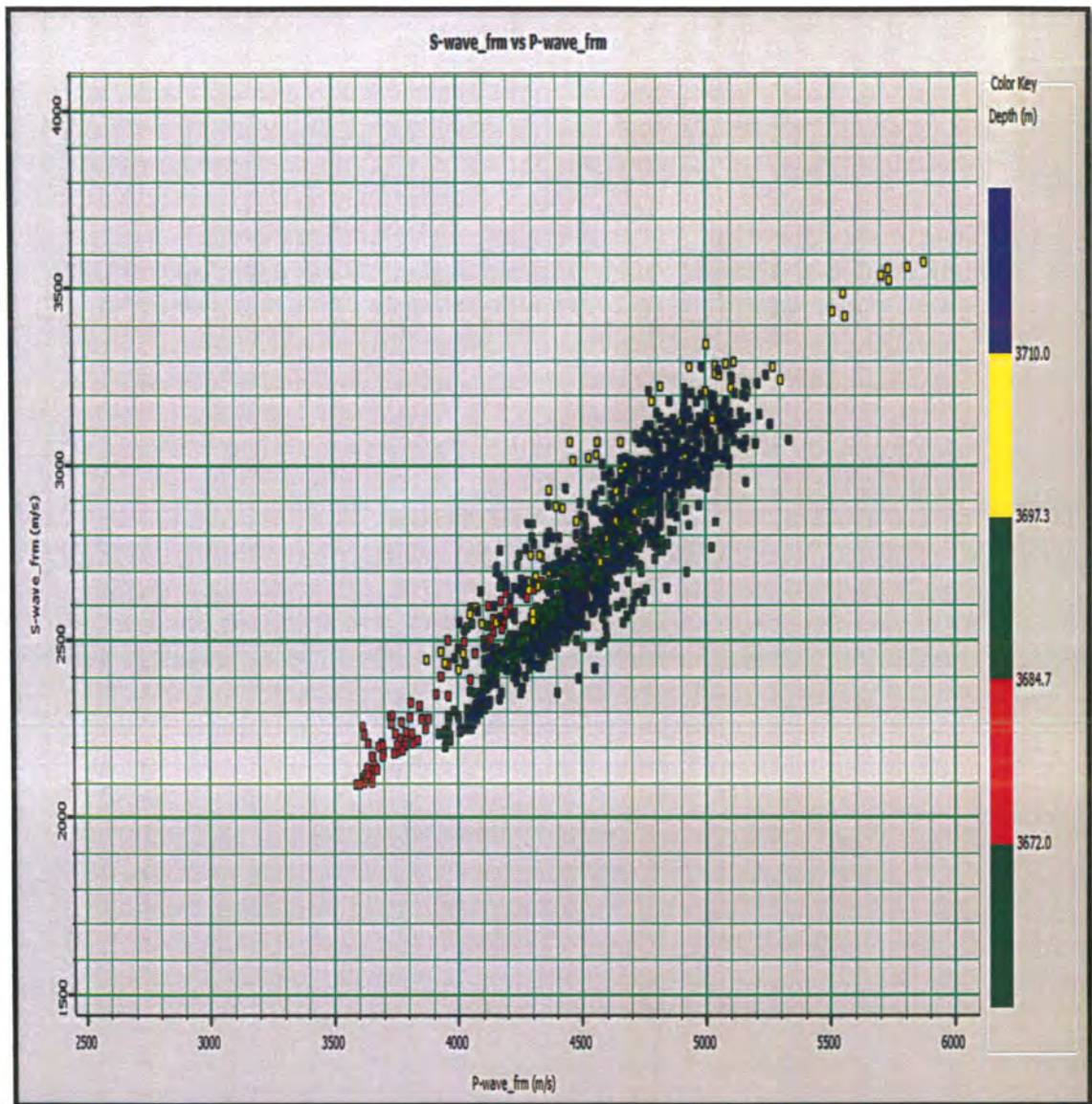
Figure 4.2: V_P/V_S cross plot of Tajjal-01 (100% Water)

In the above figure, Gassmann's Equation is applied at that specific 12 meters interval and fluid saturation is changed from gas to brine. V_P saturated is plotted against V_S saturated and results show that velocities are related in a similar way but data pattern (3672 to 3684 meters) which was originally scattered, is almost following the same pattern as shown by red points. It implies that rock physics modelling can help to predict reservoir behaviour in an accurate way.
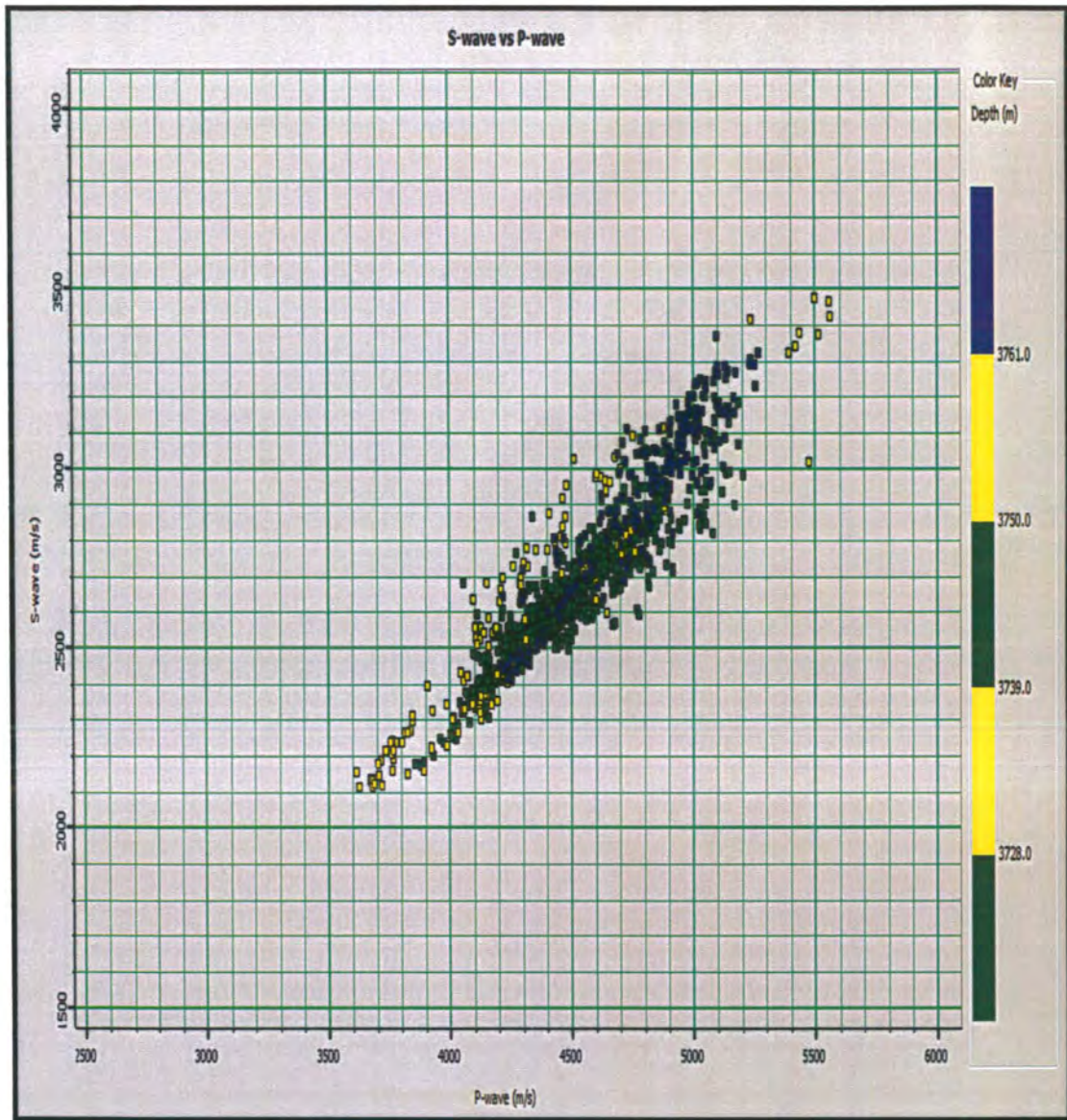
Figure 4.3: V_P/V_S cross plot of Tajjal-02 (In-situ Water)

In the above figure, V_P and V_S are cross plotted for originally water saturated well i.e. Tajjal_02 and there is no specific data scattering is observed as it is observed in case of gas producing well i.e. Tajjal_01.
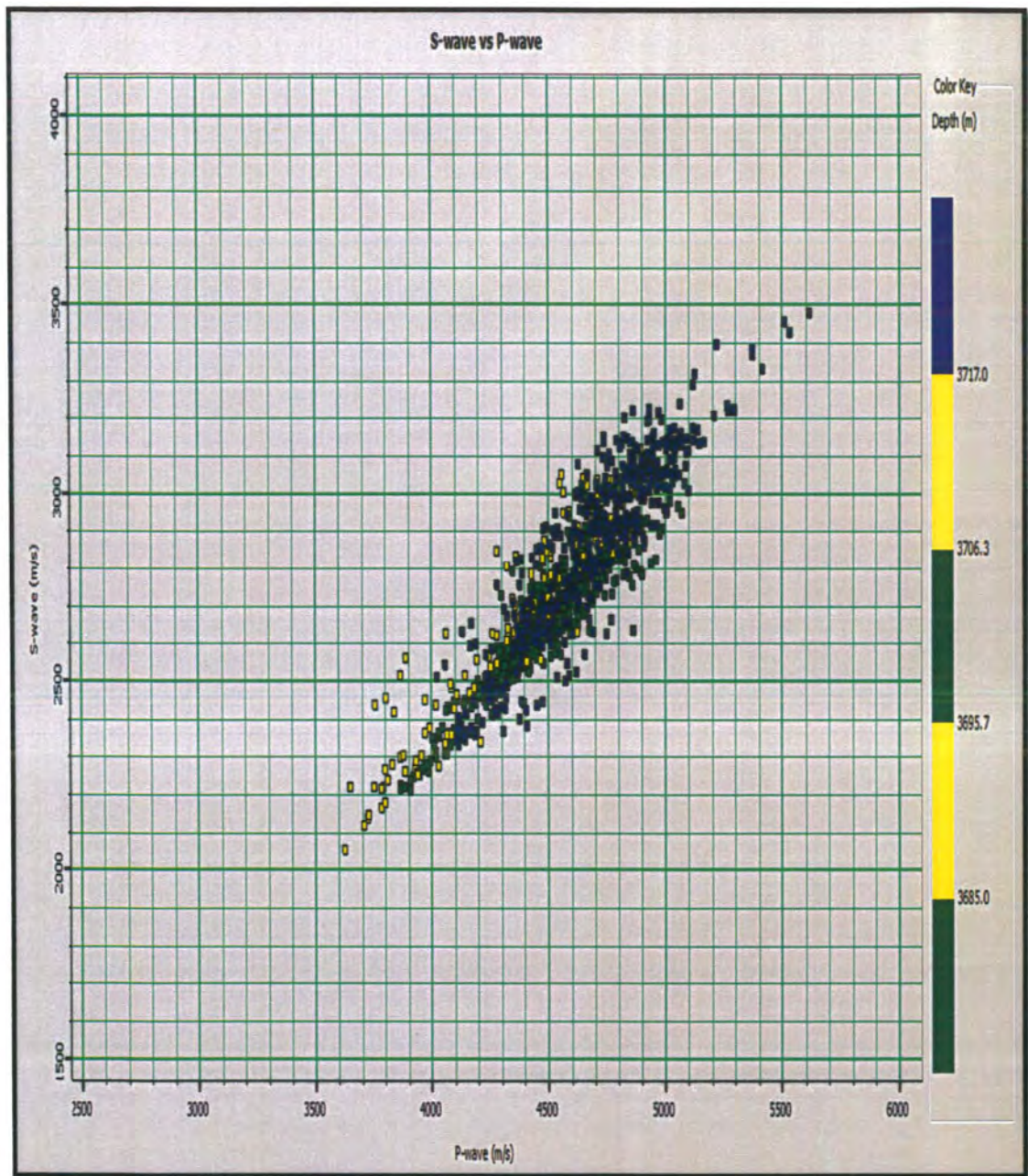
Figure 4.4: V_P/V_S cross plot of Tajjal-03 (In-situ Water)

In the above figure, V_P and V_S are cross plotted for originally water saturated well i.e. Tajjal_03 and results are same as for Tajjal_02.
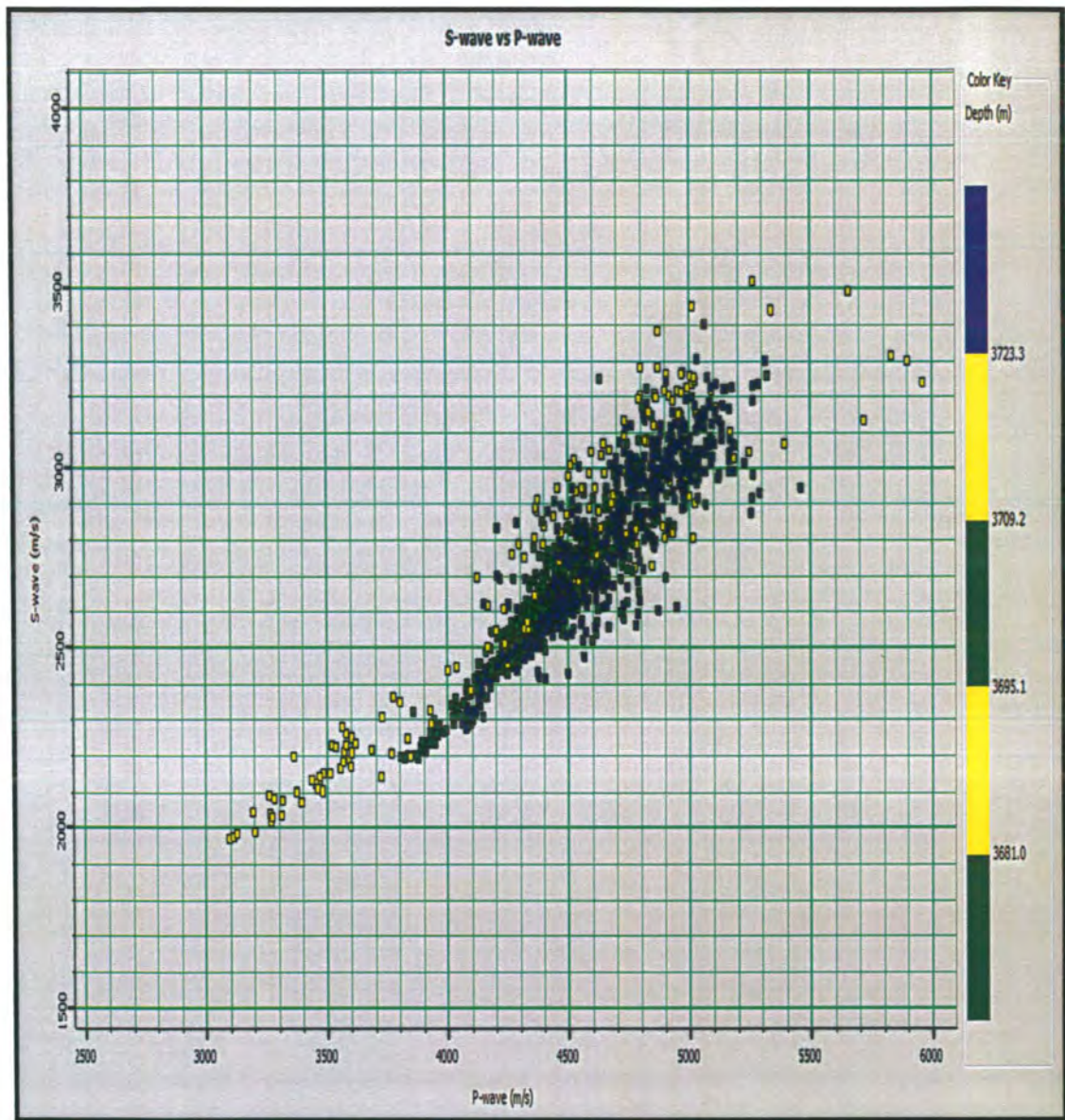
Figure 4.5: V_P/V_S cross plot of Tajjal-04 (In-situ Gas)

In the above figure, V_P and V_S are cross plotted for Tajjal_04 (Gas producing well). In this case, fluid saturation again affected the data trend and scattered data is observed at specified 12 meters interval. Velocity values are low in this zone.

Figure 4.6: V_P/V_S cross plot of Tajjal-04 (100 % Water)
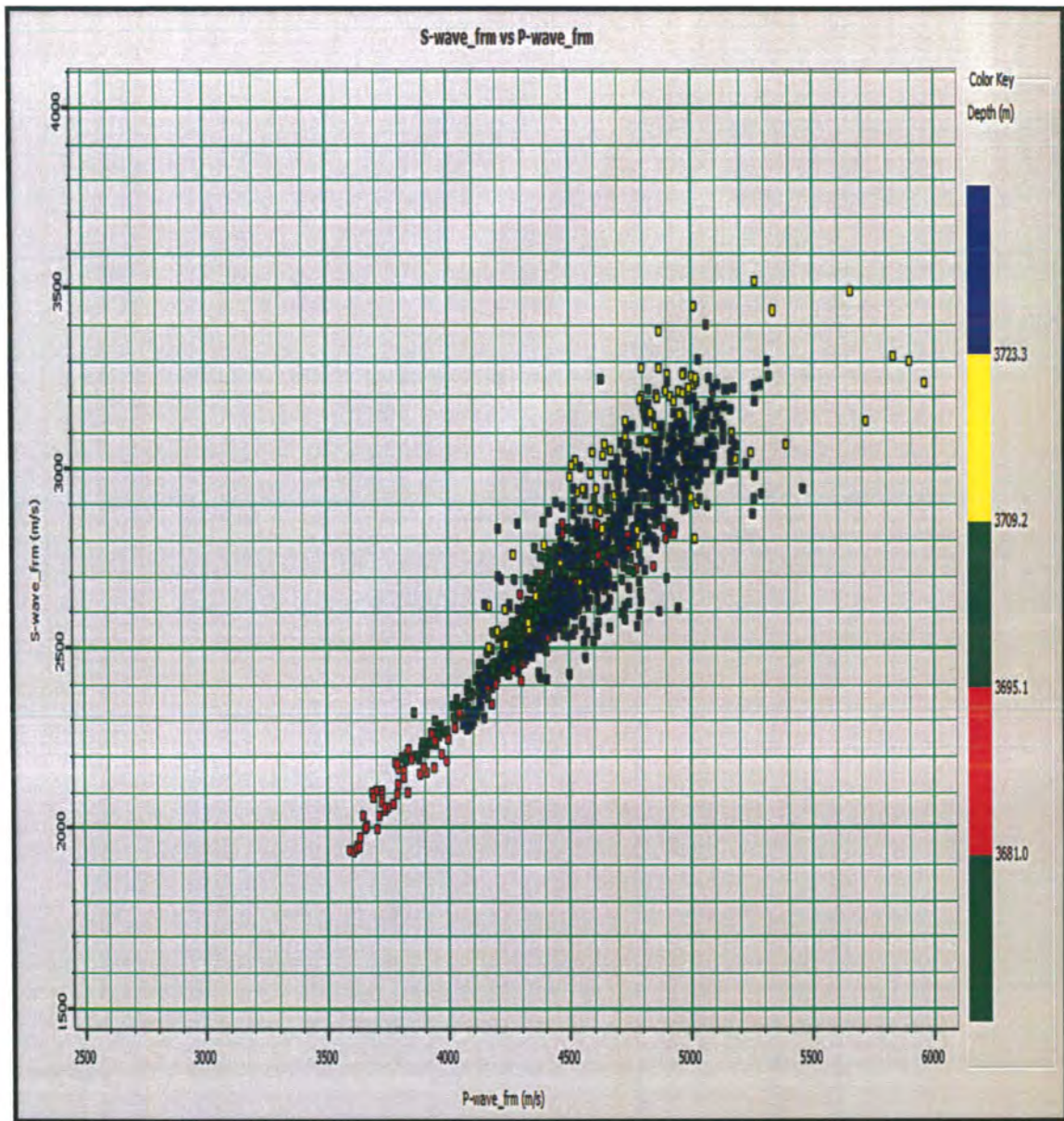
In the above figure, V_P saturated and V_S saturated are cross plotted after applying Gassmann`s Equation in the specified zone and results are same as for in-situ water saturated wells i.e. Tajjal_02 and Tajjal_03.

5. Seismic Attributes and AVO Modelling

To correctly image the structure in depth per accurate time and to correctly characterize the amplitudes of the reflections is the main objectives in most exploration and reservoir seismic surveys. We assume that amplitudes are rendering accurately a host of additional features and can be divided and used in interpretations. All these features are referred to as seismic attributes (Taner et al., 1979).

The attributes can be obtained most commonly from typical post-stack seismic data volumes. An additional information can be obtained from attributes of the individual seismic traces, prior to stacking. The variation of amplitude with offset or amplitude vs. angle (AVA), is the most common type of these attributes. To minimize the ambiguities present calibration to well data is the main interpretation of any attribute which is nonunique (Taner et al., 1979).

To correlate the attribute of interest with the well-log (or log-derived) data of interest is easy and to convince many workers that the correlation is meaningful and that seismic amplitude can be used as a proxy for porosity in reservoir characterization. There seems to be a strong correlation between seismic amplitude and porosity. On the other hand, in this approach there are many potential pitfalls (Hirsche et al., 1998). So, the following protocols should be followed:

1. To evaluate the reasonableness of the results geologic inference should be considered.
2. Statistical tests should be performed on the correlations.
3. Most importantly, the physical basis for the behavior of an observed attribute must be understood.

There should be use of simple statistical correlation, without a geological and physical basis. However, spurious correlations can readily be obtained (Kalkomey, 1997).

5.1   Classification of Attributes

The attributes can be classified into different categories depending upon the physical properties of the seismic signal. The most common categories are given as:

1. Amplitude Attributes
    i.   Mean Amplitude
    ii.   Average Energy
    iii. RMS Amplitude

  iv. Maximum Amplitude

  v. AVO Attributes

  vi. Inelastic Attenuation Factor

2. Time/Horizon Attributes

  i. Coherence

  ii. Dip

  iii. Azimuth

  iv. Curvature

3. Frequency Attributes

The use of CMP gathers, like amplitude versus offset (AVO), must be analysed pre-stack (Young and LoPiccolo, 2005), although most of the seismic attributes are post-stack. A single seismic trace or multiple traces within a defined range can be used to measure these attributes.

5.2 Post Stack Attributes

Most commonly stacked seismic data volume is used for interpretation of geological structure and seismic attributes. Top B sands of Lower Goru Formation is calculated most commonly by the attribute of amplitude, although its interpretation in beds having thin-layers is not necessarily straightforward (Robertson and Nogami, 1984). Velocity and density are strongly effected by porosity and/or liquid saturation (oil/wat vs. gas). Seismic reflections are generated at boundaries where the acoustic impedance changes. Nonhydrocarbon changes in lithology can result in large-amplitude reflections but identification of hydrocarbons 'bright-spot' is a result of this attribute. (Pennington et al., 2001).

Minimum Amplitude map for top of B-Sands is shown as:
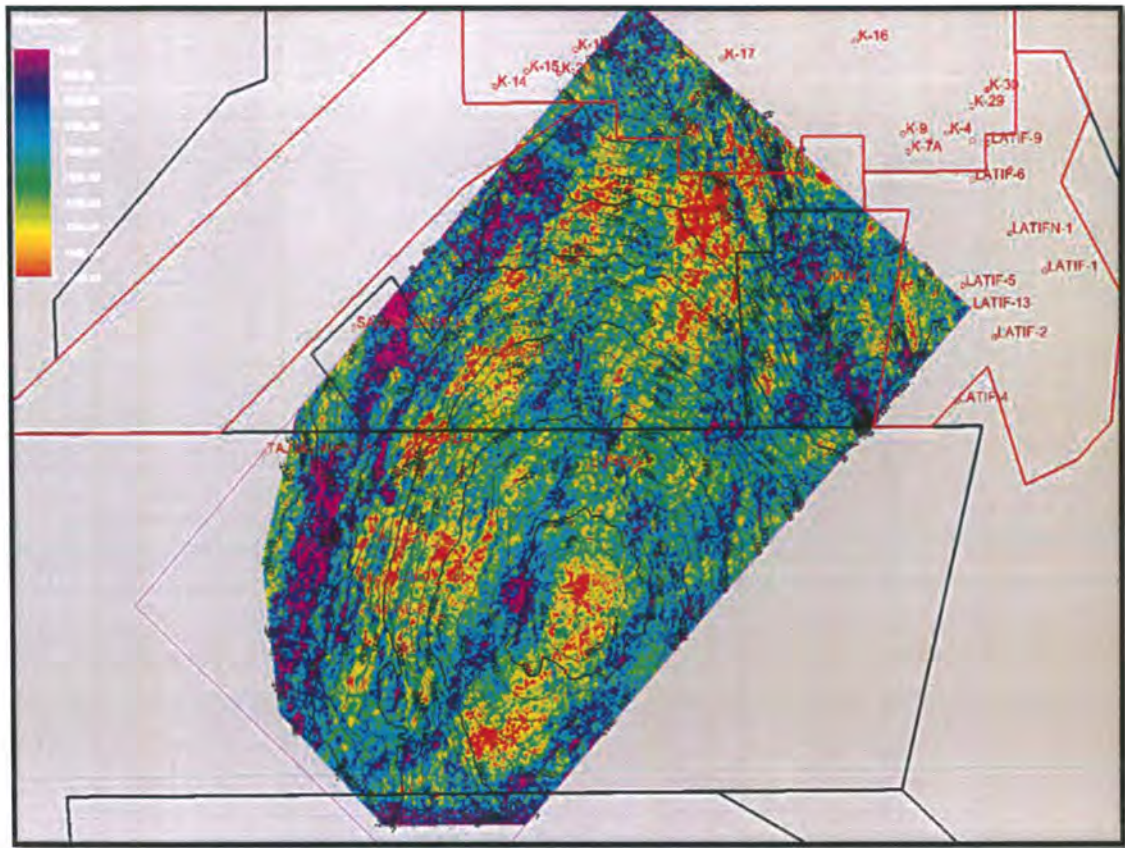
Figure 5.1: Minimum amplitude map for top of B-sands

In the above figure, minimum amplitudes are shown for Top of B-Sands and the range is varying between -500 to -4500 units. Amplitude values are relatively higher for entire volume which shows that reflection amplitudes are strong enough to apply AVO modelling on pre-stack data. However, these amplitudes are slightly weaker near fault zones. Hence, amplitude response can be proved a good tool to characterize the reservoir.

5.2.1 Variance Attribute

Variance attribute is also calculated for Top of B-Sands, it represents variability from trace-to-trace over a sample interval and therefore produces interpretable changes in acoustic impedance laterally. Discontinuities have high coefficients while similar traces produce low variance coefficients. Because faults and channels can cause discontinuities in the nearby lithologies and later in the trace-to-trace variability they become detectable in 3D seismic volumes (Taner et al., 1979). It is shown as:
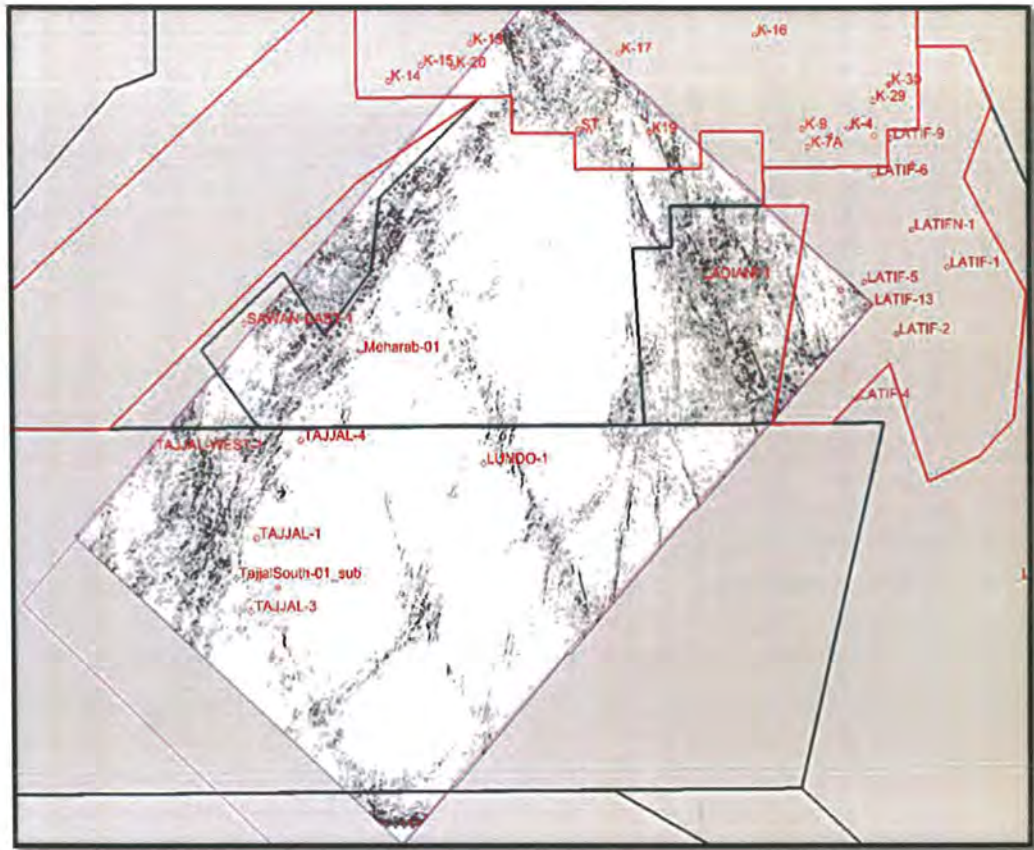
Figure 5.2: Variance slice for top of B-sands

In the above figure, variance attribute is calculated for top of B-Sands after an interval of 20ms on all seismic traces and it is shown that faults have higher values of variance coefficients shown by black color. The location of these faults is also comparable with amplitude map and depth contour map of B-Sands.

5.3   AVO Modelling

In geophysics, Amplitude versus offset (AVO) is the wide-ranging term for denoting the reliance of amplitude with the offset (distance between the source and receiver). This geophysical technique helps to determine a rock's shear wave information, fluid content, porosity, seismic velocity, etc. This phenomenon, binding the relationship between reflection coefficient and angle of incidence, has been understood since the Zoeppritz equations were calculated by Karl Zoeppritz in early 20th century. Amplitude versus angle (AVA), due to its physical origin may be taken as equivalent to AVO, but AVO is the more frequently used term because the offset is a physical term

41

that can be easily changed by the geophysicist. Aki-Richard's Equation, an approximation to Zoeppritz equations is used to understand the effect of fluid on amplitudes of synthetic data (Yilmaz, 2001).

The equation is given as:

$$R(\theta) = aR_{VP} + bR_{VS} + cR_D, \qquad (5.1)$$

$$\text{where}: \quad R_{VP} = \frac{\Delta V_P}{2\overline{V}_P}, \ R_{VS} = \frac{\Delta V_S}{2\overline{V}_S}, \ R_D = \frac{\Delta \rho}{2\overline{\rho}},$$

$$a = 1 + \tan^2 \theta, \ b = -8K \sin^2 \theta, \ c = 1 - 4K \sin^2 \theta, \text{ and } K = \left(\frac{\overline{V}_S}{\overline{V}_P}\right)^2$$

The approach is appealing because it involves separately P-wave velocity, S-wave velocity and density. These parameters are not separately observed on reflection amplitudes rather change in amplitudes is observed as a function of angle of incidence only.

The results obtained for the study area are given as:
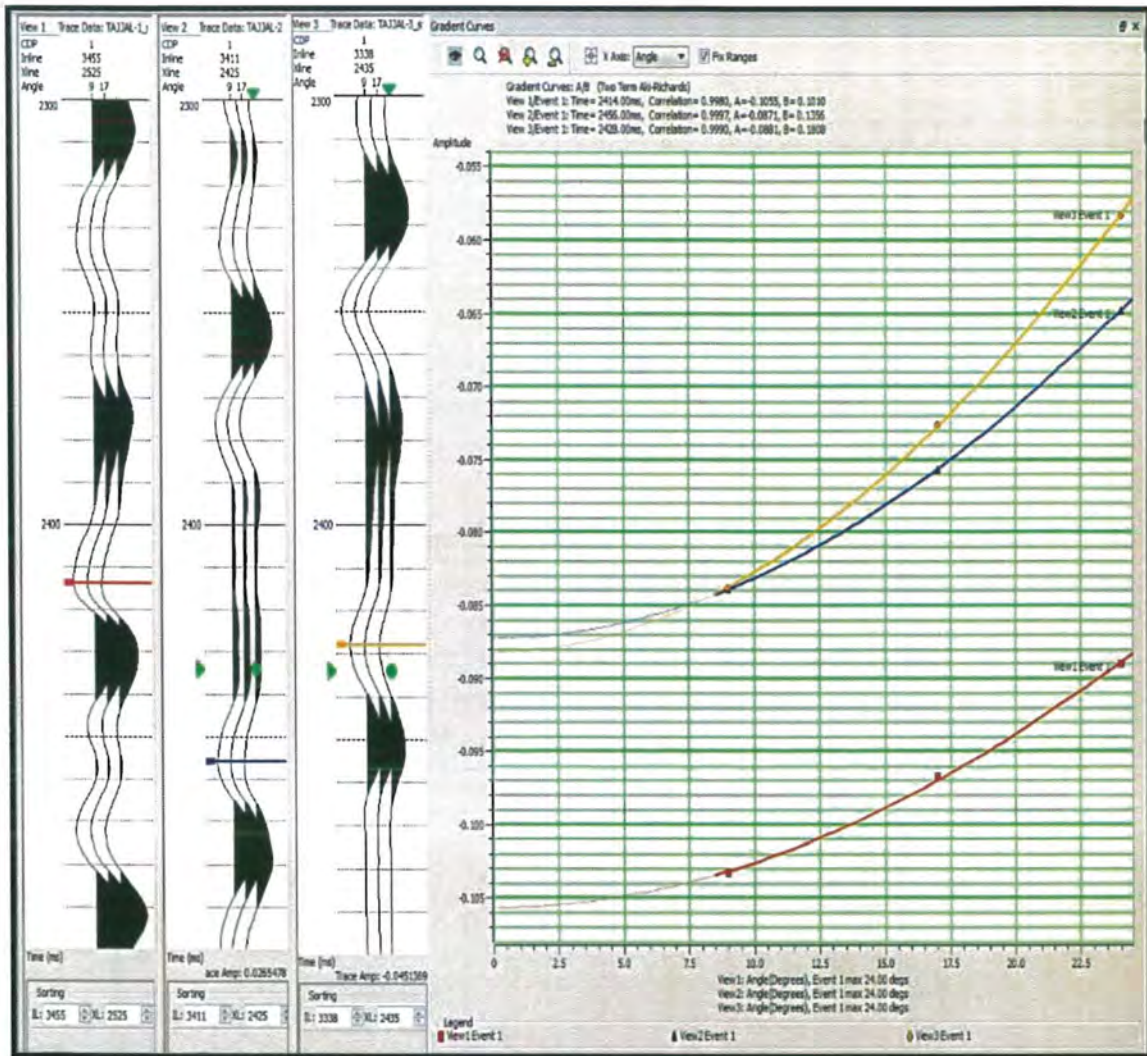
Figure 5.3: AVO Gradient analysis Tajjal-01 (Gas), Tajjal-02 & Tajjal-03

In the above figure, synthetic data is used for Tajjal_01, Tajjal_02 and Tajjal_03 to observe the effect of fluid saturation on AVO response. Three traces are generated for each well at 9 degrees, 17 degrees and 25 degrees to observe the effect of near, middle and far angles respectively. Amplitudes are cross plotted against angles and AVO response of gas producing well i.e. Tajjal_01 is entirely different from other two curves shown by red color.

43

Figure 5.4: AVO Gradient analysis Tajjal-01 (Water), Tajjal-02 & Tajjal-03

In the above figure, fluid saturation of Tajjal_01 is changed from gas to water and AVO response is observed again. In this case, AVO gradient is changed remarkably and it is comparable with other water producing wells i.e. Tajjal_02 and Tajjal_03.

44

Figure 5.5: AVO cross plot analysis Tajjal-01 (Gas), Tajjal-02 & Tajjal-03

In the above figure, AVO gradient as shown in above figures is cross plotted against intercept for similar wells and most of the data points from Tajjal_01 are scattered in first quadrant with positive values and hence class of sand can be identified which is type-IV in this case.

Figure 5.6: AVO cross plot analysis Tajjal-01 (Water), Tajjal-02 & Tajjal-03

In the above figure, cross plot of AVO gradient and intercept is analysed after altering fluid saturation in Tajjal_01 and it is observed that data trend is same as for other in-situ water saturated wells i.e. Tajjal_02 and Tajjal_03.
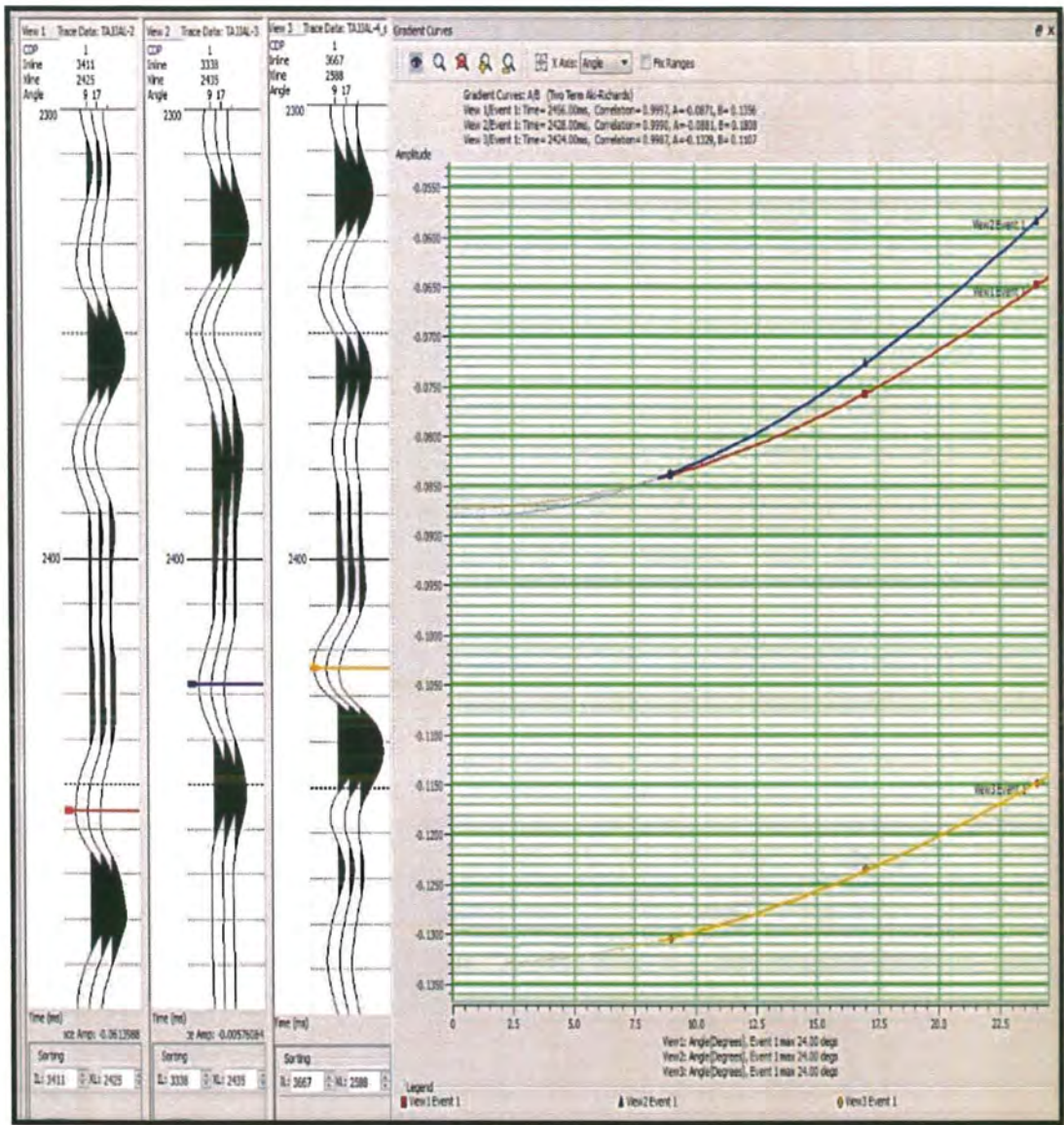
Figure 5.7: AVO Gradient analysis Tajjal-02, Tajjal-03 & Tajjal-04 (Gas)

In the above figure, AVO gradient is calculated for Tajjal_02, Tajjal_03 and Tajjal_04 based on their original fluid conditions. In this case, similar response is observed for gas producing well i.e. Tajjal_04 shown by orange color.
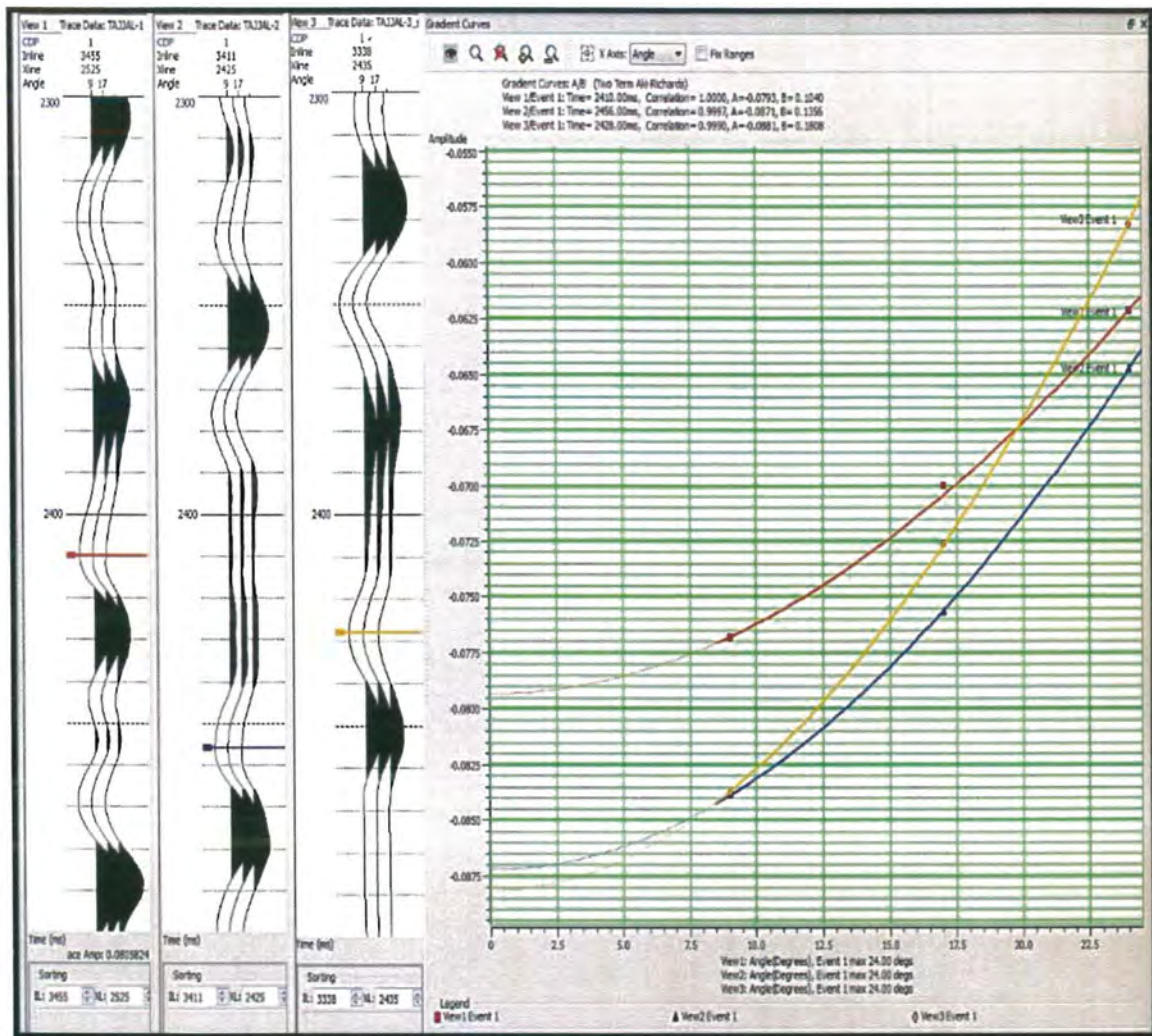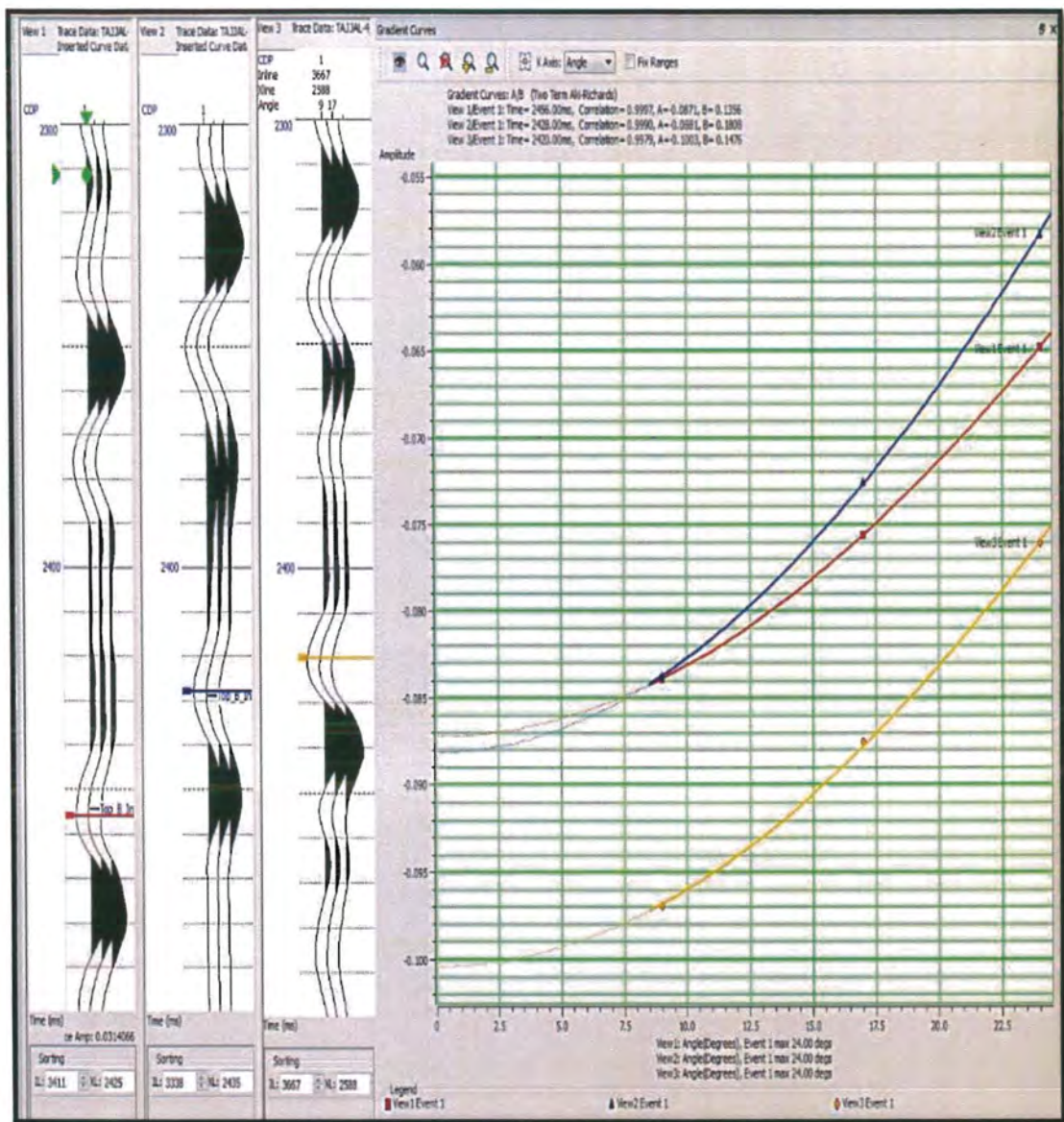
Figure 5.8: AVO Gradient analysis Tajjal-02, Tajjal-03 & Tajjal-04 (Water)

In the above figure, fluid saturation of Tajjal_04 is changed from gas to water and AVO response is observed again. In this case, AVO gradient is changed remarkably and it is comparable with other water producing wells i.e. Tajjal_02 and Tajjal_03.
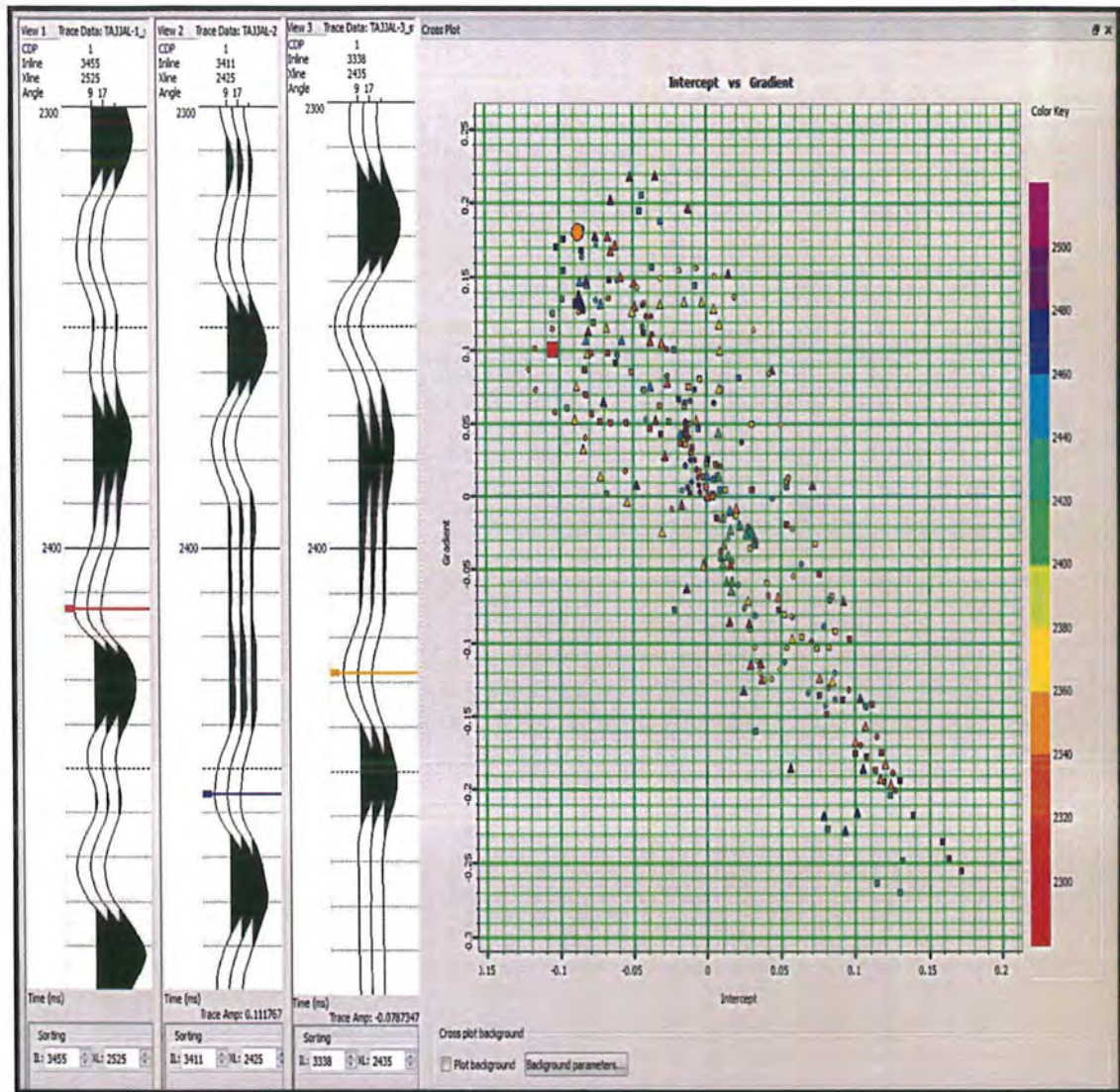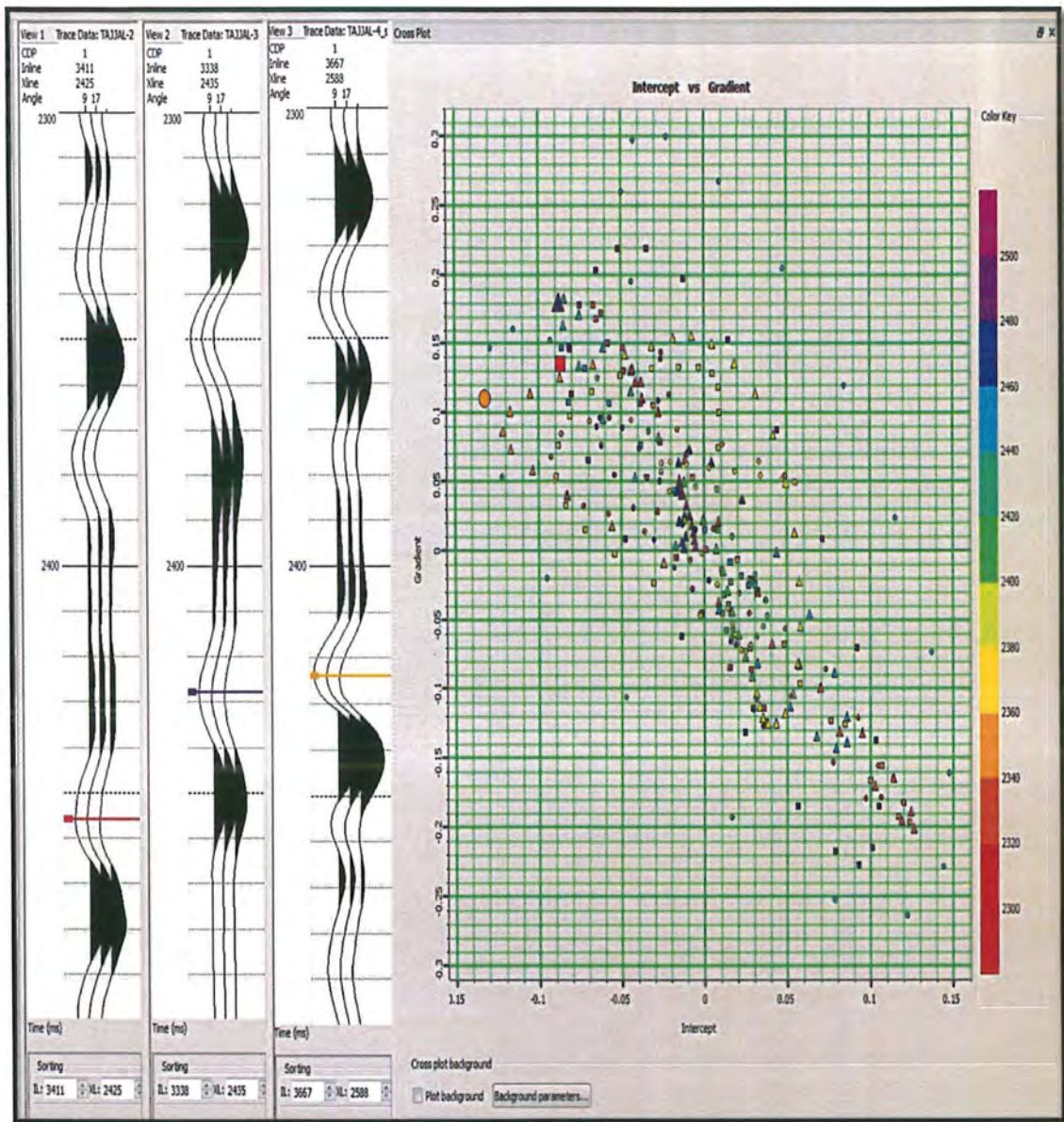
Figure 5.9: AVO cross plot analysis Tajjal-02, Tajjal-03 & Tajjal-04 (Gas)

In the above figure, AVO gradient as shown in above figures is cross plotted against intercept for similar wells and most of the data points from Tajjal_04 are scattered in first quadrant with positive values and hence class of sand can be identified which is type-IV in this case.
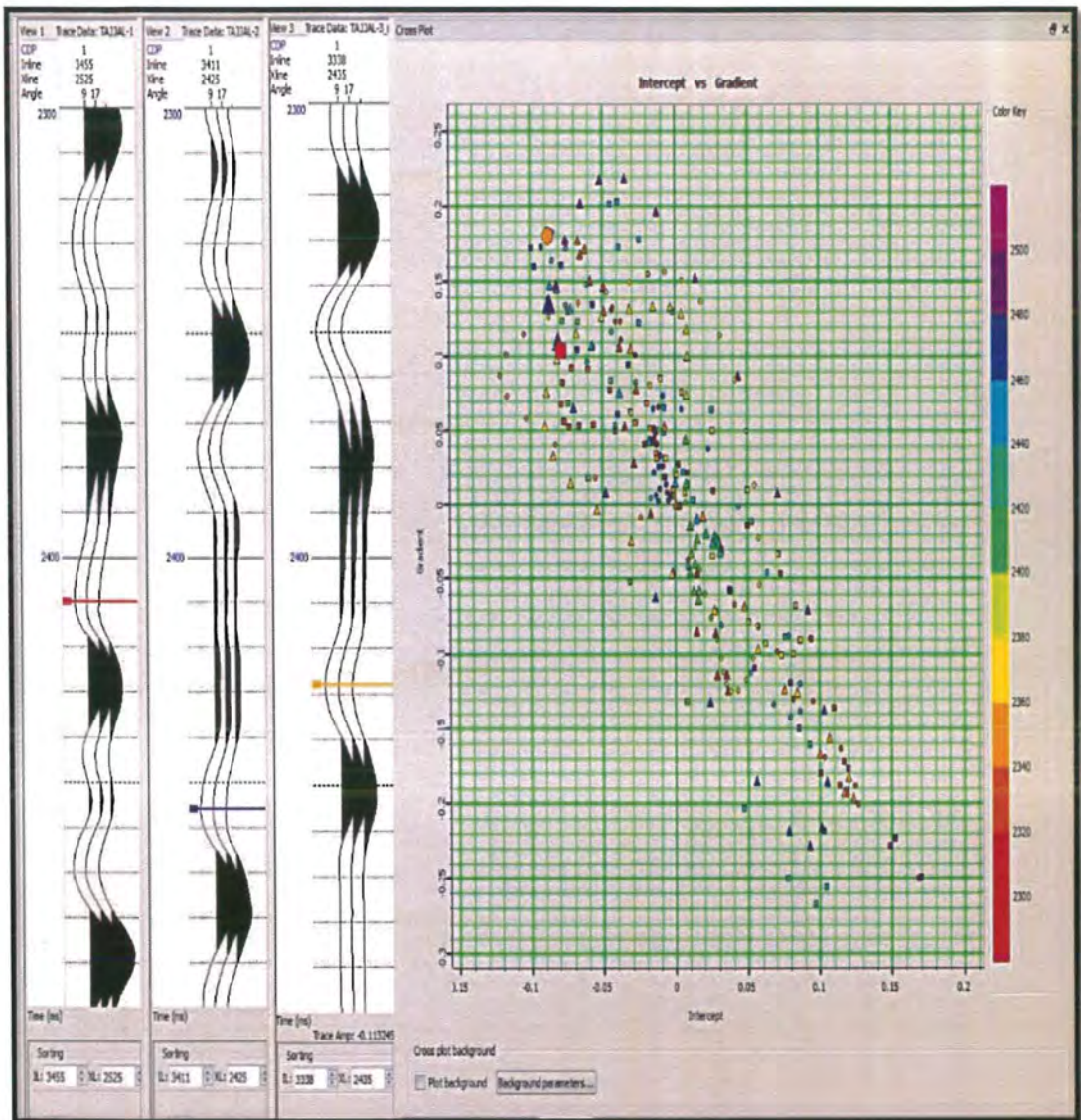
Figure 5.10: AVO cross plot analysis Tajjal-02, Tajjal-03 & Tajjal-04 (Water)

In the above figure, cross plot of AVO gradient and intercept is analysed after altering fluid saturation in Tajjal_04 and it is observed that data trend is same as for other in-situ water saturated wells i.e. Tajjal_02 and Tajjal_03.
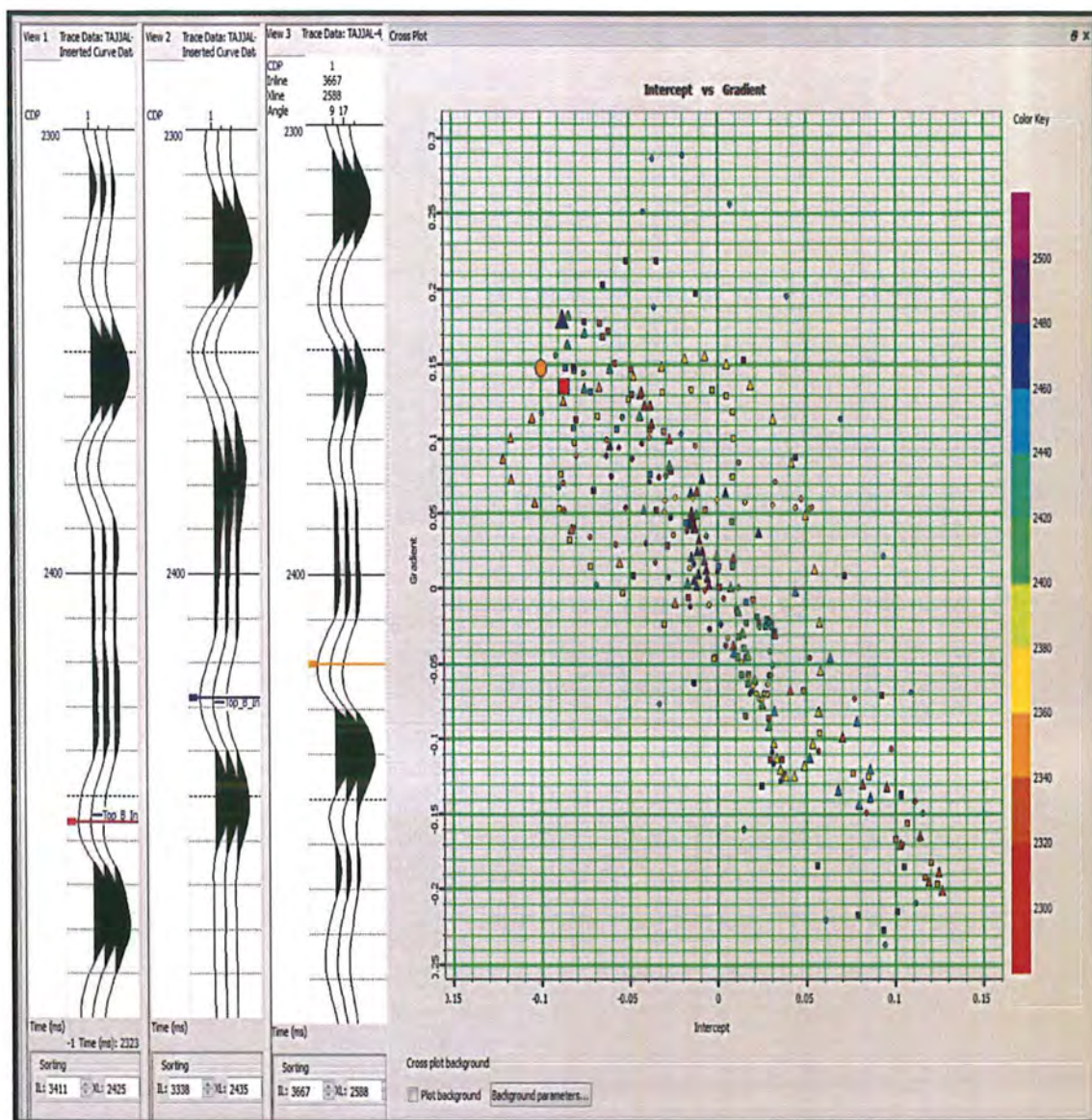
6. Post Stack Seismic Inversion

Seismic inversion converts the seismic reflection data of subsurface rocks into quantitative properties describing the subsurface geology. Seismic inversion, pre- or post- stack, includes a vast majority of calculations incorporating datasets such as cores, well logs, etc. (Yangkang et al., 2017). It also utilizes geostatistical techniques and can be applied as a deterministic or stochastic approach.

A simple qualitative interpretation of seismic data, without incorporating inversion results, can be misleading at times especially when exploring for tight sands and shale gas. While exploring for such ambiguous reservoirs, seismic inversion, because of its efficiency and quality, helps to minimize the risk by improving on the reliability and resolution of the data by estimating the rock properties such as porosity, net pay, total organic content, water saturation, etc. (Pendrel, 2006).

Seismic inversion is further categorized as:

1. Pre-Stack Inversion
2. Post-Stack Inversion

6.1 Wavelet Estimation

To estimate an accurate wavelet from the available data is crucial for the success of any seismic inversion method. The modern seismic inversion requires 1) seismic data and 2) a wavelet projected from the data. The phase and frequency of the wavelet is calculated by extracting a reflection coefficient series along the borehole. It is of paramount importance to ensure the quality of the estimated wavelet because the shape of the wavelet strongly influences the inversion results and thus have a direct effect on the reservoir quality.

Wavelet amplitude and phase spectra can be computed statistically from either 1) seismic data; or 2) a combination of seismic data and well logs namely sonic and density curves. After the estimation of seismic wavelet, it is used to estimate seismic reflection coefficients in the seismic inversion (Pendrel, 2006).

6.2 Post Stack Inversion

The major division between categories of inversion is based on stacking. Stacking is a processing sequences employed to reduce noise against the usable signal by summing up multiple traces representing the same common depth point from multiple receiver-source pairs into a single trace.

The subsequent traces mirror the acoustic impedance values for an incident wave of 90 degrees for that CMP (common-midpoint). Consequently, inversion performed on stacked seismic traces is called Post-Stack Inversion. Post-Stack inversion uses the following assumptions:

1. Gradual lateral variation of velocity
2. The average amplitude of the stacked traces is equal to the amplitude given by a trace that would be at normal-incidence to the reflector.

Post-Stack inversion can further be classified as:

1. Band Limited Inversion
2. Colored Inversion
3. Model Based Inversion

The relation of seismic inversion with other reservoir characterization techniques can simply be shown as:
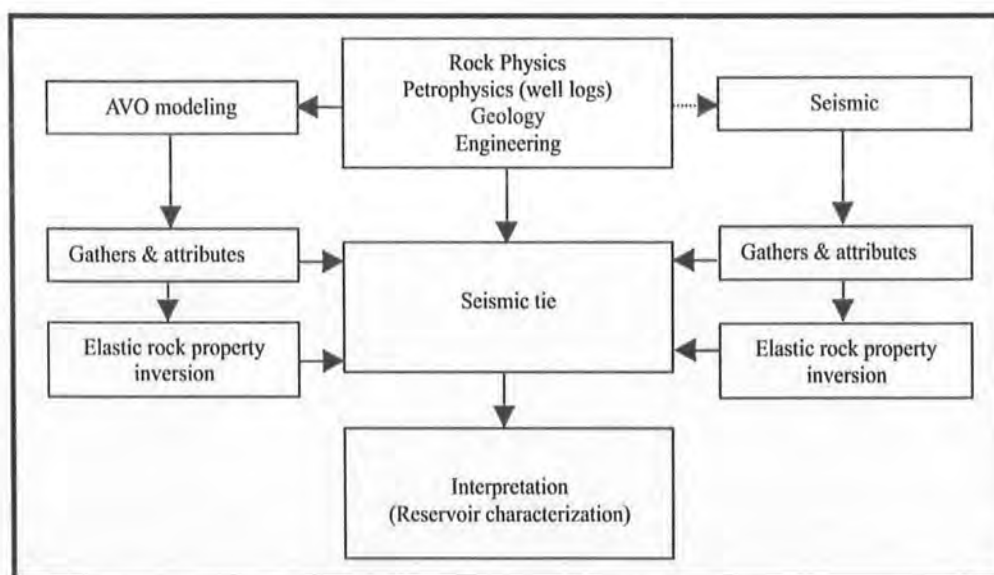
Figure 6.1: Work flow of reservoir characterization (Li et al., 2004).

Post stack seismic inversion is applied to calculate porosity and pore pressures from seismic data for the reservoir. Initially, a low frequency model (0-10 Hz) is generated for all wells to recover all missing low frequencies. Following this, seismic volume is inverted to P-impedance using average wavelet extracted from seismic data. A relation between reservoir properties (porosity and pore pressure) and P-impedance is built using well data. The results are shown as:
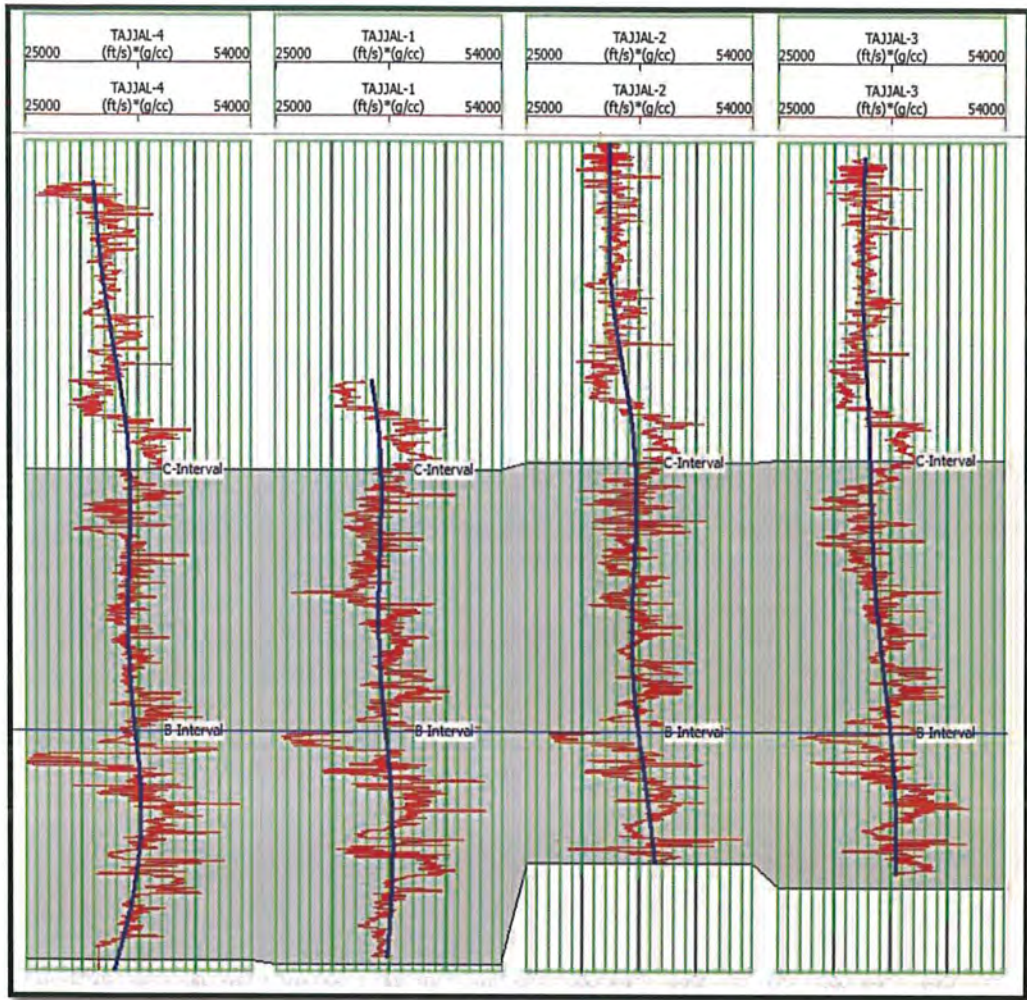
Figure 6.2: Low frequency model

In the above figure, low frequency impedance curves are generated for each well, shown by red color and blue one is the average trend for each curve. Tops of B-Sands and C-Sands are also marked. These impedance curves on convolution with extracted wavelets are used to recover low frequency data in the seismic.
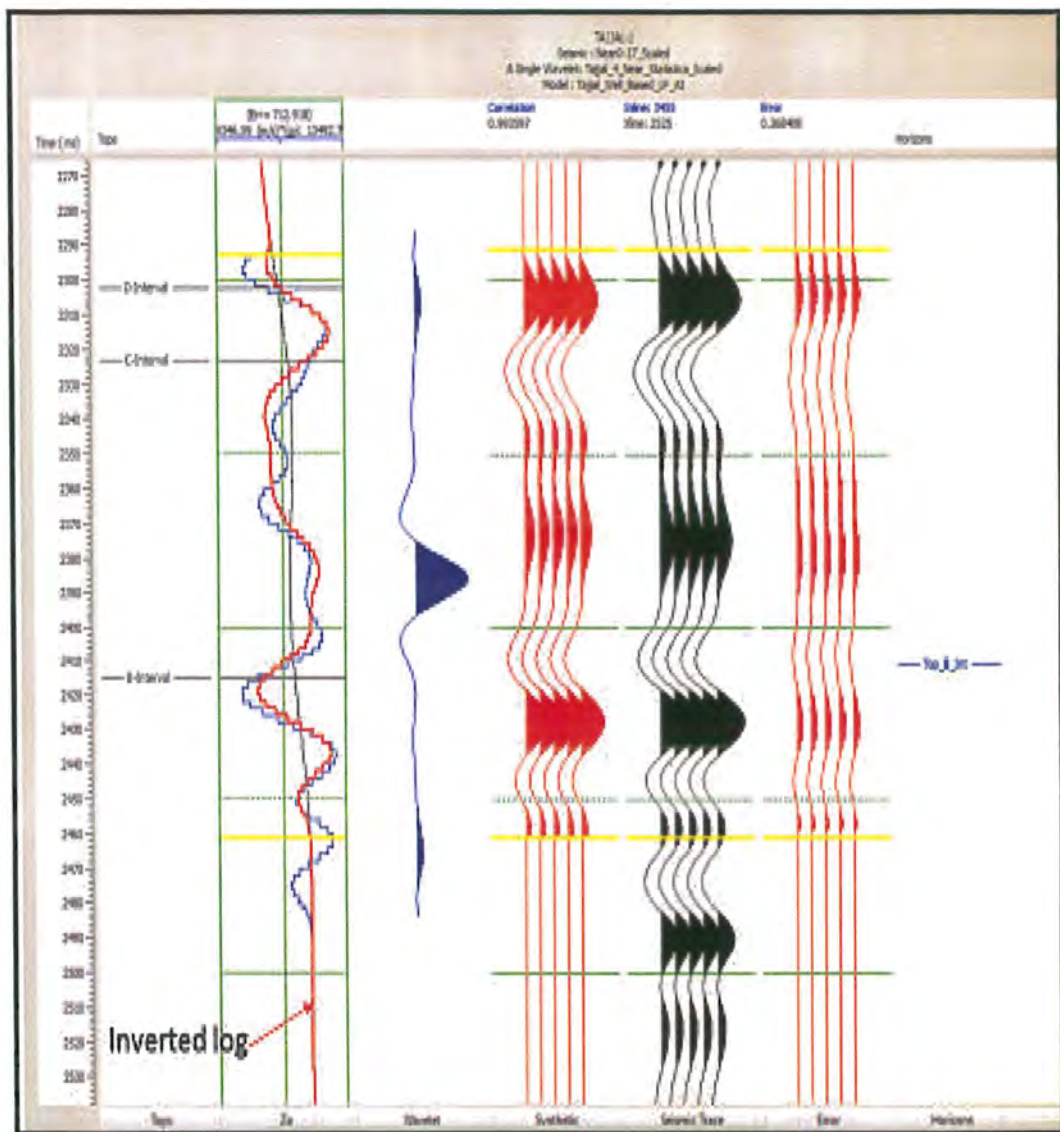
Figure 6.3: Post stack inversion analysis of Tajjal_01

In the above figure, post stack inversion is shown for Tjjal_01. Time scale is shown on left side ranging from 2270 to 2530 msec and inverted log is generated using velocity and density data. Red color shows the synthetic data while in black color original seismic data is shown. The curve shown in red color at right side is the difference between seismic data and inverted data. Correlation coefficient is 0.99 among the two which shows very strong positive relation. Tops of B-Sands, C-Sands and D-Sands are also marked.

Figure 6.4: Post stack inversion analysis of Tajjal_02

In the similar way, inverted data is calculated for Tajjal_02 and the correlation coefficient between seismic data and inverted data is 0.97 which shows a strong positive relation.
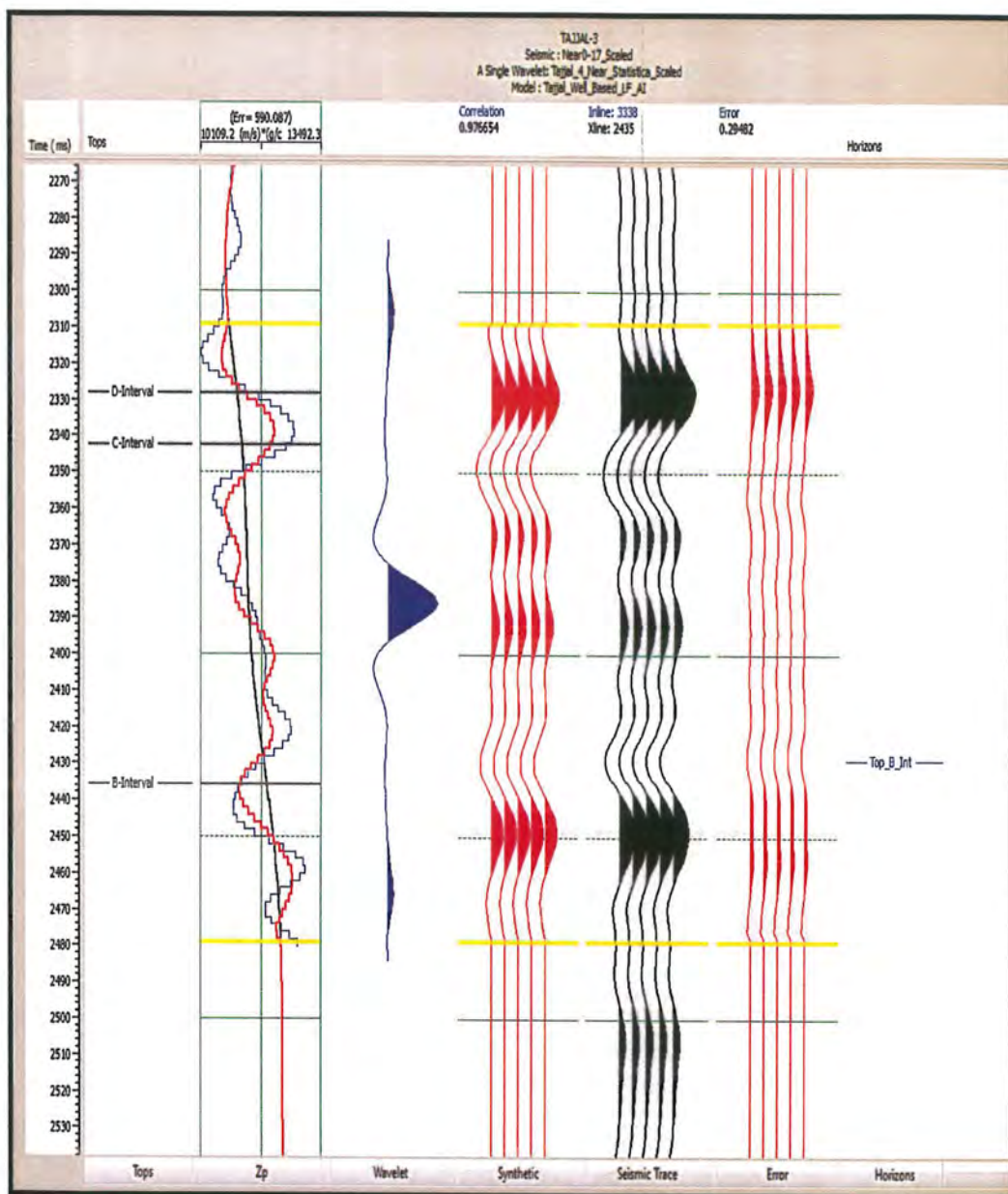
Figure 6.5: Post stack inversion analysis of Tajjal_03

In the above figure, inverted data is calculated for Tajjal_03 and the correlation coefficient between seismic data and inverted data is 0.97 which shows a strong positive relation.
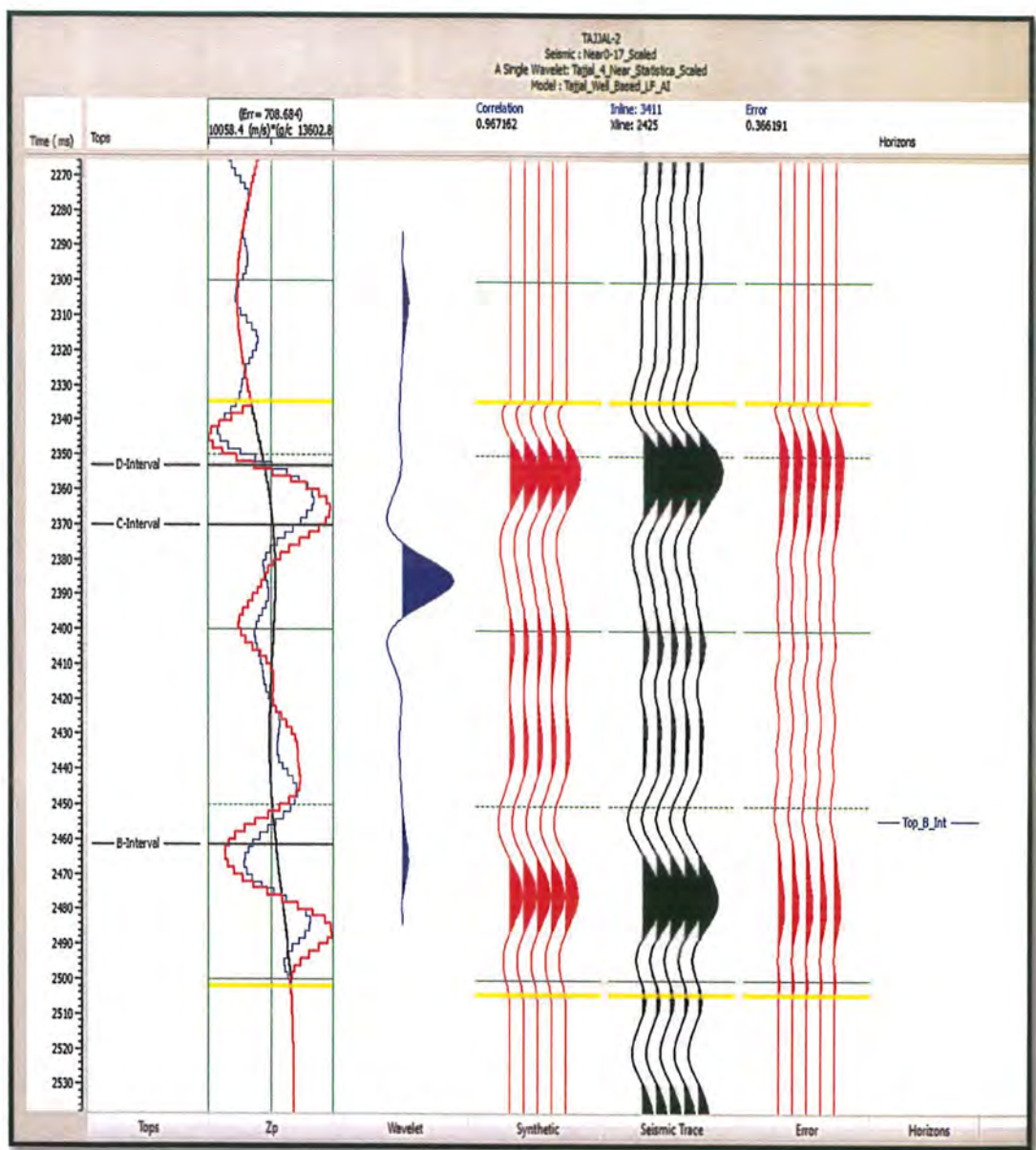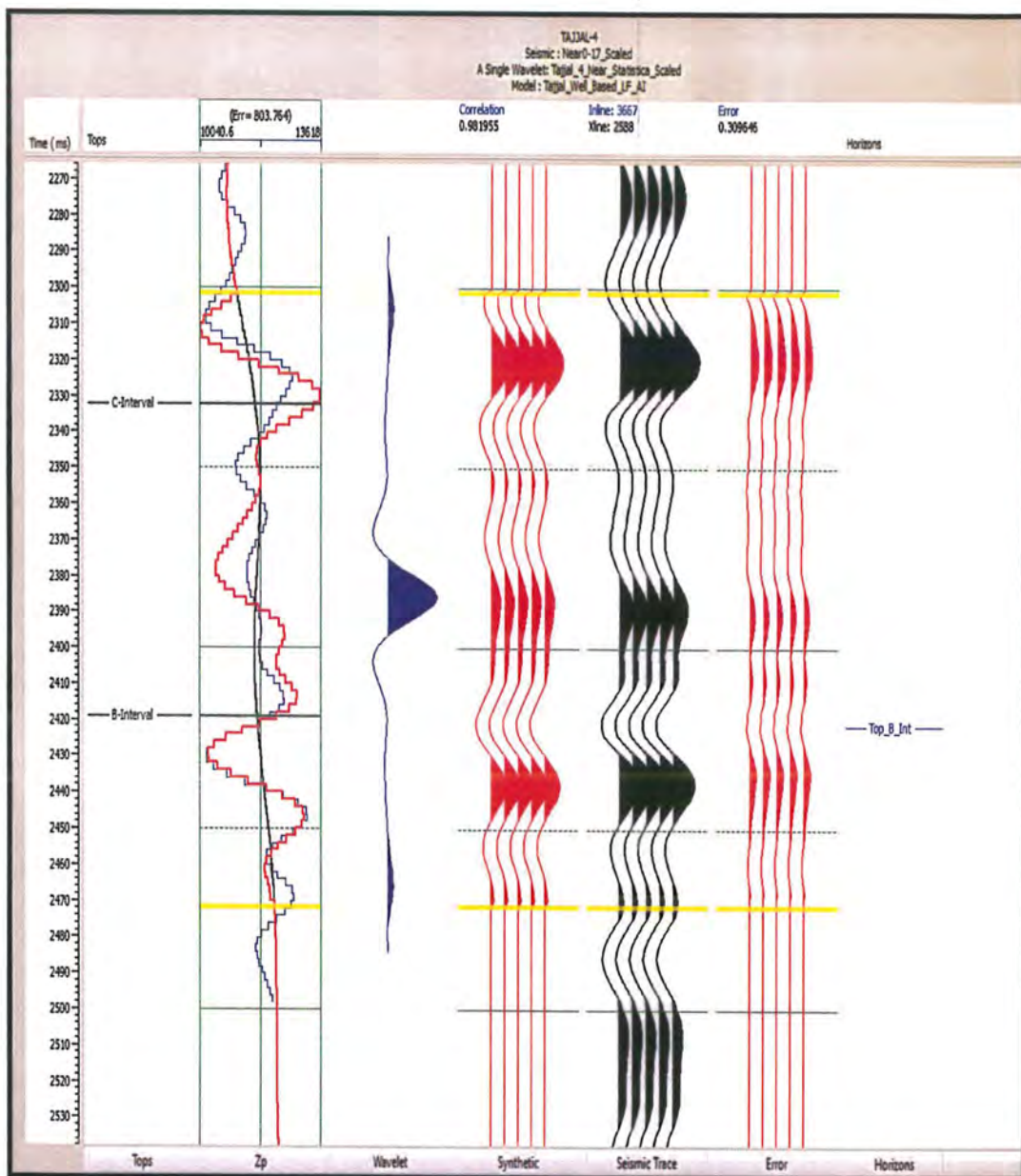
Figure 6.6: Post stack inversion analysis of Tajjal_04

In the above figure, inverted data is calculated for Tajjal_03 and the correlation coefficient between seismic data and inverted data is 0.98 which shows a strong positive relation.
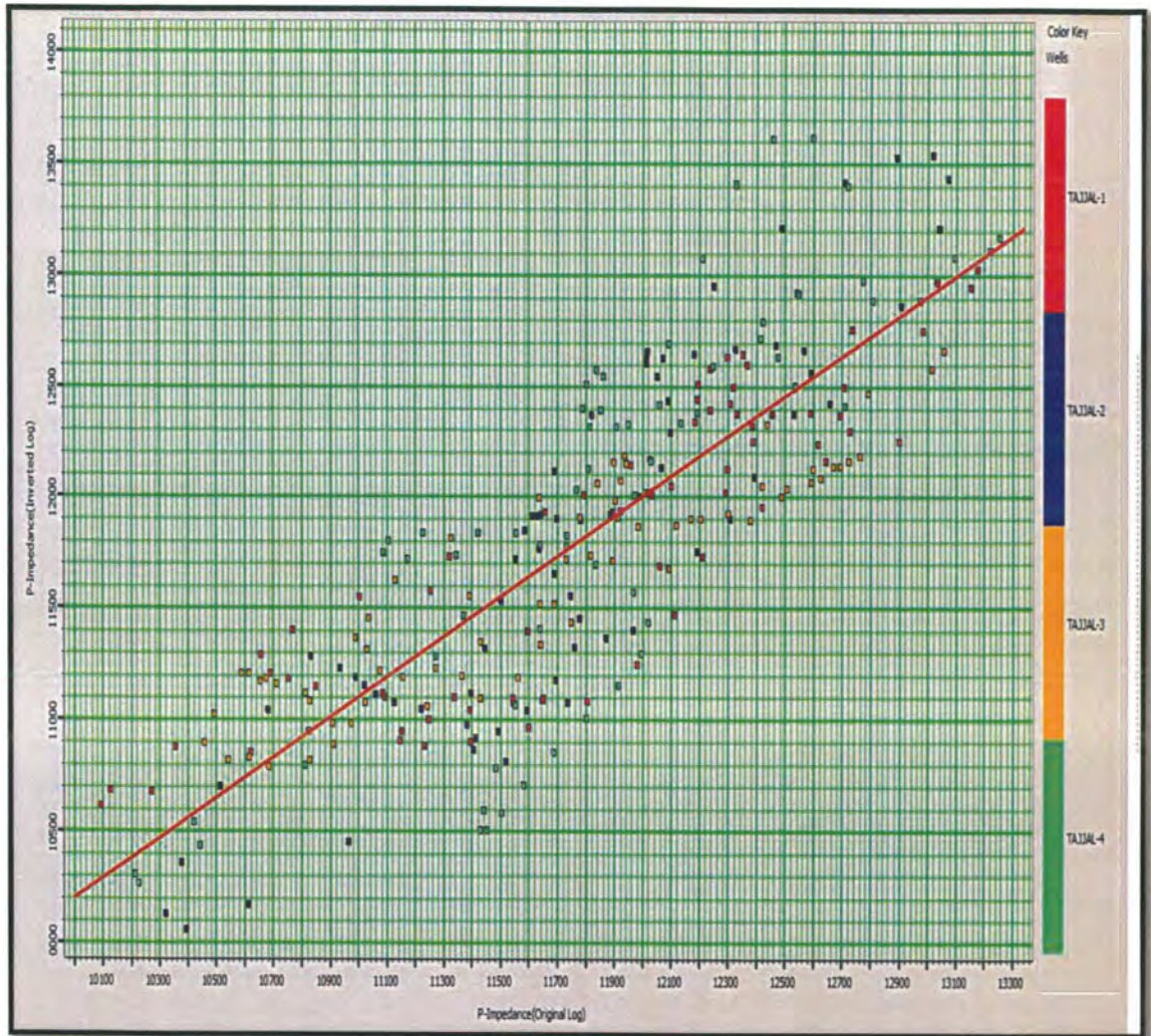
Figure 6.7: PI_Inverted logs Vs PI_Origional logs

In the above figure, P-Impedance original is cross plotted against P-Impedance inverted for all wells i.e. Tajjal_01, Tajjal_02, Tajjal_03 and Tajjal_04 shown in red, blue, orange and green colors respectively. Correlation coefficient among the two is 0.90, which shows a strong positive relation between these parameters. These inverted impedance values are further used to estimate interval velocities which are used to estimate porosity values and pore pressure for B-Sands.
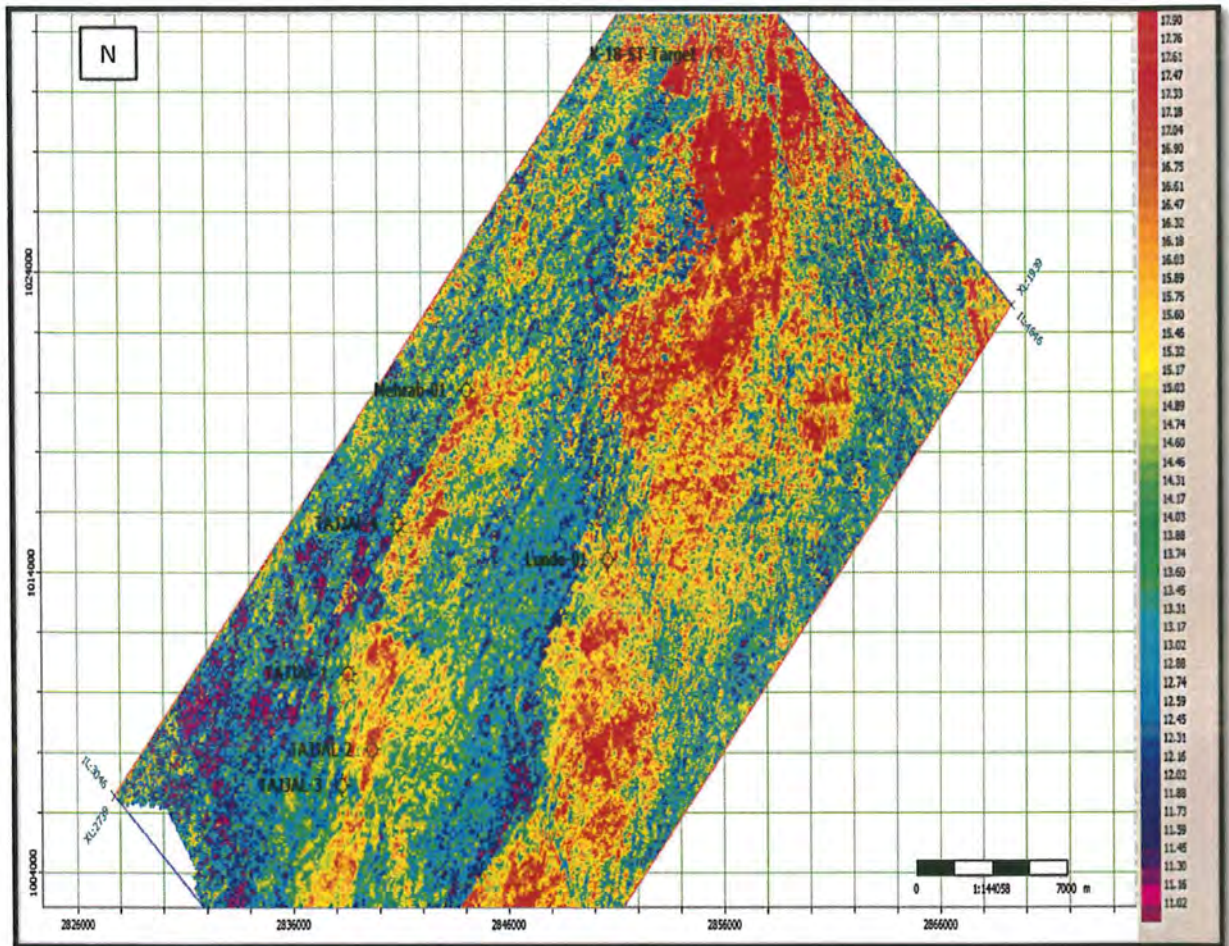
Figure 6.8: Calculated Porosity Slice for Top of B-Sands

In the above figure, calculated porosity slice for B-Sands from inverted data is shown, where porosity values are ranging between 12 to 18%.
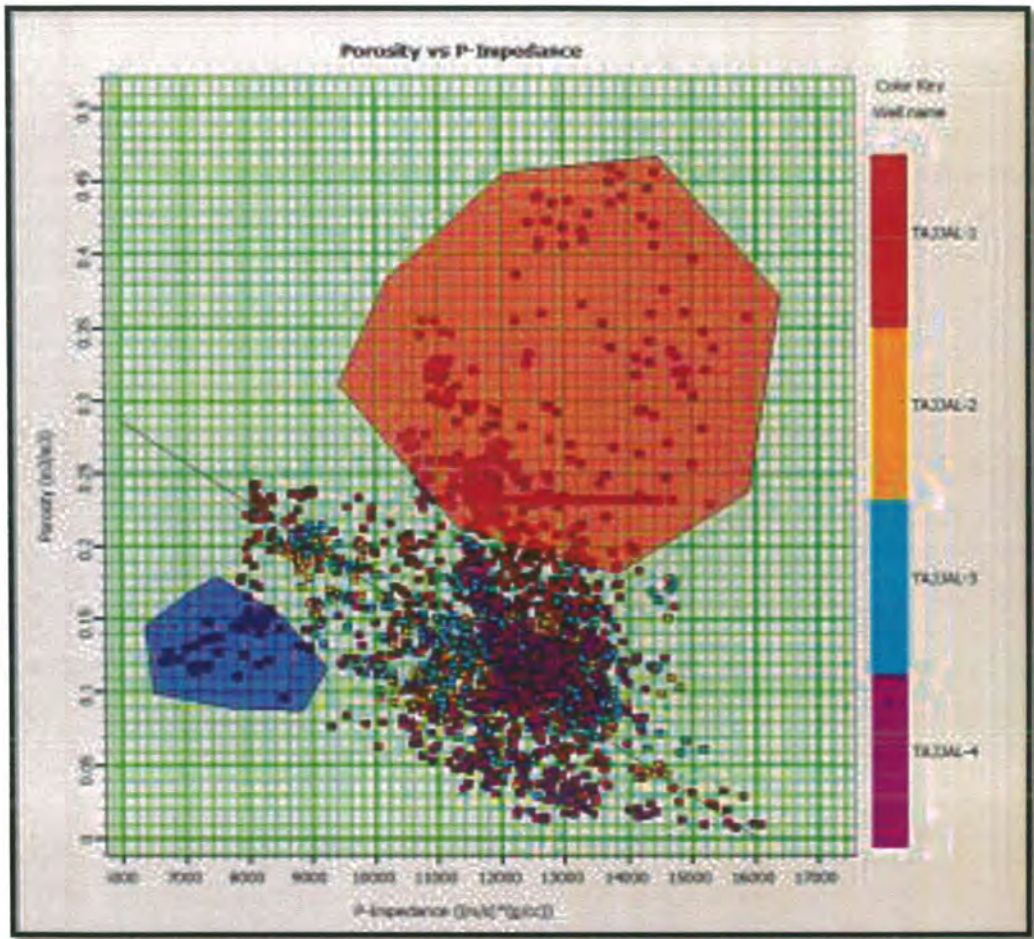
Figure 6.9: Cross plot between P-Impedance and porosity

In the above figure, porosity is cross plotted against P-Impedance for all wells i.e. Tajjal_01, Tajjal_02, Tajjal_03 and Tajjal_04. Porosity values are computed from inverted logs separately for all wells and it is observed that for Tajjal_01, these values are comparatively higher. There is an inverse relation which shows that velocity and density values are low for higher porosities.

6.3   Pore Pressure

Pore pressure is the pressure exerted by the fluid present in the rock pore on the wall of the pores of the rock volume.

$$Pore\ pressure = Pwall - Effective\ stress$$

Where Pwall the Pressure exerted by the wall of the pores on the fluid.

60

There are two main objectives of the calculation of pore pressure:

1. Provide pressure gradient curve to minimize the drilling risks as well.
2. Seal integrity of the prospect.

It can be calculated from seismic as well as well data using different approaches in both cases. Seismic data is used in most of the cases due to its wide areal extent and greater depth of penetration. Hottman and Johnson (1965), and Pennebaker (1968) used deviation of P-wave velocity from normal compaction trends to detect pore pressure. In a similar way, pore pressure is calculated using interval velocities, extracted from inverted data. The generalized trend of velocities with depth is shown as:
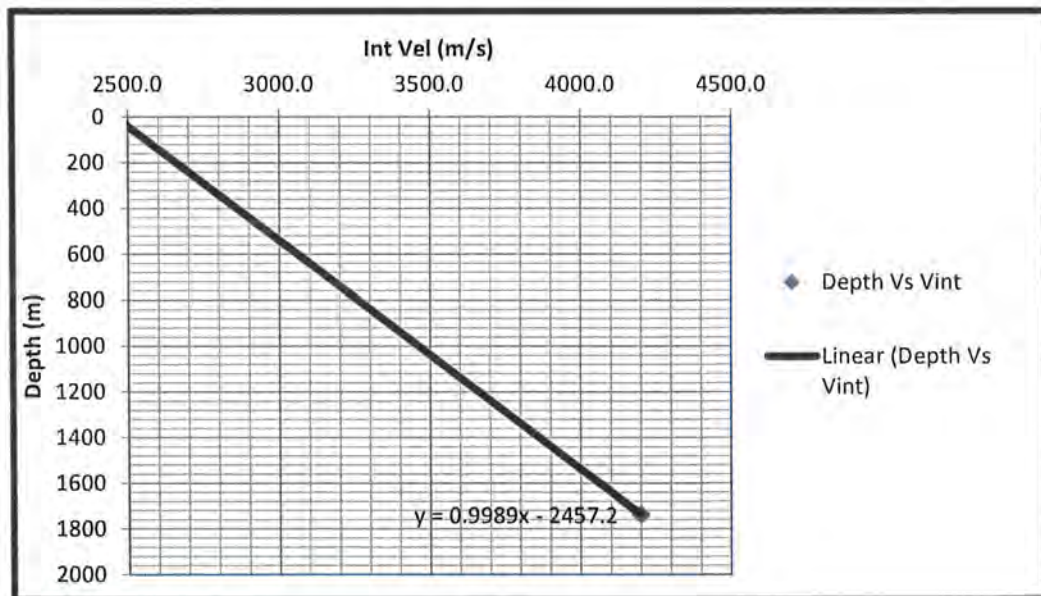
Figure 6.10: Cross plot between depth and interval velocity

In the above figure, it is shown that velocities are linearly increasing with depth in the range of 2500 to 4500 m/s. A linear relation is developed among the two parameters as shown above which can be used to predict interval velocity at any depth.

Interval velocities, effective stress and NCT (Normal Compaction Trend) are used to calculate pore pressures. NCT curves generally define the normal behaviour of a rock towards over burden and stress effects. The deviation from these curves give pore pressures which can be calculated

61

using any method as mentioned above. NCT curves are generated by cross plotting depth against velocity and pressure data. Over burden pressure and hydrostatic pressure are calculated using generalized pressure gradients. The following relation is used (Eaton, 1975):

$$\sigma = \sigma_{norm} \left(V_{int}/V_{norm} \right)^3 \qquad (6.1)$$

Where σ_{norm} and V_{norm} are calculated from the NCT curve. The results are shown as:
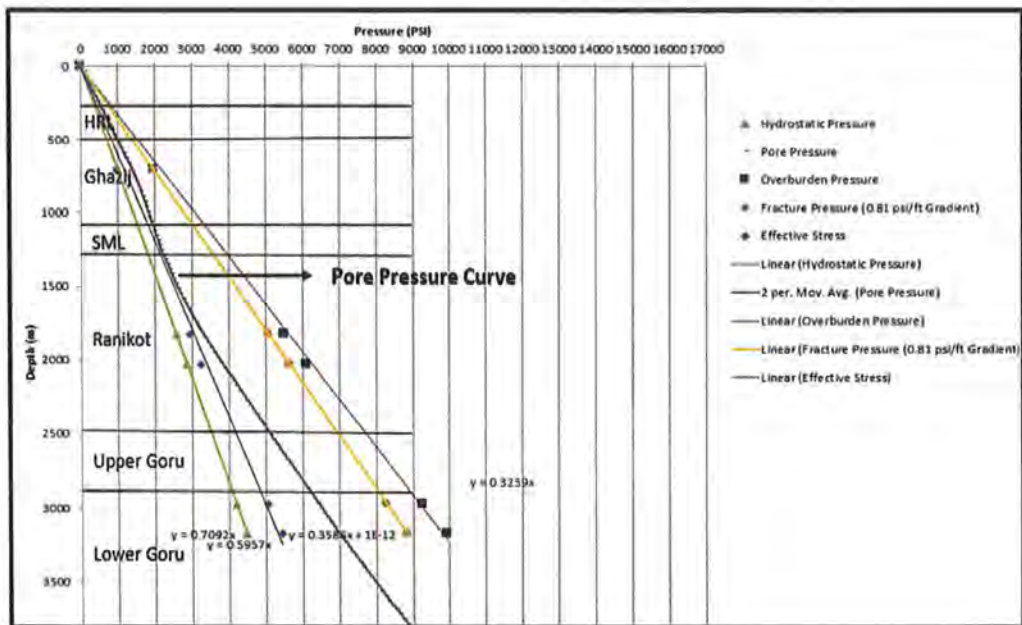
Figure 6.11: Cross plots between depth and pressure

In the above figure, hydrostatic pressure, pore pressure, effective stress and overburden pressure are plotted against depth and linear relation is calculated for each parameter against the depth which can be used to calculate pressure value at any depth. Pore pressure remains almost same in adjacent sand-shale layers. However, slight increase in the pressure is observed in Ghazij shales which is bounded by limestone at its both ends.

62

7. Results and Discussion

In the present study, Tajjal_01 and Tajjal_04 are gas saturated wells while Tajjal_02 and Tajjal_03 are water saturated wells. Rock physics modelling is applied to change saturation of Tajjal_01 and Tajjal_04 from gas to water and results are compared with originally water saturated wells. The cross plots between V_P and V_S are following a specific pattern for water saturated zones in case of Tajjal-02 and Tajjal-03. In case of Tajjal-01 and Tajjal-04 the data points are scattered away from normal trend at a specific depth interval taken from the reservoir. However, the trend gets changed in a similar way for both the wells when the fluid saturation is changed from gas to water. Hence, rock physics modelling can be implied to build relation between seismic parameters at different conditions of the reservoir. In this case, velocities of S-waves can be predicted by building a linear relation between two parameters i.e. V_P and V_S by observing the data trend. S-wave velocities are always predicted from water saturated reservoir zone instead of hydrocarbon saturated zone. The predicted S-wave velocities can further be used in AVO modelling.

Synthetics are made for three amplitude conditions i.e. near angle, mid angle and far angle for all wells to have a clear understanding of AVO response. AVO gradients of all wells for in-situ condition clearly predict true characterization of the reservoir but as soon as the situation gets changed i.e. after fluid substitution in gas producing wells (Tajjal_01 and Tajjal_04). The amplitude trend shifts towards the water saturated wells (Tajjal_02 and Tajjal_03). Similarly, AVO cross plots i.e. gradient and intercept can clearly indicate the class of sand and to some extent presence of hydrocarbons as well. The data trend indicates that the reservoir consists of class-IV sands. In this case, fluid saturation is effective in a similar way as in AVO gradient analysis. The results can be verified from pre-stack data, where reflection coefficients are plotted against the incidence angles. Hence, AVO modelling can characterize the reservoir in an accurate way, if it is applied properly by considering all conditions and assumptions on which this approach is based.

Seismic and inverted data are correlated such that amplitude error between the two is roughly between 0.3 and 0.4 units which shows good results. P-Impedance original and P-Impedance inverted are linearly related to each other, as there is a clear positive data trend in cross plot of the two, which shows the strong correlation between these two parameters. The porosity values are good for zone of interest i.e. B-Sands of Lower Goru ranging from 12 – 18%. Cross plot between porosity and P-Impedance shows comparatively higher values for Tajjal_01, which is a gas

producing well. Pore pressure is estimated using Eaton method, lying in the range 0-8000 psi and its deviation from NCT curve is remarkable at a depth of 2000m and greater than that which shows intense pressure conditions at that depth.

Conclusions

- 3D Seismic data is interpreted for Gambat Block and flower structure is observed in the area which is formed due to strike slip faulting.

- B-sand of lower Goru formation in the area is characterized using petrophysics, rock physics modelling, seismic attributes, AVO modelling and post stack seismic inversion.

- Rock physics analysis showed that relation between V_P and V_S is dependent upon fluid saturation and based on this dependence, V_S can be predicted from V_P. Tajjal_01 and Tajjal_04 are modelled by changing the saturation from gas to water and results are comparable with Tajjal_02 and Tajjal_03, which are water producing wells.

- AVO Modelling clearly indicated class of sand (Type IV) of the reservoir and showed variable response at variable fluid saturation. The results can be confirmed by plotting reflection coefficients against incident angles, if Pre-Stack seismic data is available.

- Post Stack Inversion showed that P-Impedance original and P-Impedance inverted are linearly related to each other. The porosity values are good for zone of interest ranging between 12-18% and pore pressures are more at 2000m which shows intense pressure conditions.

References

- Coffeen, J.A., 1986. "Seismic exploration fundamentals, Penn Well Publishing Company, Tulsa, Oklahoma."

- Dobrin, M. B., & Savit, C. H., 1988. "Introduction to Geophysical Prospecting. Mcgrew Hill Company."

- Eaton, B.A., 1975. "The equation for GeoPressure prediction from Ell logs." SPE 50th Annual Fall Meeting Proceedings SPE 5544.

- Grana, D., 2014. "Probabilistic approach to rock physics modeling."

- Han, D., & Batzle, M., 2004. "Gassmann's equation and fluid-saturation effects on seismic velocities." The Leading Edge.

- Hirsche, K., Boerner, S., Kalkomey, C., & Gastaldi, C., 1998. "Avoiding Pitfalls in Geostatistical Reservoir Characterization: A Survival Guide." The Leading Edge 17 (4): 493.

- Johansen, T.A., Jensen, E.H., Mavko' G., & Dvorkin, J., 2013. "Inverse rock physics modeling for reservoir quality prediction."

- Kalkomey, C.T. 1997. "Potential risks when using seismic attributes as predictors of reservoir properties." The Leading Edge 16 (3): 247.

- Kazmi, A.H., & Jan, M.Q., 1997. "Geology and Tectonics of Pakistan, Graphic Publishers Karachi, Pakistan."

- Li, Y., Downton, J., & Xu, Y., 2004. "AVO Modeling in Seismic Processing and Interpretation Part III. Applications." Canadian society of Exploration Geophysicists Vol 29. No. 02.

- Pendrel, J., 2006. "Seismic Inversion; A critical tool in reservoir characterization", Scandinavian Oil-Gas Magazine, No. 5/6, p. 19-22.

- Raza, H.A., Ahmed, R., Ali, S.M., Sheikh, A.M., & Shafique, N.A., 1989. "Exploration performance in sedimentary zones of Pakistan." Pakistan Journal of Hydrocarbon Research v. 1/1, p. 1-7.

- Robertson, J.D., & Nogami, H.H., 1984. "Complex seismic trace analysis of thin beds." Geophysics 49: 344.

- Robinson, E.S., and Coruh, C., 1988. "Basic Exploration Geophysics, John Wiley & Sons, IncNewyork."

- Shah, S.M.I., Ahmed, R., Cheema, M.R., Fatmi, A.N., Iqbal, M.W.A., Raza, H.A., & Raza, S.M., 1977. "Stratigraphy of Pakistan. Geological Survey of Pakistan." Memoirs, v. 12, p.137.

- Shah, S.M.I., 2009. "Stratigraphy of Pakistan. Geological Survey of Pakistan." Memoirs, v.22.

- Taner, M.T., Koehler, F., & Sheriff, R.E. 1979. "Complex seismic trace analysis." Geophysics 44 (6): 1041.

- Telford, W. M., Sheriff, R. E., & Geldart, L. P., 1990. "Applied geophysics." Cambridge University Press.

- Yangkang, C., Xiang, H., **Chen, K., 2017.** "Geological structure guided well log interpolation for high-**fidelity full waveform inversion**". Geophysical Journal International. **209** (1): 21-31.

- Yilmaz, 2001. "Seismic Data Analysis and Processing, Inversion and Analysis of Seismic Data." Society of Exploration Geophysics, Tulsa.

- Younas, U., Khan, B., Ali, M., Arshad, C.M., Farid, U., Zeb, K., Rehman, F., & Mehmood, Y., 2016. "Pakistan Geothermal Renewable Energy Potential for Electric Power Generation."

- Young, R., & LoPiccolo, R., 2005. "AVO analysis demystified." E&P.